University of Birmingham

School of Biosciences

The Comparison of the unnatural amino acid Napthylalanine NfsB mutant and wild type NfsB activity for the pro-drug CB1954 and Menadione.
Investigating the effect of the poly histidine tag on wild type NfsB substrate reduction.

&

G protein coupled cytokines fMLP & LPA Induced Potentiation of PDGF Receptor Signaling.
Protein Kinase C: A possible point of signal integration for PDGF β receptor recycling.

A research project report submitted by

ASHA HASSAN

as part of the requirement for the

degree of MRes in Molecular and Cellular Biology

This project was carried out at: The University of Birmingham

Under the supervision of: Dr Eva Hyde and Dr Carina Hellberg

Date: July 2012

This thesis consists of the combination of two projects:

The first project investigated the enzyme NfsB from *Eschericia coli* (a bacterial Nitroreductase), which has now entered the clinical trial stage with the pro-drug [5-(aziridin-1-yl)-2,4-dinitrobenzamide] (CB1954) as the enzyme reduces this inert pro-drug into its toxic hydroxylamine derivative.

The second project investigated the Platelet derived growth factor tyrosine kinase receptor PDGF β, which investigated the current hypothesis that Protein Kinase C (PKC) is a point of signal integration for PDGF receptor recycling.

To my mother: Dr Maryan Qasim

My Secure Foundation

&

To my son: Nasir Hassan

My Engine

Acknowledgements

I would like to express my deep gratitude to Dr Carina Hellberg and Dr Eva Hyde for the amazing support, patience and continuous guidance they have given me throughout the two projects as this thesis would otherwise have not been completed

I would also like to thank Wei Zheng and Martin Day for the support they have given me during the projects and the unwavering help offered whenever I required it.

Finally a great big thank you to the 5th floor Biosciences, I will greatly miss the routinely Friday meetings of lecturers arguing!

Contents

List of figures

List of tables

Appendix I Section 3 Table 3.2 The kinetic parameters of reduction of Menadione by NapA

Abbreviations

CB1954	(5-[aziridin-1-yl]-2,4-dinitrobenzamide)
DMSO	Dimethyl sulfoxide
FMN	Flavomononucleotide
NapA	Unnatural amino acid mutant Napthylalanine at position 124. NfsB
NiNTA column	Nickel-Nitrilotriacetic acid column
NQO1	NAD(P)H: Quinone oxidoreductase 1
SDS-PAGE	Sodium dodecyl sulphate polyacrylamide gel electrophoresis
WT NfsB	Wild type never his-tagged NfsB
WT HT NfsB	Wild type his-tagged NfsB
WT CL NfsB	Wild type cleaved his-tag NfsB

E. coli	*Escherichia coli*

First Thesis

Abstract

The enzyme NfsB from *Eschericia coli* is a bacterial Nitroreductase, which has now entered the clinical trial stage with the pro-drug [5-(aziridin-1-yl)-2,4-dinitrobenzamide] (CB1954) as the enzyme reduces this inert pro-drug into its toxic hydroxylamine derivative. In this study the poly histidine tag which was added onto the wild type NfsB (to allow affinity purification) was investigated and it was determined that it had a negative effect on the specificity constant (k_{cat}/K_m) of wild type NfsB for CB1954, reducing to half the original value, however a statistical significance was not observed. In addition once the histidine tag was cleaved, the original level of activity did not return as the recombinant enterokinase did not cleave the entire tag and a statistical significance was observed for the rate of menadione reduction when comparing to WT NfsB. Furthermore the activity of wild type NfsB and the unnatural amino acid mutant napthylalanine with menadione were also determined, concluding that menadione is a far better substrate for both the wild type and napthylalanine NfsB mutant, improving the specificity constant by 40/50 times. Nevertheless, the napthylalanine NfsB mutant showed a statistically significant lower activity with the pro-drug in comparison to the wild type NfsB, which was due to the low concentration and impurity of the sample obtained for napthylalanine NfsB. Finally a crystal of the cleaved wild type NfsB was grown, however this was twinned and the diffraction pattern could not be solved.

1. Introduction

1.1Background

On average 12.7 million individuals are diagnosed with cancer annually around the globe, with 267 cases for every 100,000 individuals within the U.K making it the 22nd highest cancer rate in the world (WCRFI, 2011). This disease has been identified and acknowledged as a disorder with high morbidity and mortality rates; therefore highlighting the great need for developing therapeutic solutions (WCRFI, 2011). Malignant neoplasm, commonly referred to as cancer, is a term used to cover a vast number of different cancerous types. Generally the cells in cancer patients replicate uncontrollably and result in the formation of tumours. These can be classified as either benign or malignant tumours; in the benign form the tumour doesn't spread and remains localized (Davis and Balentine, 2012). However in malignant tumours, the cancer cells are undergoing rapid replication, infiltrating and spreading into other and distant parts of the body, through the lymphatic system and bloodstream (Davis and Balentine, 2012). These malignant transformations occur as oncogenes are over expressed through the inhibition, destruction or mutation of the tumour suppresser genes, resulting in uncontrollable replication of both normal and abnormal cells. Generally, a number of genes are required to transform within the normal cells in order to produce a cancerous cell (Davis and Balentine, 2012). Nevertheless, the mortality of cancer has reached significant figures, with an average of 7.6 million deaths reported in 2008 (WHO, 2008)

Chemotherapy is one of the major treatments of cancer, which holds an important position in the struggle against this disease; however there are several limitations, which result in the failure of such methods. It involves the use of antineoplastic drugs in order to treat cancer;

these drugs target rapidly dividing cells which consequently affect the bone marrow, digestive tract and hair follicles (Goldwein and Vachani, 2010). These types of drugs include DNA alkylating agents, which damage the DNA and nucleotide analogues functioning as anti-metabolites and preventing DNA replication. The main issues surrounding this treatment includes the deficiency in drug delivery to the tumour site, toxicity caused and most significantly the insufficiency of selectivity for tumour cells causing high system toxicity (Xu and McLeod, 2001). The success of a therapeutic cancer treatment is generally defined by the percentage of drug delivery to the tumours in addition to limiting system toxicity (Wu & Chang, 2010). The majority of chemotherapeutic drugs aren't specific to tumour cells and do not accumulate at these sites, with only a small percentage of the dosage delivered to the tumour, and approximately 75-90% of the dose accumulating in other organs (Ropert, 1999). As well as system toxicity, multidrug resistance has been one of the major causes for the lack of success in chemotherapy (Kowalski *et al.*, 2002). There have been a vast number of approaches in order to address these setbacks, one of which is recruiting liposomes as a gene delivery system (Ropert, 1999; Wu and Chang, 2010; Krishna and Mayer, 1997). This approach targets tumour associated endothelial cell receptors (on the cell surface) via encapsulating the chemotherapeutic drugs with liposomes that bind these receptors (Wu and Chang, 2010; Suzuki *et al.*, 2007).

The developments for methods addressing multidrug resistance in particular, are important as it is a significant obstacle; occurring as the tumour cells exposed to 1 type of chemotherapeutic drug, develop a form of resistance to that specific cytotoxic agent in addition to a range of other drugs which can differ in both structure and function (Thomas and Coley, 2003). This is caused by an increased expression of specific proteins, which affect the cell membrane (e.g. related membrane transporters) and cause an increase efflux of the

cytotoxic drug; decreasing intracellular concentrations (Thomas and Coley, 2003). However in some cases resistance has developed in the absence of previous drug administration.

Since the establishment of gene therapy in 1990, new treatments became available via gene therapy combined with other therapeutic agents/methods which improved chemotherapy delivery (Davidoff, 2007; Suzuki *et al.,* 2007). Gene therapy was initially established from the theory that disorders caused by a gene defect can be cured by the replacement or modification of the affected genes, therefore enabling the host cells to reverse the disease phenotype (via the transgene expression). Cancer in particular is ideal for this form of treatment due to its genetic foundation and potential for cellular exploitation. This includes targeting fundamental processes such as different phases of the cell cycle (Goldwein and Vachani, 2010). These type of drugs can be cell cycle non specific, allowing it to destroy a cell during any phase. However other chemotherapeutic agents can also be cell cycle specific, only able to initiate cell destruction during specific phases. Generally during chemotherapy treatment, these drugs are combined in order for the two to complement one another (Goldwein & Vachani, 2010).

Although chemotherapy was established beforehand; the use of gene therapy has been exploited and adapted significantly since its breakthrough in 1990 (base for gene directed enzyme pro-drug therapy) (Prosser, 2011). This led to many therapeutic advances towards the treatment of cancer by combining cancer drugs with anti-tumour genes and resulting in gene directed enzyme pro-drug therapy (GDEPT) (Kowalski *et al,* 2002). This has proved to be an appealing area for local cancer treatment and tumour selectivity (Mitchel & Minchin, 2008). Treatment involves two main phases; initially the enzyme which will activate the biologically inert pro-drug, converting it into a potent toxic metabolite, must be expressed in the tumour. Therefore upon the administration of the non toxic pro-drug, it (the pro-drug) can be

converted into an active anticancer drug (Xu and McLeod, 2001). Although the pro-drug distribution within the body is extensive, the cytotoxicity caused will be limited to the cells expressing the transgene. This enables the use of higher concentrations of chemotherapy drugs, consequently improving the therapeutic index (Both, 2009).

Furthermore, there are many vectors used for the delivery of the transgene in the target cell, however 2/3 of ongoing gene therapy have employed the use of viral vectors (figure1.1.1) (Herod, 2010). This is further categorized into 6 main virus vectors, with adenovirus vectors favoured for the delivery and packaging of the nitroreductase transgene (Herod, 2010). This is delivered either locally into the tumour or systemically, which will then express the transgene (in tumour cells that have taken up the vector) and produce the corresponding protein. This will then convert the administered pro-drug into its toxic metabolite as well as transfecting neighbouring cells, also referred to as the bystander effect (figure 1.1.2) (Prosser, 2011).

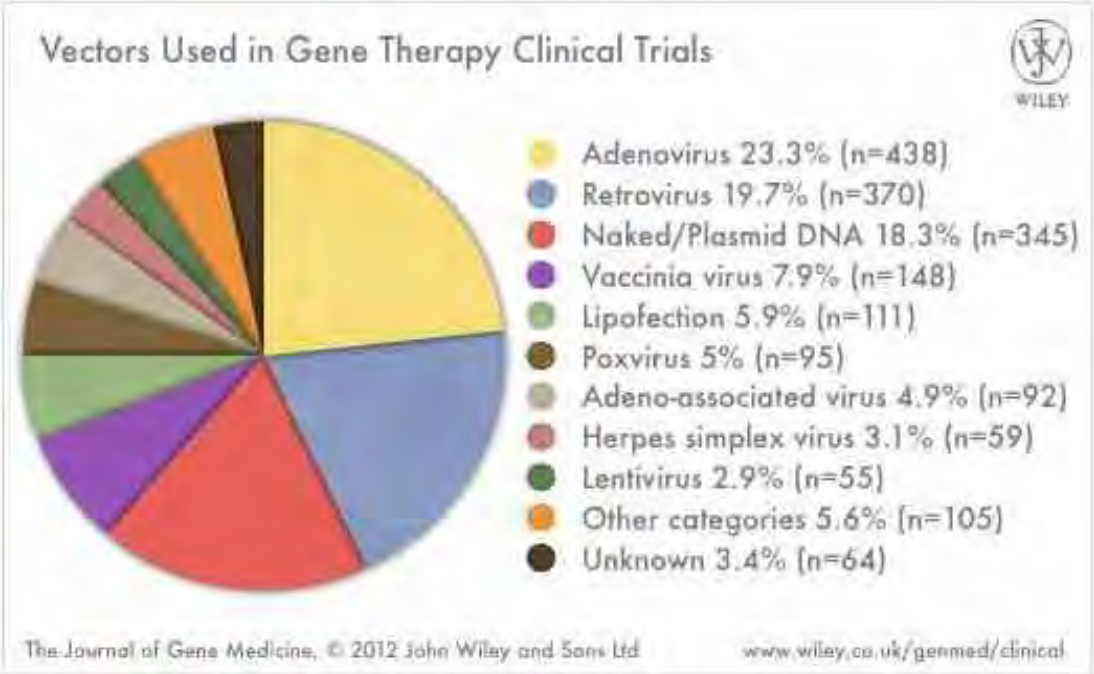

Figure 1.1.1: Vectors used in gene therapy clinical trials (Herod, 2010).

The most common vector is a viral one which encapsulates the transgene, delivering the genetic material through transduction. The favoured viral vector for the delivery of the nitroreductase transgene in molecular chemotherapy is the adenovirus vector, which is one of the most common viral vectors used. It is a non-enveloped icosohedral virus, which can hold great sections of the DNA, in addition to being able to rapidly infect a vast variety of human cell (Genomics, 2011).

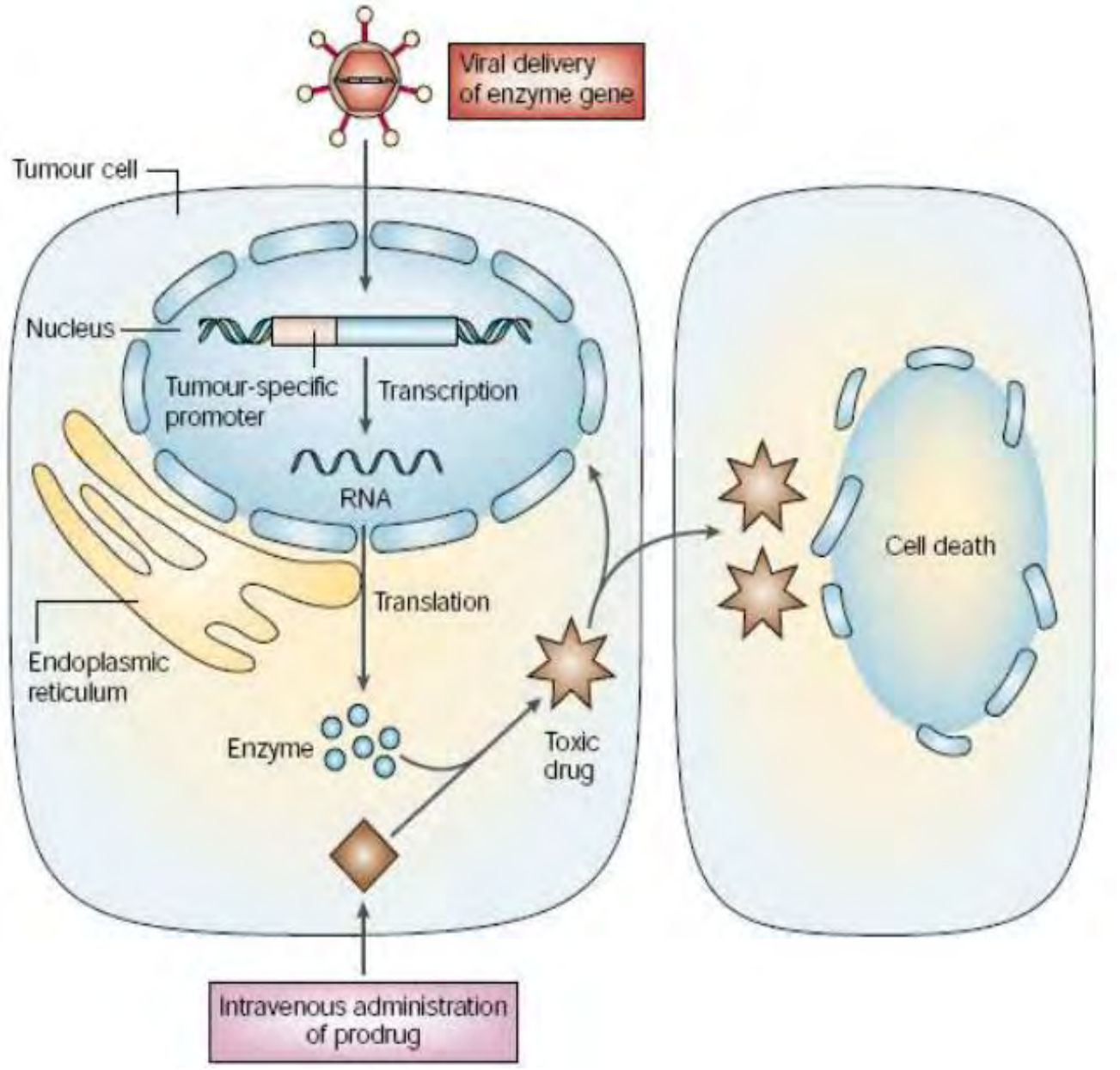

Figure 1.1.2: Schematic Diagram of gene directed enzyme pro-drug therapy via the use of a viral delivery vector system to administer the enzyme gene (Prosser, 2011).

The transgene is packaged and delivered either directly or systemically into the tumour. This then transcribes the transgene and translates the enzyme/protein. The inert pro-drug is administered intravenously and the enzyme/protein translated converts it (the pro-drug) into its toxic metabolite. This then damages the cell, killing it as well as transfecting neighbouring cells and causing the same result (bystander effect) (Prosser, 2011).

The nitro-aromatic pro-drug 5-(Aziridin-1-yl)-2,4-dinitrobenzamide (CB1954) is a monofunctional alkylating agent with low toxicity, which had proved itself significant as an antitumour drug, against the rat Walker 256 carcinoma (Cobb *et al*, 1969). The pro-drug was initially discovered during the investigation of N-substituted-aziridine compound effects on the cancer model system; rat Walker-256 carcinoma. The CB1954 antitumour pro-drug had completely regressed and cured this carcinoma (Cobb *et al*, 1969). Further studies identified that the CB1954 pro-drug was enzymatically activated and its 4 nitro group (4-NO_2) reduced to a 4-hydroxyl amine derivative (5-(aziridin-1-yl)-4-hydroxylamino-2-nitrobenzamide: 4-NHOH) (Friedlos *et al.*,1992). This reduction was catalysed by NAD(P)H: Quinone oxidoreductase 1 (NQO1), an oxygen insensitive reductase (Knox *et al*. ,2000 ; Prosser, 2011).

This reduction causes the compound to undergo both structural and electronic alterations within the aromatic ring; the alteration of electrons increases the hydrophilic ability of the ring and consequently increases DNA binding properties (Prosser, 2011). Alternative studies proposed that a non enzymatic interaction occurs between the 4-hydroxylamine and intracellular thioesters (specifically the acetyl-CoA) forming an N-acetoxy derivative. This is an extremely toxic compound which results in the formation of DNA-DNA inter-strand cross links within the cancer cells. The inability to repair this damage to the DNA correctly causes cell death (figure 1.1.3) (Christofferson, 2009; Prosser, 2011)

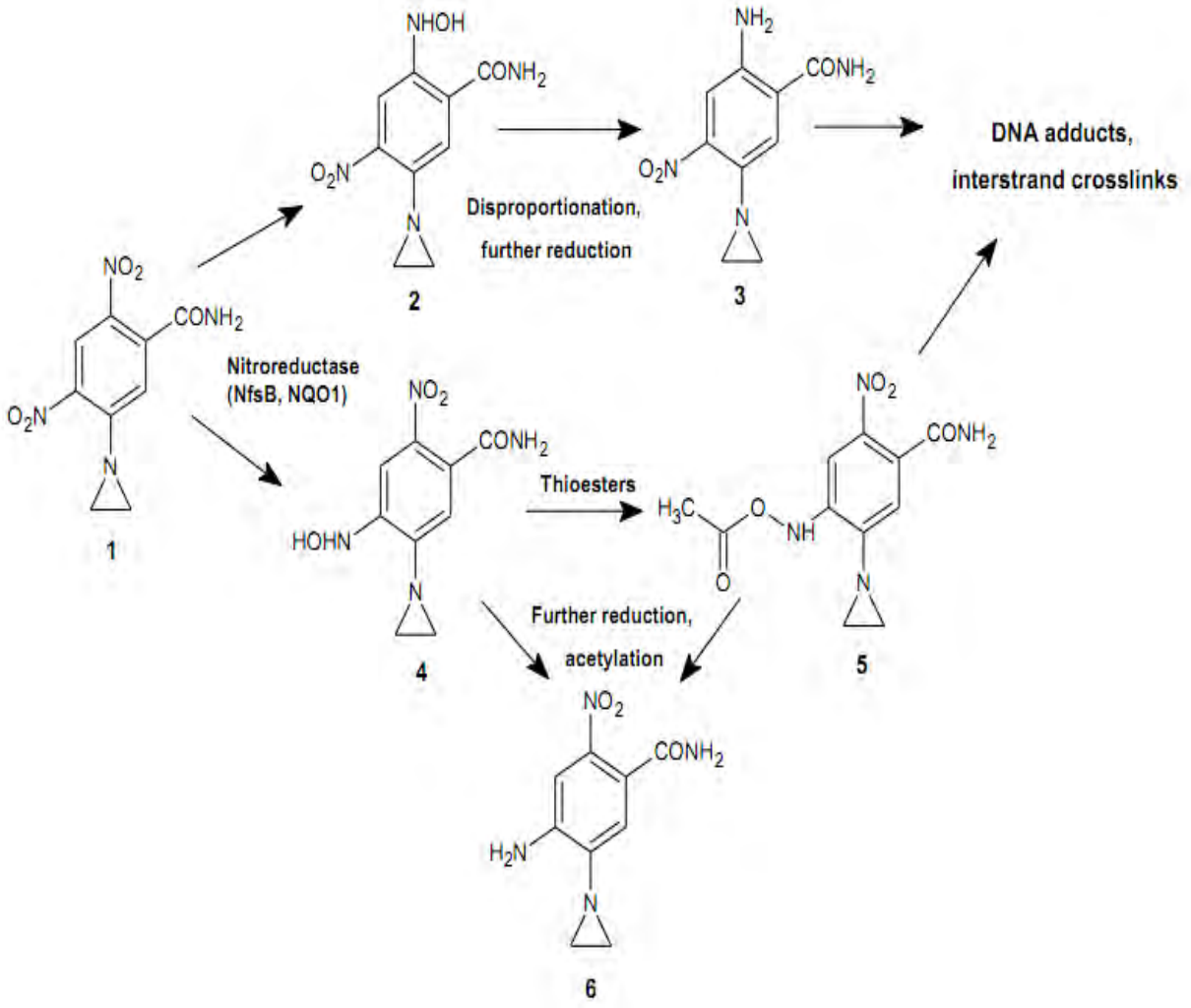

Figure 1.1.3: The Bioactivation of CB1954 (Prosser, 2011).

The initial step is the enzymatic nitroreduction of the pro-drug, into either 2-hydroxylamine (2NHOH) or 4-hydroxylamine (4NHOH). Depending on which of the two the parental pro-drug is reduced to, different products will be formed. In the case of 2NHOH, it is unstable and disproportionate in aqueous solutions. This produces nitroso derivates (compounds with functional group as RNO), not shown, and amine derivates (compound 3). Although it is unstable it has good bystander effects. In the case of the parental pro-drug reduction to 4NHOH, it undergoes a further reduction to compound 6, a non toxic amine. However 4NHOH can also react with the intracellular thioesters (specifically the acetyl-CoA) forming an N-acetoxy derivative, compound 5. Finally an increased acetylation of compound 5 can

result in the formation of compound 6, with only compounds 3 and 5 being able to form intra and inter strands cross-links with DNA forming monoadducts. (Prosser, 2011).

This enzyme (NQO1) is also present in human cells, however due to a difference at residue 104 (tyrosine to glutamine) the metabolism of the CB1954 pro-drug by the human NQO1 is significantly inferior (Xu and McLeod, 2001). Kinetic analysis comparing the enzyme activity of the human and rat form of this enzyme, showed them both to have comparable activity. However the human NQO1 enzyme was significantly lower in the activation of CB1954, with a k_{cat} of 0.64/min; in comparison to the rat NQO1 enzyme, with an enzyme activity of K_{cat} of 4.1/min (Green *et al.*, 2004). However subsequent studies have shown the nitroreductase encoded by the NfsB gene of *E. coli*, enhances the efficiency of this bioreduction by nearly a 100 fold in comparison to the NQO1 enzyme in rats (Green *et al.*, 2004). This drug is excellent for the use in GDEPT, as the administration of CB1954 is non toxic at therapeutic levels, as well as the inability of normal human enzymes to activate this pro-drug to toxic levels (human NQO1 is a poor analogue) (Xu and McLeod, 2001). In addition, CB1954 is not cell cycle specific and thus can kill the cells independently of the cell cycle (Christofferson, 2009).

The nitroreductase NfsB found in *E. coli* is part of the superfamily enzymes; bacterial nitroreductases, which are diverse and also found in prokaryotes (Prosser, 2011). These flavoproteins were initially discovered in 1940, for their effect on the antibiotic chloramphenicol, where they reduced the nitro group (Merkel and Steer, 1953). The NfsB NTR is made up of two subunit dimers; each containing 217 amino acids, and a FMN cofactor at its active site (Christofferson, 2009). Nitroreductases are a group of flavoproteins which have been found to reduce a diverse range of nitroaromatic compounds either aerobically (oxygen sensitive class I) or anaerobically (oxygen insensitive class II) (Koder *et*

al.,2002). This is through either 1 or 2 electron reduction steps with class I nitroreductases employing only one step and class two employing a single, simultaneous 2 electron transfer step (figure 1.1.4) (Koder *et al.*,2002; Prosser,2011).

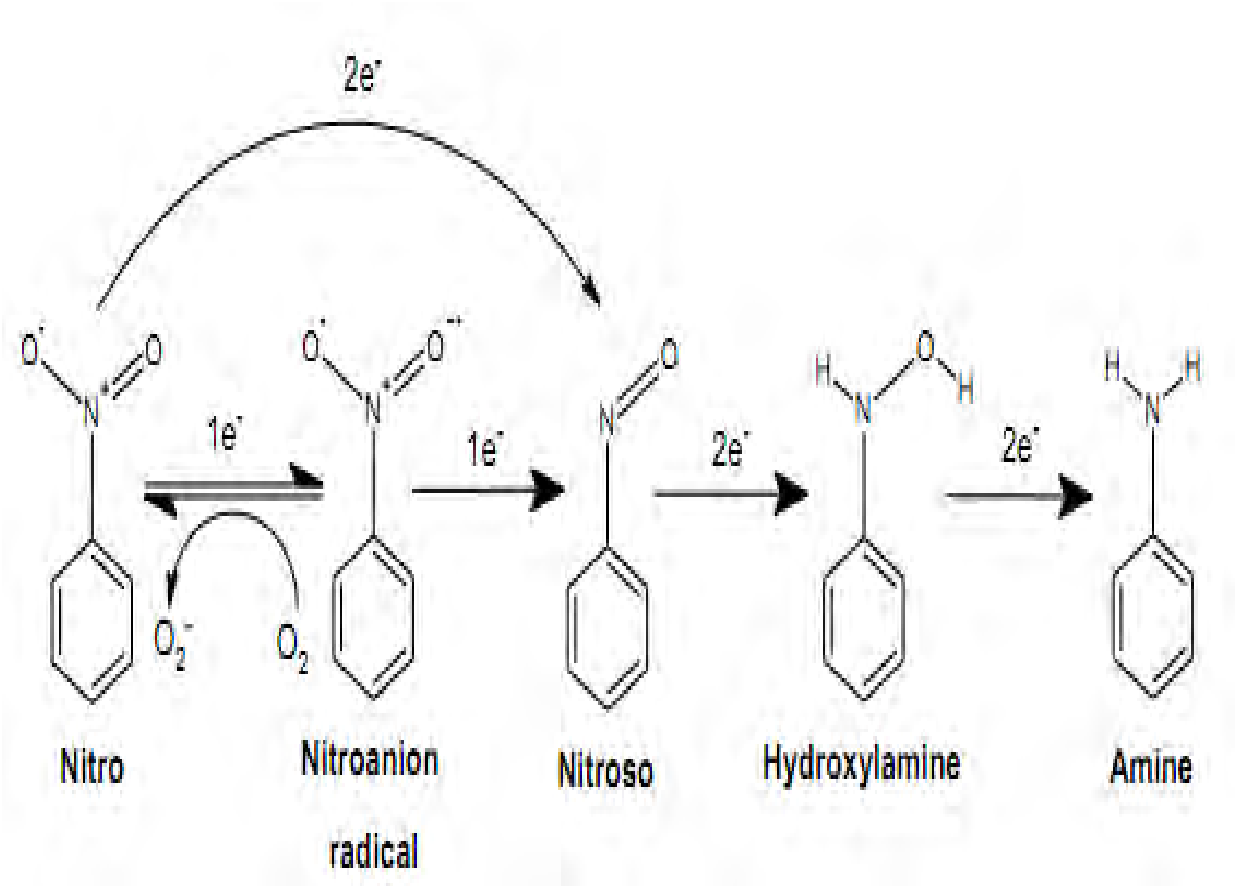

Figure 1.1.4: Schematic overview of the electron steps reduction of nitroaromatic compound (Prosser, 2011).

Upon the reduction ($1e^-$) of the initial nitroaromatic, an unstable nitro-anion radical is formed, which can be reversed to the parental nitroaromatic (through reacting with O_2 – class I). In a further reduction of $1e^-$ (either in absence in O_2, with class 1 or – class II) the nitro group is converted, in an irreversible reaction to a nitroso metabolite and upon the reduction of a further $2e^-$ the hydroxylamine derivative is produced. Finally a further reduction of $2e^-$ the amino reaction product is produced (Koder *et al*., 2002; Prosser, 2011)

There have been three oxygen insensitive nitroreductase proteins identified in *E. coli*: NfsA (the major nitroreductase), NfsB and NfsC with minor nitroreductase activities. In comparison to NfsC, the other two proteins have been studied in a greater depth and identified to have similar enzymatic properties. NfsA and NfsB both employ flavomononucleotide (FMN) as a prosthetic group and use this to reduce the nitrocompounds via the Ping Pong Bi Bi mechanism. These NTRs use NAD(P)H as the reducing agent via a 2 electron step reduction (figure 1.1 IV). In the first step of the reaction FMN (Enzyme.FMN) is reduced via NAD(P)H and $NAD(P)^+$ is released with the formation of $E.FMNH_2$. In the second step of the reaction, different quinones and nitroaromatic substrates are reduced.(figure 1.1.5) (Anlezark *et al,* 2002; Lovering *et al,* 2001). The substrates (aromatic compounds/quinones) bind the active site of the reduced enzyme (Lovering *et al*, 2001).

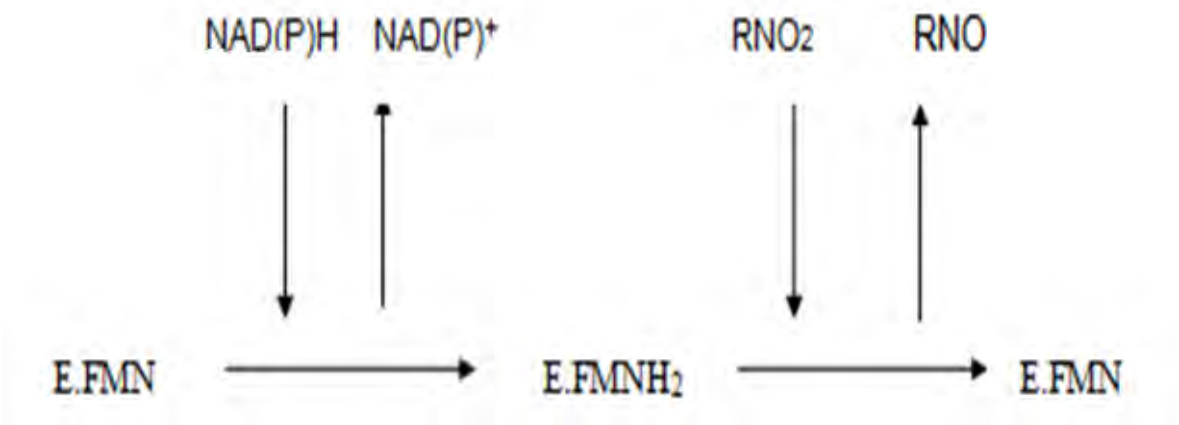

Figure 1.1.5: Schematic overview of the Ping Pong Bi Bi mechanism reduction of nitrocompounds (Anlezark *et al,* 2002; Lovering *et al,* 2001).

Furthermore, although the wild type NfsB enhances the bio-reduction of CB1954 by nearly a 100 fold; the affinity of the NTR for the pro-dug is still considerably low, as it is not a natural substrate (Christofferson, 2009). The result in a low percentage yield of pro-drug, activated into its toxic metabolite. The investigation of the exact mechanism is important as this can help determine vital amino acids at the active site, in order to mutate them and increase pro-

drug activation (Christofferson, 2009). Therefore the 9 residues at the active site of the nitroreductase and surrounding the FMN co-factor were selected for site directed mutagenesis with a single mutation. These include ; Phe124, Ser40, Tyr68, Phe70, Asn71, Gly120, Glu165, Gly166, Thr41, from which the potential amino acid substitution were made and subsequently cloned into an *E.coli* bacteria (Grove *et al,* 2003). These showed a significant enhancement in the sensitization of the cells to the pro-drug enhanced sensitisation to CB1954 in an E. coli cell-killing assay; the decrease in bacterial was growth monitored (*E. coli* cell killing assay), implying the improved activity of the pro-drug. The most active single mutants were found at the Phe124 site, which had 15 amino acids replaced, resulting in an increased drug activity (Grove *et al*, 2003). It has been proposed that this is due to the hydrophobic side chain, partially restricting binding of the substrate (Grove *et al*, 2003). Other improvements were also at the Ser40 site, by mutating it to residues which have small side chains (e.g. alanine/glycine). In constrast Thr41 only showed improvements with long hydrophobic, glycine or polar groups. Tyr68 also improved with glycine and in addition asparagines (Grove *et al*, 2003). Phe70, however, is located near the opening of the active site, which resulted in several residues that caused an improvement. This is most likely due to its location, and that it allowed an increased admission to the active site in addition to reducing product release. Finally Asn71 only produced an improvement with a polar residue (e.g. Serine) (Grove *et al,* 2003).

The Phe124 site had emerged as an important factor in the binding of the substrate and thus different single unnatural amino acids were incorporated at the phe124 site (Jackson *et al,* 2006). These all had different effects on the activation of CB1954, however F124 & F124N were revealed to be the most significant as they increased the cell sensitivity to the pro-drug by five times (Jackson *et al,* 2006). Studies have suggested that this is due to the Phe12 pi stacking with the aryl ring of either the CB1954 or NAD(P)H as a response to the occupation

of the active site. Therefore it is considered that the Phe124 interacts with the substrate bound to the cofactor, and as the active site becomes occupied, it also interacts with the opposite subunit (Jackson *et al*, 2006).

This has led to the incorporation of unnatural amino acids into the active site, which further enhanced the activity of the pro-drug over the most successful natural amino acid (figures 1.1.6/7) (Jackson *et al*, 2006).

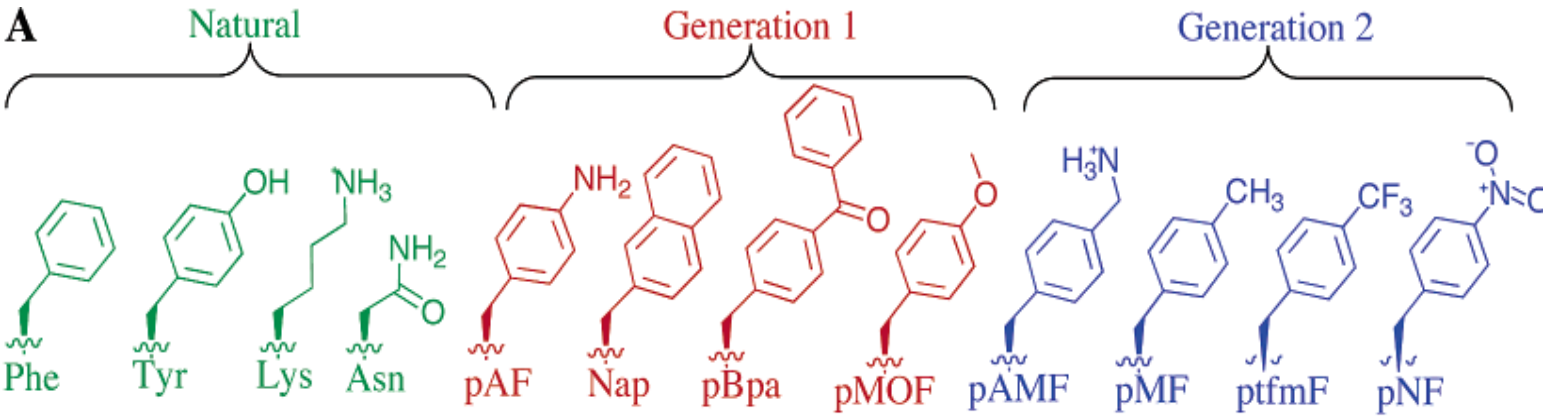

Figure 1.1.6: Nitroreductase modifications; natural and unnatural amino acids incorporated at site 124 (Jackson *et al*, 2006).

Generation 1: p-aminophenylalanine (pAF), naphthylalanine (Nap), p-benzoylphenylalanine (pBpa), p-methyoxyphenylalanine (pMOF). **Generation 2**: p-aminomethylphenylalanine (pAMF), pmethylphenylalanine (pMP), p-trifluoromethylphenylalanine (ptfmF), p-nitrophenylalanine (pNF) (Jackson *et al*, 2006).

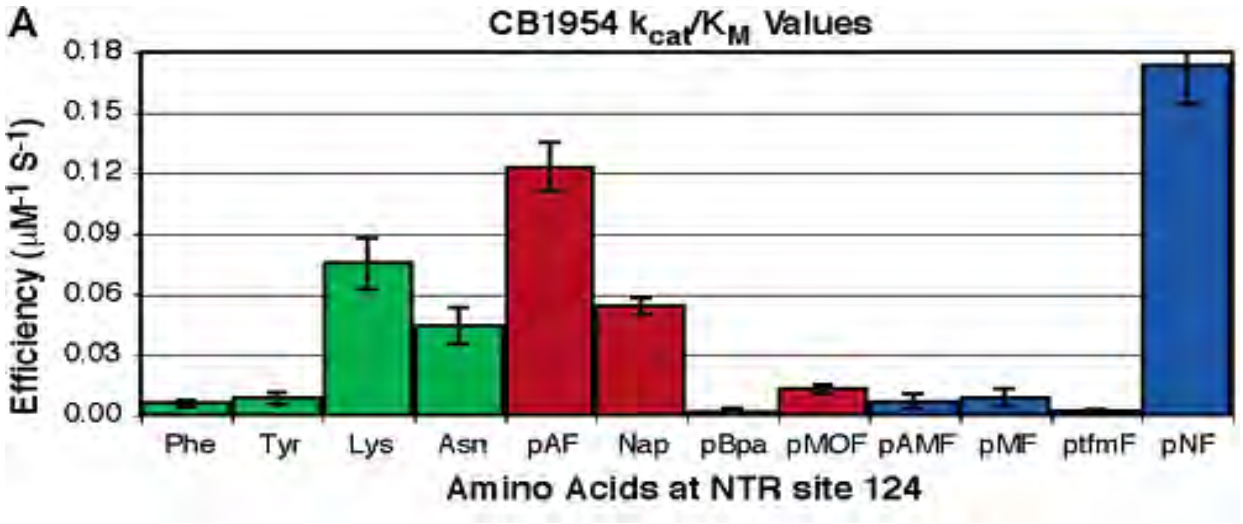

Figure 1.1.7: CB1954 k_{cat}/K_m with the different natural and unnatural modifications at site 124. This figure illustrates the improvement of CB1954 activation by incorporating unnatural amino acids (Jackson *et al*, 2006).

This project investigated the wild type NfsB protein and the single unnatural amino acid mutant Napthylalanine at position 124, and comparing the rate at which these can reduce the CB1954 pro-drug as the aforementioned studies have shown it to have a higher specificity constant for the pro-drug, in comparison to wild type NfsB (Jackson *et al,* 2006; Grove *et al*, 2003). However the wild type NfsB used in this project was expressed with the addition of a poly-histidine tag, to allow for affinity purification on a nickel NTA column. Therefore the initial objective was to investigate whether the poly-histidine tag had an effect on the enzyme's capabilities of substrate reduction. Furthermore, the steady state kinetics of the wild type NfsB were assessed and compared with those of the unnatural amino acid mutant Napthylalanine at position 124. In addition although the unnatural amino acid Napthylalanine NfsB at position 124 increases the specificity of the protein for the pro-drug, there are still a vast number of combinations of potential residue mutations. This makes it nearly impossible to improve the NTR any further, without specific knowledge of the substrate binding to the active site and the general reaction mechanism. Therefore the second part of the project investigated the enzymes reduction of another substrate: menadione. This is important as the binding orientation of different substrates and their reduction by FMN can help to increase the knowledge of how CB1954 is reduced by FMN (Christofferson, 2009). Finally the NfsB protein was crystallized in order to produce a 3-D image of the enzyme via X-ray crystallography, illustrating the different bonds and interactions of the pro-drug with FMN (Nelson, 2011).

The NfsB protein will benefit GDEPT as the enzyme pro-drug combination is already in cancer trial stages, due to its significant potential. Since the main issues lie in the lack of improving the NfsB preference for the CB1954 pro-drug, this project will mainly investigate the kinetics of NfsB with different substrates (CB1954 and menadione).

In this project the Wild type NfsB never his-tagged is referred to as WT NfsB. The wild type with the his-tag is referred to as WT HT NfsB and finally the wild type with the cleaved his-tag as WT CL NfsB. Finally the single unnatural amino acid mutant napthylalanine at position 124 of NfsB is referred to as NapA. However the NapA is also his-tagged as it is simply the WT HT NfsB protein but with the unnatural amino acid napthylalanine inserted at position 124.

1.1Summary of aims & objectives

The aims and objectives were separated into three parts for the project.

1. Comparing the activity & rate of reduction by WT NfsB , WT HT NfsB and WT CL NfsB; with the pro-drug CB1954 and Menadione

This assessed the effect of the poly histidine tag on the rate of substrate reduction by NfsB.

2. Comparing the rate of substrate reduction of NapA with WT NfsB

This assessed whether the NapA shows an improvement for substrate reduction in comparison to the WT NfsB.

3. Comparing the reduction of CB1954 and Menadione to determine whether Menadione is a better substrate for NapA than CB1954.

This assessed whether Menadione is a better substrate for NapA than CB1954.

2. Materials & methods

2.1 Material

All reagents were bought from Sigma Aldrich unless otherwise stated

2.2 Methods

2.2.1 Over expression of NapA

The clone expressing the NapA was a gift from Dr Ryan Mehl (Oregon State University, USA) and the protein was produced by the method described in the paper Jackson *et al*. 2006. The cells were *E. coli* strain DH10B, transformed with the pBAD plasmid (with ampicillin antibiotic resistance) encoding the WT HT NfsB with the Phe124 codon mutated to UAG (previously a stop codon) and the pDule plasmid (with tetracycline antibiotic resistance) encoding the aminoacyl- tRNA synthetase/$tRNA_{CUA}$ which will incorporate the appropriate unnatural amino acid when it recognises the stop codon (UAG). The E. coli cells were plated onto selective LB agar plates with antibiotics (Tetracycline 25 μg/ml & Ampicilin 100 μg/ml) and the plates were incubated for 24 hours at 37^0 C. A single colony from the agar plate was allowed to grow in 50 ml of LB media containing Tetracycline (25 μg/ml) and Ampicilin (100 μg/ml); this was placed in a shaking incubator at 37^0 C, and allowed to grow. Once it reached saturation, 2.5 ml of the culture was added to 500 ml of arabinose autoinduction media made up following the protocol in the paper Hammill *et al*, 2007, however with the following modifications:

The addition of the fluorine probe (tfmF) to the auto-induction media in step 8 of the protocol was replaced with 1 mM Napthylalanine. The optical growth curve for the E. coli with this medium had already been established by Martin Day, which was 23 hours until saturation. An optical density greater than 4 but less than 6 had to be obtained at 600 nm.

2.2.2 Over expression and purification of WT NfsB

The WT NfsB with the poly histidine tag was expressed and purified by Martin Day on a nickel-nitrilotriacetic acid column (NiNTA) (Pharmacia Biotech). WT NfsB was purified previously as in the paper by Lovering et al 2001.

2.2.3 Purification of NapA

Cultures were harvested by centrifuging at 7,500 g for 10 minutes; the centrifuge cooled the cultures to approximately 4 ^{0}C. The supernatant was removed and the pellet re-suspended in 30 ml of STE buffer (10 mM Tris pH 7.0, 100 mM NaCl, 1 mM EDTA). This was centrifuged at 7500 g for 30 minutes. The supernatant was removed again and re-suspended in 30 ml buffer (10 mM Sodium Phosphate pH 7.0, 300 mM NaCl, 10 mM Imidazole, 20 µM FMN, and a EDTA free protease inhibitor (Roche). The enzyme mixture was sonicated (using Ultrasonic Processor Heat Systems) at level 5 (275 W) with each pulse cycle lasting 15 seconds on and off for 20 seconds (for 3 minutes). The sonicated enzyme mixture was then centrifuged for 30 minutes at 35,000 g and the supernatant filtered through Acrodisc Syringe Filter with a 0.2 µM Super Membrane (from Pall Corporations).

Prior to column purification process, 200 µl of the protein solution was removed for purposes of SDS-PAGE in order to compare it to the protein after purification with the NiNTA column.

The NiNTA column (Pharmacia Biotech) was pre-equilibrated with 10 mM Imidazole, 300 mM NaCl, and 50 mM Sodium phosphate buffer; with a 100 mM NiNTA resin of 10 cm^3 volume. The filtered supernatant was loaded onto the column and the fractions collected. Other proteins within the solution passed through the column; the NapA was bound on the

column, as the poly-histidine tag bound with the nickel ions immobilized on the resin. NapA was eluted from the column with a concentration gradient of Imidazole (20 – 200 mM imidazole) in a buffer containing 50 mM sodium phosphate, 300 mM NaCl pH 8). The imidazole buffer was in a volume of 200 ml to which 20 μM of FMN was added. The flow rate of the column was 0.77 ml/minute, and 5.4 ml/fraction collected.

2.2.4 SDS-PAGE

The purity of WT NfsB, WT HT NfsB and WT CL NfsB was assessed via SDS-PAGE analysis. A Biorad Protean II apparatus was used with 12% w/v acrylamide and 0.32% bisacrylamide. The gels contained HyperPAGE, a protein molecular marker from Bioline and the method from Laemmli, 1970 was followed (Laemmli, 1970).

2.2.5 Small scale optimization of Recombinant Enterokinase cleavage of the poly histidine tag from WT HT NfsB

The optimized conditions for cleavage of the WT HT NfsB with the recombinant enterokinase (rEK) purchased from Novagen were determined by conducting a small scale optimization (SSO). The SSO consisted of mixing 93 μl of rEK cleavage buffer (500 mM NaCl, 200 Mm Tris-HCl, 20 Mm $CaCl_2$ at pH 7.4) with 2 μl WT HT NfsB (13 mg/ml) and 5 μl of diluted rEK (1/50 dilution). The rEK and WT HT NfsB ratio is 0.001 Units (rEK): 260 μg WT HT NfsB (in a 100 μl).

Furthermore following the same protocol, a small scale optimization with 0.0001 Unit of rEK : 260 μg WT HT NfsB (in a 100 μl) was conducted.

Subsequently, 10 μl samples were taken to which 5 μl protein loading dye and 1 μl of PMSF (a protease inhibitor) were added. The final concentration of the protein loading dye contained 50 mM Tris-HCl pH 6.8, 2% SDS, 10% glycerol, 1% β-mercaptoethanol, 12.5 mM EDTA and 0.02 % bromophenol blue. The samples were taken at 2-4 hour

intervals (upt0 48 hours) and were stored in a -20 freezer. The samples were assessed by SDS-PAGE stained with Coomassie brilliant blue R.

Once the optimum conditions were established, the poly histidine tag of the WT HT NfsB was cleaved using the following protocol:

1 ml of NfsB (13 mg/ml) was added to 0.5 µl rEK (final ratio was 13 mg/ml WT HT NfsB: 0.0005 Unit of rEK). The reaction was stopped at 24 hours using 1 µl of PMSF and 10 µl samples were taken (as for the optimization) from 0-24 hours. These were analysed by SDS-PAGE. Following the cleavage, the 1 ml of WT HT NfsB containing the rEK was loaded onto a NiNTA column in 10 mM Imidazole buffer containing 50 mM sodium phosphate, 300 mM NaCl pH 8 (Pharmacia Biotech). The ploy histidine tag from the WT HT NfsB bound to the nickel ions immobilized on the column and the WT CL NfsB eluted off the column. The fractions were collected and assessed by SDS-PAGE and Bradford assay.

2.2.6 Protein concentration of all NfsB

Protein concentrations of all NfsB samples were determined by Bradford assays, which were calibrated using bovine serum albumin (0-10 µg/ml).

2.2.7 NapA activity assays

The fractions of Napthylalanine NfsB with high protein concentration were pooled together and dialysed into 10 mM Potasium phosphate and 20 mM NaCl buffer pH 7.0 (overnight at 4 ^{0}C). The dialysed protein was then concentrated using Amicon Spin Concentrator (with a 10 kDa membrane) to 2 ml.

The activity assay was conducted to determine the specific activity of all the NfsB samples. The reaction consisted of 100 µM NADH and 200 µM menadione as the enzyme substrates, in the presence of 800 µM cytochrome C. The substrates were made up in 10

mM Tris-HCl pH 7.0 to a total volume of 1 ml in a quartz cuvette. The reaction was monitored by measuring the reduction of cytochrome C as each $2e^-$ reduction of menadione to menadiol, results in 2 single e^- reductions of cytochrome C. This was monitored at 550 nm using ε 21,100 M^{-1} cm^{-1}.

2.2.8 Steady state enzyme kinetics

This was performed with either menadione, or CB1954 as the variable substrate against a fixed concentration of NADH.

For menadione kinetic studies, the reaction was performed in 10 mM Tris-HCl (pH 7.0),with either 60 or 200 μM NADH, 1000 μM cytochrome C, 150 mM NaCl, 0.5 – 300 μM menadione in 4% DMSO (the DMSO was in 10 mM Tris pH 7). The reaction was initiated by adding approximately 10 nM of enzyme and the absorbance change measured at 550 nm on the Uvikon Spectrophotometer (Kontron instrument model 923). The molar absorbance for cytochrome c at 550 nm is ε 21,100 M^{-1} cm^{-1} , which was used to convert the absorbance change rate to change in concentration of product. The value is divided by 2 as for every mole of menadione reduced; 2 moles of cytochrome C are also reduced.

$$\frac{\text{Activity change in absorbance/s}^{-1}}{2{,}100} \div 2$$

For CB1954 kinetic studies, the same procedure was followed with the following alterations: The menadione in DMSO was replaced with CB1954 (0.141 – 3.525 μM) in N-methyl pyrrolidone and Poly ethylene glycol 300 (2: 7 v/v ratio) in a total volume of 50 μl. The reaction was initiated by adding approximately 10 nM of enzyme and measured at 420 nm on Uvikon Spectrophotometer (Kontron instrument model 923). This reaction monitored the reduction of CB1954 into its 2-/4- hydroxylamine derivative; the initial rate of CB1954 reduction per unit time was calculated. The 2-/4- hydroxylamine have significantly different UV spectra, but at 420 nm the extinction coefficients for both are exactly the same. Therefore, allowing the reaction to be monitored at one wavelength.

Furthermore at 420 nm the molar absorbance is ε 1,200 M^{-1} cm^{-1} , which was used to convert the absorbance change rate to change in concentration of product.

$$\frac{\text{Activity change in absorbance/s}^{-1}}{1{,}200}$$

2.2.9 Determination of the kinetic parameters

The initial rate v_i divided by the enzyme concentration [E] is plotted against the varying concentrations of menadione and CB1954. This was then fitted to the following single substrate Michaelis Menten equation:

$$\frac{Vi}{[E]} = \frac{K_{catapp}[A]}{K_{mAapp} + [A]}$$

[E] = Enzyme concentration

V_i = Initial rate of reduction

[A] = Concentration of the variable substrate

k_{catapp} = Apparant k_{cat}

K_{mAapp} = Apparant K_m for [A] at the concentration of [B]

Finally [A] is the variable substrate (CB1954 or menadione) and [B] is the constant substrate (NADH). Furthermore k_{cat}/K_m was accurately estimated using the following equation, as the apparent values k_{cat} and K_m depend on the concentration of the second fixed substrate (NADH).

$$\frac{v_i}{[E]} = \frac{k_{catapp}[A]}{\left(\frac{k_{cat}}{K_{mA}}\right)}$$

Figure 2.2.9.1: Single substrate Michaelis Menten equation for the determination of k_{cat}/K_m

The data was analysed by non-linear regression using SigmaPlot 11 and the P and t values were calculated.

2.2.10 Crystallization

The proteins used for crystallization were WT HT NfsB and WT CL NfsB. The crystallization trays were set up using both a sitting and hanging drop vapour diffusion method.

The tray used for the hanging drop vapour method was a 24 well tray from Molecular Dimensions Limited and all crystals were allowed to grow in 18^0 C. The conditions tried for the hanging drop vapour method were as the follows; the mother liquor was made up to a total of 1 ml, which consisted of PEG 4000 (10-20 %), Sodium acetate (10 mM pH 4.6), Nicotinic acid (15 mM pH 4.6), ethylene glycol (0-15 %) and finally filtered distilled water (to make up to 1 ml). The trays used for the sitting drop vapour method was a 24 well tray from Emerald Biosystem and all crystals were allowed to grow in 18^0 C. The conditions tried for the sitting drop vapour method were as follows; the mother liquor was also made up to a total volume of 1 ml, which consisted of PEG 8000 (15-30 %), either sodium acetate (0.6-10 Mm pH 4.6) or potassium phosphate (15-45 mM pH 7.0), ethylene glycol (0-15 %), additive (Na Maleate 50 mM). Finally filtered distilled water (to make up to 1 ml). Finally the drops of protein used for both the cover slip (hanging drop) and on the sitting wells (sitting drop) were 2 µl.

2.2.11 Analysis of crystal structures and images

Diffraction data was collected, for the WT CL NfsB on I04 at Diamond Light Source Ltd, Diamond House, Oxfordshire., UK by Martin Day; however these were not solved.

3. Results

3.1 Expression and purification of WT NfsB, WT HT NfsB, WT CL NfsB and NapA

Three different wild type NfsB proteins were investigated: Wild type NfsB which had never been his-tagged, wild type his-tagged NfsB which had been his-tagged and wild type NfsB with the his-tag cleaved off by using a recombinant enterokinase. In this project the Wild type NfsB never his-tagged is referred to as WT NfsB. The wild type with the his-tag is referred to as WT HT NfsB and finally the wild type with the cleaved his-tag as WT CL NfsB. The single unnatural amino acid mutant napthylalanine at position 124 of NfsB is referred to as NapA. The vector used for incorporating the histidine tag into the protein is pTrcHisA, which added an NH_2 terminal his6-tag, in order to allow affinity purification.

The WT NfsB with the poly histidine tag was expressed and purified by Martin Day on a nickel-nitrilotriacetic acid column (NiNTA) (Pharmacia Biotech). WT NfsB was purified previously as in the paper by Lovering *et al* 2001. A Bradford assay was conducted to determine the protein concentration of the WT NfsB and WT HT NfsB, followed by SDS-PAGE to assess purity and expression of protein. Furthermore 1 ml of the WT HT NfsB was cleaved with recombinant enterokinase to remove the his-tag and produce the WT CL NfsB, which was purified using a NiNTA column and followed by a Bradford assay to determine the protein concentration. Finally a SDS-PAGE was conducted for assessing the purity of the sample and also whether the his-tag was removed successfully.

The NapA was expressed as in the paper hammill *et al*, 2007 (refer to method 2.2.1) and purified using a NiNTA column, followed by a Bradford assay and SDS-PAGE.

The WT HT NfsB has a known molecular weight of around 23 kDa and the SDS-PAGE gel illustrated that the NfsB protein was present and quite pure in all WT NfsB, WT HT NfsB and WT CL NfsB samples. However the NapA was significantly impure and the NfsB band was very faint. In addition the NfsB band which had appeared for the NapA was significantly lower than the normal molecular weight expected for NfsB. Furthermore, once the his-tag had been removed, the molecular weight of the WT HT NfsB should decrease and produce a slight lower (by 1-2 kDa) NfsB band (figure 3.1 1).

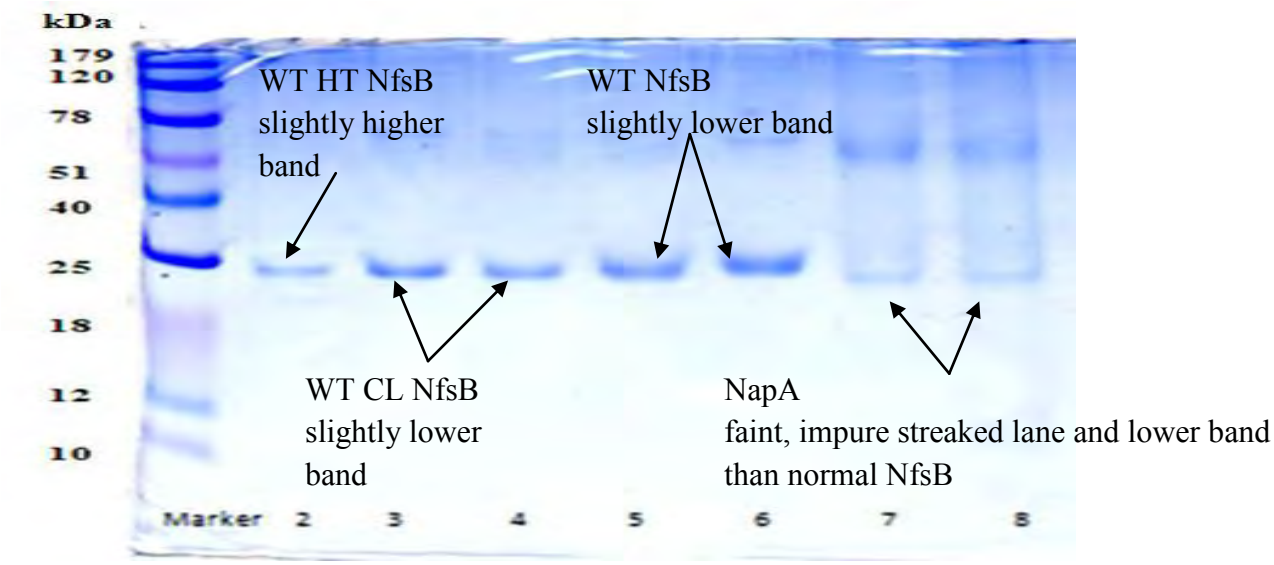

Figure 3.1.1: A 12% w/v acrylamide and 0.32% bisacrylamide gel for the purity of the NfsB samples.

The molecular marker from bioline is on lane 1. The WT HT NfsB, is on lane 2 with a 1/20 dilution. The WT CL is on lanes 3 (in acetate buffer) and on lane 4 (in phosphate buffer), both diluted 1/5. Lanes 5 and 6 contain other purified WT NfsB samples. The undiluted NapA is on lanes 7 and 8.

3.2 Cleavage of the poly histidine tag from WT HT NfsB with recombinant enterokinase

Prior to cleaving the his-tag off the WT HT NfsB with the recombinant enterokinase (rEK), the optimized incubation time and rEK concentration were established by conducting a small scale optimization to determine optimum conditions, followed by a large scale to remove the his-tag from the WT HT NfsB. Furthermore the optimized conditions for digestion of the NfsB with the recombinant enterokinase were established and analysed using SDS-PAGE, where the concentration and incubation time of the rEK were varied.

The gel on figure 3.2.1 contains the rEK at 0.001 Units and 260 µg/ml WT HT NfsB, where samples were taken from zero to 48 hours. The gel shows significant secondary digestion of the protein as many lower bands have appeared on the gel confirming further unwanted proteolysis at secondary sites. However a band has appeared below the NfsB band at 23 kDa, confirming the his-tag was removed from the WT HT NfsB; although before 4 hours there is no digestion and after 28 hours the digestion stops (figure 3.2.1).

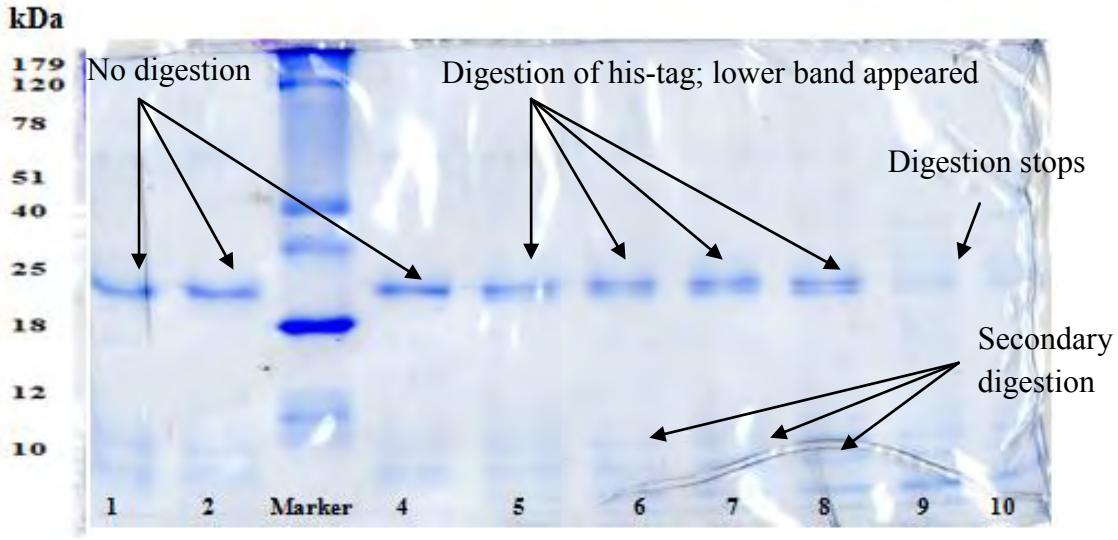

Figure 3.2.1: A 12% w/v acrylamide and 0.32% bisacrylamide gel, for the optimization of rEK digestion of WT HT NfsB with high rEK concentration.

Digestion times with rEK:

Lane1: zero hours, lane2: 2 hours, lane3: Marker (Bioline), lane4: 4 hours, lane5: 22.5 hours, lane6: 24.5 hours, lane7: 26.5, lane8: 28.5, lane9: 46 hours, lane10: 48 hours

The concentration of the rEK was too high which caused unwanted proteolysis; therefore another optimization was carried as before however only 0.0001 Units of rEK was used in a ratio with 260 µg/ml WT HT NfsB. The samples were taken as before and assessed by SDS-PAGE (figure 3.2.2). The gel illustrates that there wasn't enough rEK present to fully digest the WT HT NfsB sample, however although the bands are very faint, the digestion of the his-tag can still be seen after 4 hours and in an excess of 22 hours the digestion stops.

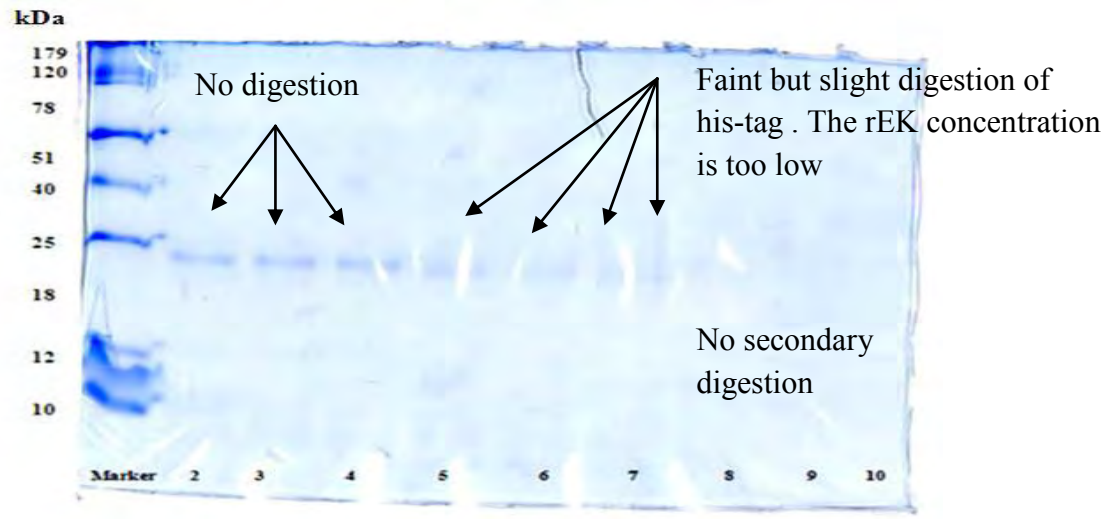

Figure 3.2.2: A 12% w/v acrylamide and 0.32% bisacrylamide gel, for the optimization of rEK digestion of WT HT NfsB with low rEK concentration.

Digestion times with rEK:

Lane one: molecular Marker (Bioline), lane2: zero hour, lane3: 2 hours, lane4: 4 hours, lane5: 20 hours, lane6: 22 hour, lane7: 24 hours, lane8: 43 hours, lane9: 46 hours

From these optimizations, the optimum conditions were determined, which was an incubation time for at least 22 hours (to ensure the his-tag is removed from all NfsB) and a

concentration of 0.0005 Units for the rEK (this is an average of the two optimizations as one was too high and the other too low). By using these conditions 1 ml of the WT HT NfsB was incubated with 0.0005 Units of rEK for 24 hours and the reaction was stopped with PMSF. As for the optimization, samples were taken in order to monitor the digestion of the his-tag by SDS-PAGE (figure 3.2.3). This showed that the his-tag was successfully digested as a lower band appeared below the NfsB band, confirming digestion.

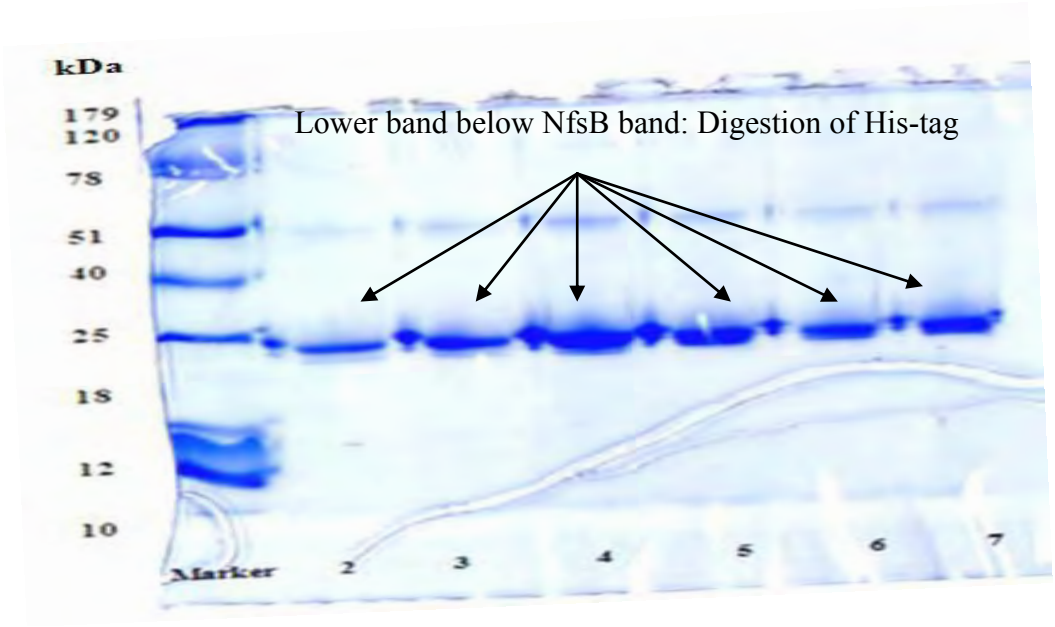

Figure 3.2 .3: A 12% w/v acrylamide and 0.32% bisacrylamide gel of the digestion of the WT HT NfsB.

Digestion times with Rek:

In lane one is the Marker (Bioline), lane 2: zero hours, lane 3: 2 hours, lane 4: 4 hours, lane 5: 20 hours, lane 6: 21 hours, lane 7: 24 hours.

Finally the digested wild type NfsB protein was loaded onto a NiNTA column, which was subsequently followed by a SDS-PAGE of the fractions collected (figure 3.2.4). This illustrated that the his-tag had been successfully cleaved as the lower histidine band was observed on the SDS-PAGE. However there were still two bands on the gel following purification with the NiNTA column. This indicates that not all of the WT HT NfsB protein had been cleaved successfully (figure 3.2.4/5).

Both figures illustrate fractions of WT CL NfsB after purification with a NiNTA column. There are still two bands which conclude that the his-tag was not removed from all of the NfsB protein within the WT CL NfsB samples.

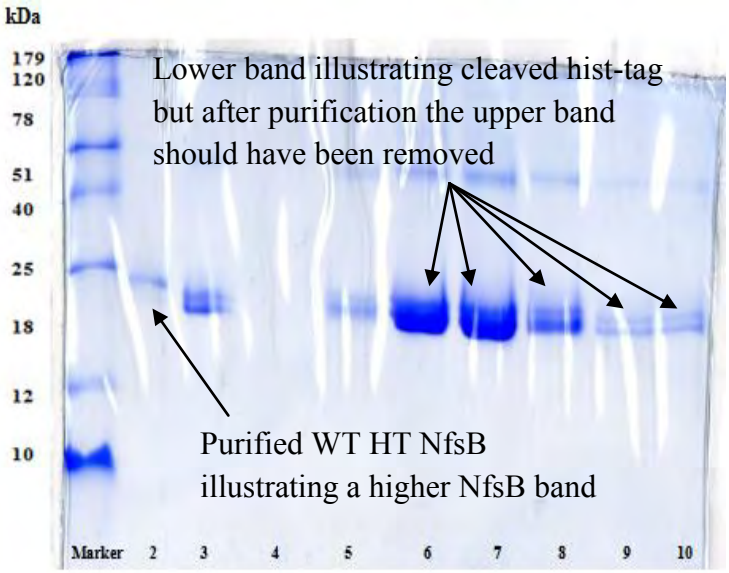

Figure 3.2.4: A 12% w/v acrylamide and 0.32% bisacrylamide gel of the WT CL NfsB Lane1: Marker, Lane 2: Purified NfsB with His-tag, Lane 3: NfsB + rEk at zero hours, Lane 4: fraction 4, Lane 5: fraction 5, Lane 6: fraction 6, Lane 7: fraction7, Lane 8: fraction 8, Lane 9 and 10: fraction 9

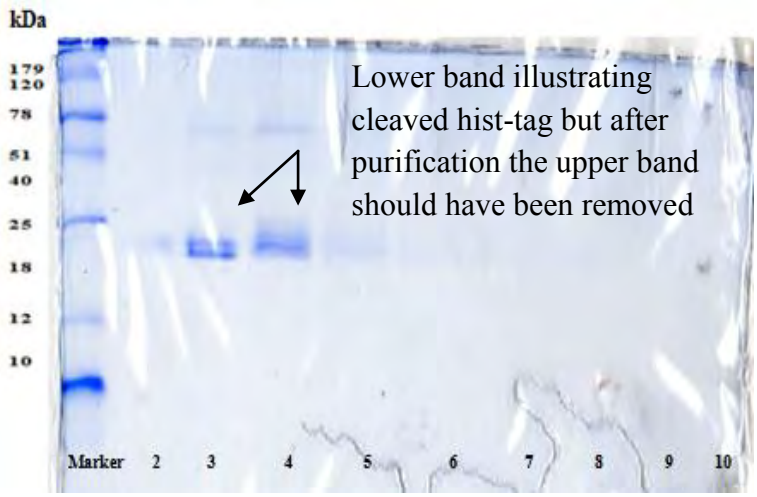

Figure 3.2.5: A 12% w/v acrylamide and 0.32% bisacrylamide gel of the WT CL NfsB

Lane1: Marker, Lane 2: Purified NfsB with His-tag, Lane 3: NfsB + rEK at zero hours, lane 4: fraction 10, Lane 5: fraction 12, Lane 6: fraction 13, Lane 7: fraction 14, Lane 8: fraction 15, Lane 9: fraction 16, Lane 10: fraction 17

3.3The steady state kinetics of all NfsB proteins for CB1954; the effects of the poly histidine tag on the rate of CB1954 reduction

Steady state kinetics was conducted for the three NfsB proteins in order to assess whether the his-tag had an effect on the rate of CB1954 reduction by the protein in the presence of cytochrome C. For each of the kinetic assay, a constant NADH concentration of either 60 μM or 200 μM was used and a varied concentration of the pro-drug CB1954 (141-3525 μM).

This reaction monitored the reduction of CB1954 into its 2-/4- hydroxylamine derivative; the initial rate of CB1954 reduction per unit time was calculated at 420 nm ε 1,200 M^{-1} cm^{-1} , which was used to convert the absorbance change rate to change in concentration of product. Furthermore the k_{cat}/K_m was estimated from the fit of each dataset to the Michaelis Menten equation on figure 2.2.9 1. (The kinetic parameter tables can be found in Appendix I section 1).

Finally, NADH is required as the reducing agent to reduce FMN which will subsequently reduce the substrate (CB1954), therefore the more NADH present in the reaction, the higher the K_m value as well as the rate of reduction.

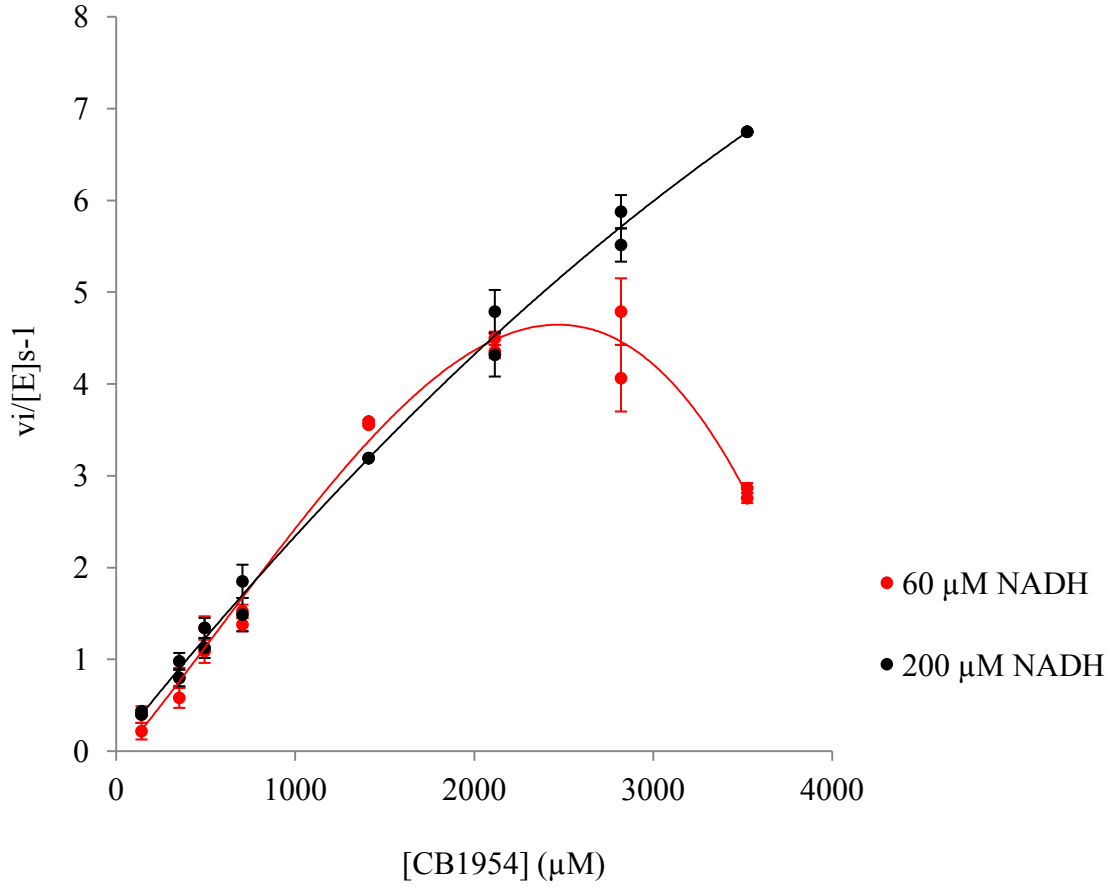

Figure 3.3.1: The rate of CB1954 reduction by the WT NfsB at fixed 60 µM (red) and 200 µM (black) NADH concentrations, fitted to the equation on figure 2.2.9 1

This plots initial rate of CB1954 reduction by WT NfsB (v_i) divided by the enzyme concentration [E] using 60 or 200 µM NADH (as the cofactor) at a range of CB1954 concentrations. The lower concentration of NADH (red 60 µM), illustrates the line curving (fitted to a hyperbola), as K_m is reached. However there is substrate inhibition as high concentration levels of CB1954 are used. Furthermore with the higher NADH concentration (black 200 µM) the line is linear which indicates that K_m is very high and that the line shown is presenting the initial rate of reaction of the hyperbola.

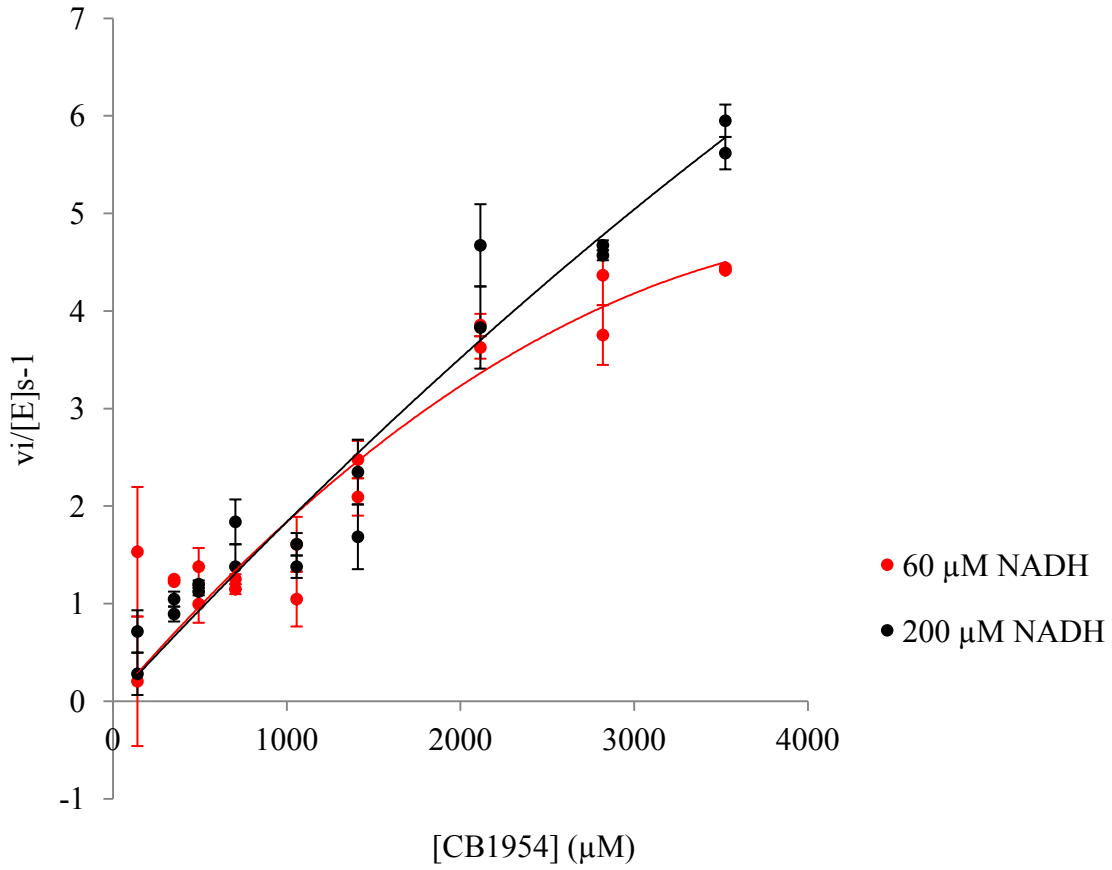

Figure 3.3.2: The rate of CB1954 reduction by the WT HT NfsB at fixed 60 µM (red) and 200 µM (black) NADH concentrations, fitted to the equation on figure 2.2.9.1

This plots initial rate of CB1954 reduction by WT HT NfsB (v_i) divided by the enzyme concentration [E] using 60 or 200 µM NADH (as the cofactor) at a range of CB1954 concentrations.

The lower concentration of NADH (red 60 µM), illustrates a linear line, however at 3525 µM CB1954 it begins to curve. The higher NADH concentration (black 200 µM) has a linear rate of reduction which indicates that K_m is very high and that the line shown is presenting the initial rate of reaction of the hyperbola.

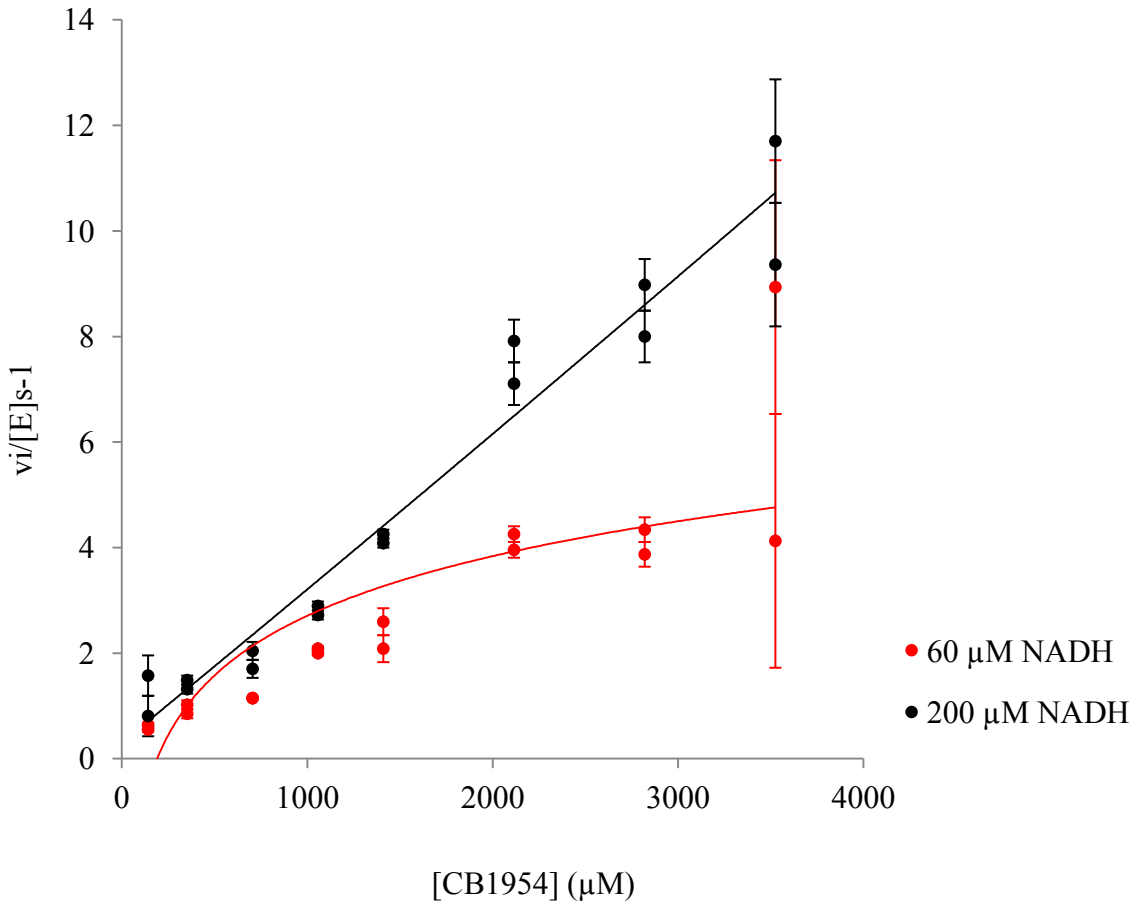

Figure 3.3.3: The rate of CB1954 reduction by the WT CL NfsB at fixed 60 µM (red) and 200 µM (black) NADH concentrations, fitted to the equation on figure 2.2.9.1

This plots initial rate of CB1954 reduction by WT CL NfsB (v_i) divided by the enzyme concentration [E] using 60 or 200 µM NADH (as the cofactor) at a range of CB1954 concentrations.

The lower concentration of NADH (red 60 µM), illustrates the line beginning to curve and thus beginning to reach K_m , however the higher NADH concentration (black 200 µM) illustrate a linear line, which indicates that K_m is very high and that the line shown is presenting the initial rate of reaction of the hyperbola.

3.4 Statistical analysis of the poly-histidine tag's effect on the rate of CB1954 reduction

From observing the figures 3.3.1-3, it can be observed that the addition of the his-tag slightly decreases the rate of CB1954 reduction by the NfsB protein. However in order to determine this accurately a Mann-Whitney U Rank Sum Test was conducted as the sample sizes were not the same and the normality test failed. This concluded that when comparing the values observed for WT NfsB and WT HT NfsB for the rate of reduction of the pro-drug, there was no statistical significant difference (P= 0.986 for 60 μM NADH and P= 0.617 for 200 μM NADH).

Furthermore once cleaved there was no statistical significance observed when comparing to the values observed for WT NfsB (P= 0.836 for 60 μM NADH and P= 0.127 for 200 μM NADH).

3.5 The steady state kinetics of WT NfsB, WT HT NfsB, WT CL NfsB for Menadione to determine the effects of the poly histidine tag on the rate of substrate reduction

Steady state kinetics was conducted for the three NfsB proteins in order to assess whether the his-tag had an effect on the rate of menadione reduction by the protein in the presence of cytochrome C. For each of the kinetic assays, a constant NADH concentration of either 60 μM or 200 μM was used and the concentration of the substrate (menadione) was varied (0.5-300 μM). The reaction was monitored by measuring the reduction of cytochrome C as each $2e^-$ reduction of menadione to menadiol, results in 2 single e^- reductions of cytochrome C. This was monitored at 550 nm using ε 21,100 M^{-1} cm^{-1}. Furthermore the k_{cat}/K_m were estimated from the fit of each dataset to the Michaelis Menten equation on figure 2.2.9.1. (The kinetic parameter tables can be found in Appendix I section 2).

Finally, NADH is required as the reducing agent to reduce FMN which will subsequently reduce the substrate (menadione), therefore the more NADH present in the reaction, the higher the K_m value as well as the rate of reduction

For all the graphs illustrating the rate of Menadione reduction by the three NfsB proteins:

This plots initial rate of menadione reduction by NfsB (v_i) divided by the enzyme concentration [E] using 60 or 200 μM NADH (as the cofactor) at a range of menadione concentrations (0.5-300 μM)

Both the higher and lower concentration of NADH used for the rate of menadione reduction, illustrate a good fit to the hyperbola curve and thus K_m has been reached; menadione is a better substrate than CB1954 for all NfsB proteins.

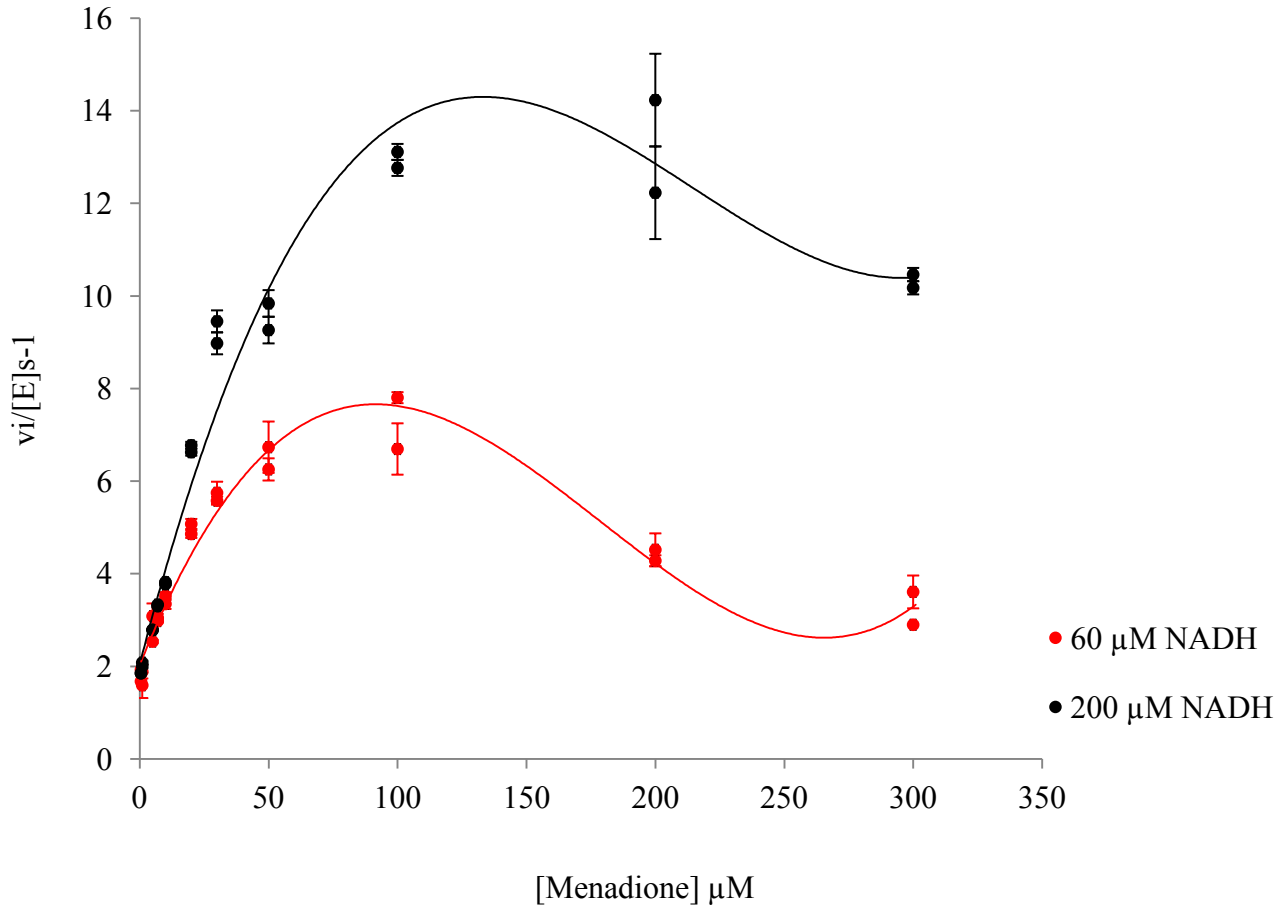

Figure 3.5.1: The rate of Menadione reduction by the WT NfsB at fixed 60 µM (red) and 200 µM (black) NADH concentrations, fitted to the equation on figure 2.2.9.1

This plots initial rate of menadione reduction by WT NfsB (v_i) divided by the enzyme concentration [E] using 60 or 200 µM NADH (as the cofactor) at a range of menadione concentrations.

Both the concentration of NADH (red 60 and black 200 µM), illustrates the product/substrate inhibition of menadione reduction.

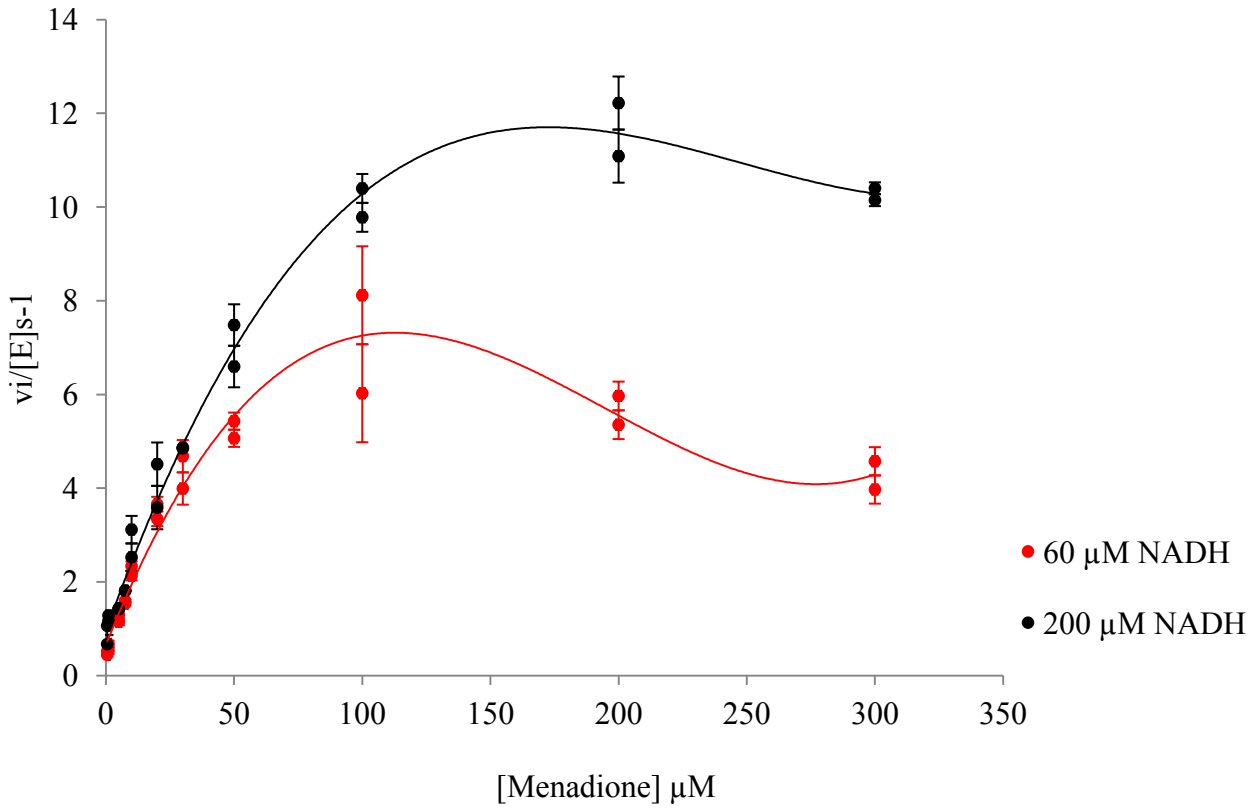

Figure 3.5.2: The rate of Menadione reduction by the WT HT NfsB at fixed 60 µM (red) and 200 µM (black) NADH concentrations, fitted to the equation on figure 2.2.9.1

This plots initial rate of menadione reduction by WT HT NfsB (v_i) divided by the enzyme concentration [E] using 60 or 200 µM NADH (as the cofactor) at a range of menadione concentrations.

Both the concentration of NADH (red 60 and black 200 µM), illustrates the product/substrate inhibition of menadione reduction.

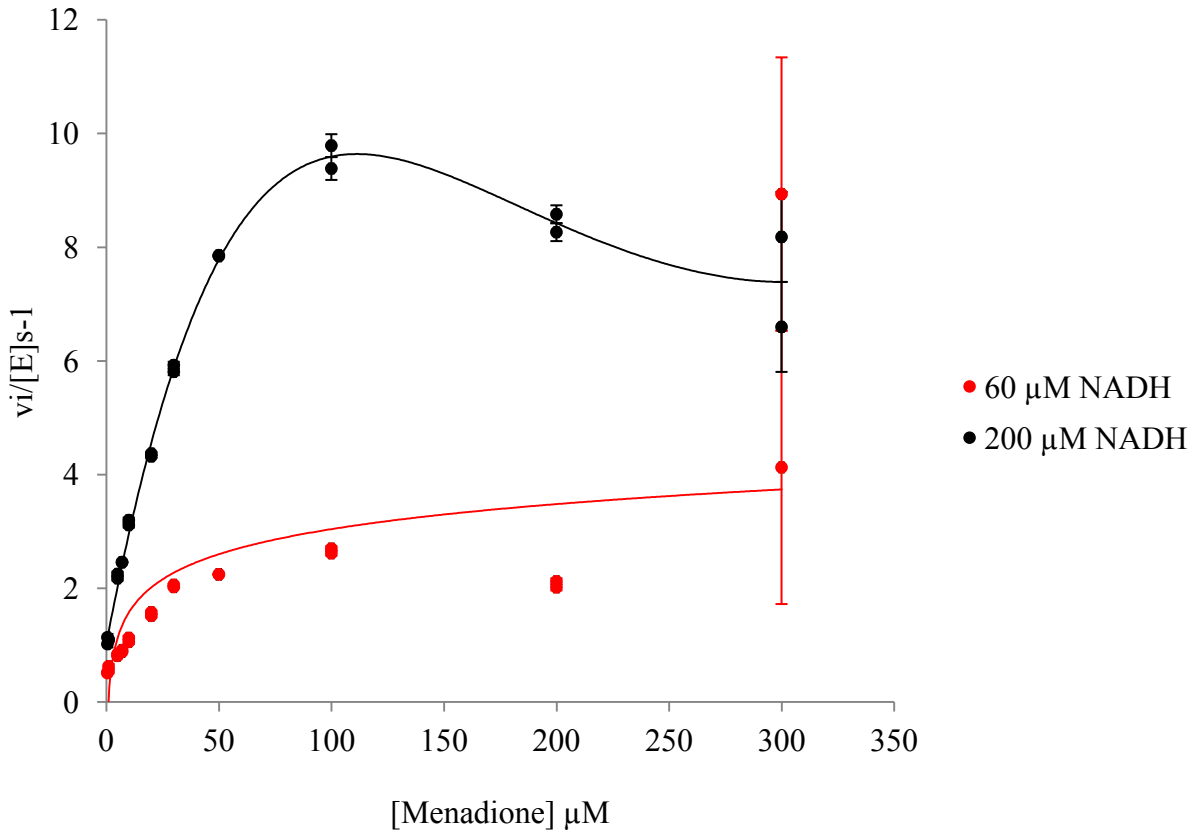

Figure 3.5.3: The rate of Menadione reduction by the WT CL NfsB at fixed 60 µM (red) and 200 µM (black) NADH concentrations fitted to the equation on figure 2.2.9.1

This plots initial rate of menadione reduction by WT CL NfsB (v_i) divided by the enzyme concentration [E] using 60 or 200 µM NADH (as the cofactor) at a range of menadione concentrations.

The higher concentration of NADH (black 200 µM), illustrates the product/substrate inhibition of menadione reduction. However due to the standard error being very high for the last two values recorded for the lower concentration of NADH (red 60 µM), the substrate inhibition cannot be observed.

3.6 Statistical analysis of the poly-histidine tag's effect on the rate of Menadione reduction

From observing the figures 3.5.1-3, it can be observed that the addition of the his-tag slightly decreases the rate of menadione reduction by the NfsB protein. However in order to determine this accurately a Two tailed T-Test was conducted.

This concluded that when comparing the values observed for WT NfsB and WT HT NfsB for the rate of reduction of the pro-drug, there was no statistical significant difference ($P= 0.202$ for 60 μM NADH and $P= 0.098$ for 200 μM NADH).

However once cleaved there a statistical significance observed when comparing to WT NfsB, and the difference in the median values between the two groups is greater than that which would be expected by chance ($P= <0.001$ for 60 and 200 μM NADH).

3.7 The steady state kinetics of NapA for the pro-drug CB1954

Steady state kinetics was conducted for the NapA with the pro-drug CB1954, in order to assess whether NapA has better kinetics with CB1954 in comparison to the WT NfsB proteins. For the kinetic assay, a constant NADH concentration of either 60 μM or 200 μM was used and the concentration of the substrate (CB1954) was varied (141-3525 μM).

The reaction monitored the reduction of CB1954 into its 2-/4- hydroxylamine derivative; the initial rate of CB1954 reduction per unit time was calculated at 420 nm ε 1,200 M^{-1} cm^{-1} , which was used to convert the absorbance change rate to change in concentration of product. Furthermore the k_{cat}/K_m was estimated from the fit of each dataset to the Michaelis Menten equation on figure 2.2.9 1. (The kinetic parameter tables can be found in Appendix I section 3).

Finally NADH is required as the reducing agent to reduce FMN which will subsequently reduce the substrate CB1954, therefore the more NADH present in the reaction, the higher the K_m value as well as the rate of reduction.

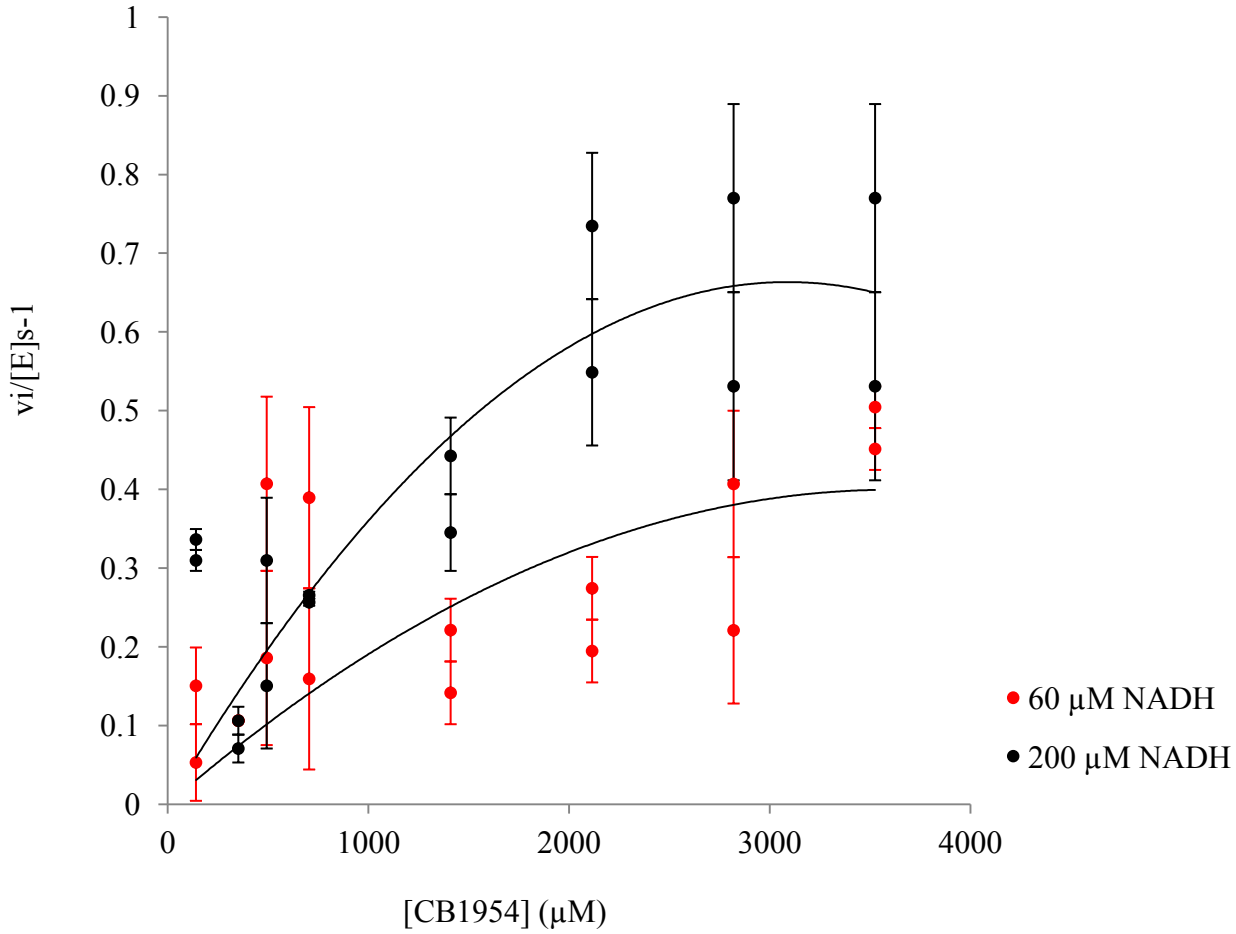

Figure 3.7 .1 : The rate of CB1954 reduction by the NapA at fixed 60 µM (black) and 200 µM (red) NADH concentrations, fitted to the equation on figure 2.2.9 1.

This plots initial rate of CB1954 readuction by NapA (v_i) divided by the enzyme concentration [E] using 60 or 200 µM NADH (as the cofactor) at a range of CB1954 concentrations.

The rate of CB1954 reduction is very significantly low. However the NapA was not pure and there wasn't much of the protein present in the sample, hence the high standard error each recording.

3.8 The steady state kinetics of NapA for Menadione

Steady state kinetics was conducted for the NapA with the menadione, in order to assess whether NapA has improved kinetics with menadione in comparison with CB1954. For the kinetic assay, a constant NADH concentration of either 60 μM or 200 μM was used and the concentration of the substrate (menadione) was varied (0.5-100 μM). The reaction was monitored by measuring the reduction of cytochrome C as each $2e^-$ reduction of menadione to menadiol, results in 2 single e^- reductions of cytochrome C. This was monitored at 550 nm using ε 21,100 M^{-1} cm^{-1}. Furthermore the k_{cat}/K_m were estimated from the fit of each dataset to the Michaelis Menten equation on figure 2.2.9.1 (The kinetic parameter tables can be found in Appendix I section 4). NADH is required as the reducing agent to reduce FMN which will subsequently reduce the substrate CB1954, therefore the more NADH present in the reaction, the higher the K_m value as well as the rate of reduction.

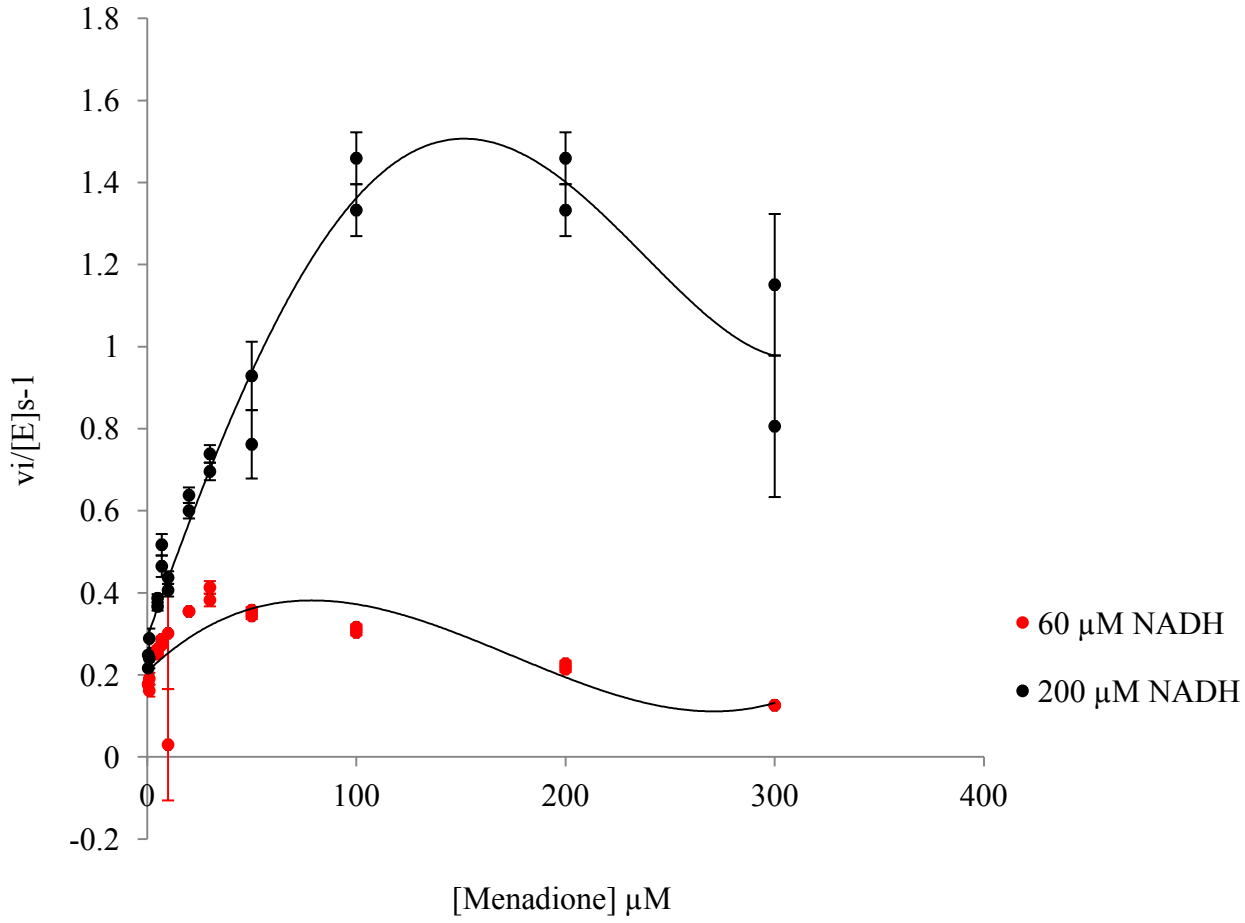

Figure 3.8.1: The rate of Menadione reduction by the single amino acid mutant Napthylalanine NfsB at fixed 60 µM (red) and 200 µM (black) NADH concentrations, fitted to the Michaelis Menten equation (figure 2.2.9.1)

This plots initial rate of menadione reduction by NapA (v_i) divided by the enzyme concentration [E] using 60 or 200 µM NADH (as the cofactor) at a range of menadione concentrations.

The rate of menadione reduction is significantly higher than the rate of CB1954 reduction by NapA.

3.9 Statistical analysis comparing the rates of Menadione and CB1954 reduction by NapA

From observing the figures 3.6.1 and 3.7.1, it can be observed that the rate of menadione reduction is higher than that of CB1954 by NapA. In order to determine this accurately a Mann-Whitney U Rank Sum Test was conducted as the sample sizes were not the same and the normality test failed. This concluded that at 60 μM NADH there is no statistically significant difference between the rates of menadione and CB1954 by NapA (P= 0.843).

However at 200 μM NADH there was a statistically significant difference observed concluding that the difference in median values observed for the rates of menadione and CB1954 by NapA is greater than that which would be expected by chance (P=0.032).

4. Crystal structures and diffraction pattern

Crystal trays were set up using the His-tagged and cleaved wild type NfsB via the sitting and hanging drop vapour methods and the crystals were allowed to grow in a crystallization room at 18 ^{0}C. The His-tagged NfsB did not crystallize through either method; however the cleaved wild type NfsB crystallized using both methods. The crystal which formed in the sitting drop method was in mother liquor consisting of 15 mM Nicotinic acid, 10 mM Sodium acetate, 20 % of PEG 4000, 5 % ethylene glycol and made up to 1 ml with filtered distilled water (figure 4.1).

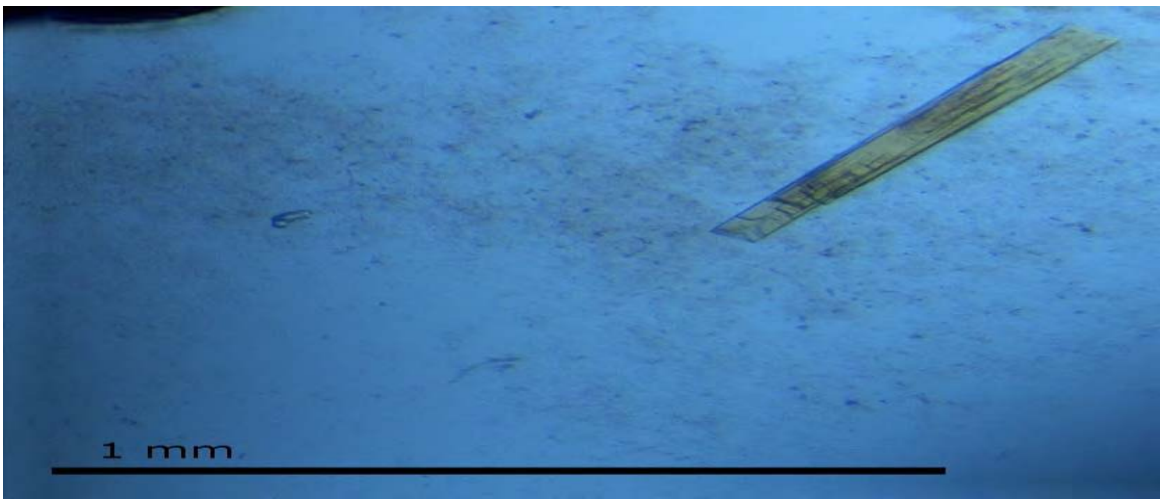

Figure 4.1: The cleaved wild type NfsB crystal in acetate buffer (hanging drop vapour method)

This is a crystal of the wild type NfsB; however the crystal appears to be twined where two or more separate crystals are sharing the same crystal lattice points; the image illustrates an intergrowth of several crystals.

The cleaved wild type NfsB crystal which formed using the sitting drop methods was in a mother liquor consisting of 10 mM Nicotinic acid, 10 mM Sodium acetate, 22 % PEG 8000, 15 % ethylene glycol, 50 mM Sodium Maleate and filtered distilled water made up to 1 ml.

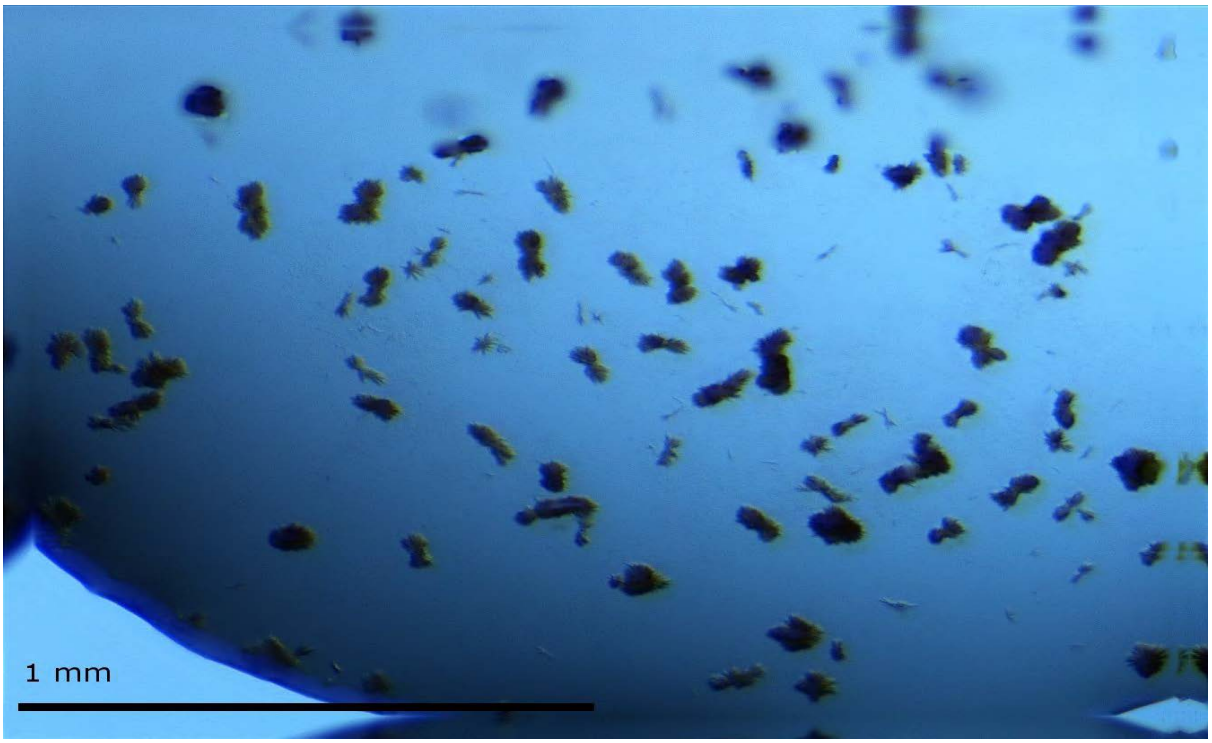

Figure 4.2: The crystals formed by cleaved wild type NfsB in acetate buffer (sitting drop vapour method). The crystals are clustered and did not grow efficiently.

Furthermore only the crystal from figure 4.1 diffracted, however due to the intergrowth of lattices the diffraction pattern could not be solved.

Figure 4.3: The diffraction pattern of the cleaved wild type NfsB crystal in acetate buffer (hanging drop vapour method).

5. Discussion

The main aims in this study were to assess the following:

a) Whether menadione is a better substrate for NapA than CB1954
b) Whether NapA shows an improvement for substrate reduction in comparison to the WT NfsB
c) The effect of the poly histidine tag on the rate of substrate reduction by the three NfsB proteins.

In this project the Wild type NfsB never his-taggded is referred to as WT NfsB. The wild type with the his-tag is referred to as WT HT NfsB and finally the wild type with the cleaved his-tag as WT CL NfsB. The single unnatural amino acid mutant napthylalanine at position 124 of NfsB is referred to as NapA. However the NapA is also his-tagged as it is simply the WT HT NfsB protein but with the unnatural amino acid napthylalanine inserted at position 124.

The concentration of NapA protein obtained was significantly low and impure (figure 3.1.1). In addition there was a low molecular weight band observed on the SDS-PAGE, which was potentially due to truncated proteins; there were some proteins made which terminated at the stop codon (UAG). This would then translate on the gel as a high mobility band; however this can be resolved by using a C terminal affinity tag, which will only purify the full length proteins as the C terminal is at the end of the protein; therefore any truncated proteins will be removed (Hammill *et al*, 2007). Furthermore in order to ensure that the band obtained for the NapA on the SDS-PAGE is actually the protein, an inhibitor such as Dicoumarol can be used which will reduce the rate of substrate reduction

by NapA. If the rate is not reduced significantly, then the protein present in the sample is not NapA as this would have been inhibited (Rau and Stolz, 2003).

The specificity constant (k_{cat}/K_m) of NapA with the pro-drug, measured how efficiently NapA reduced the substrate. As the results showed that rate of CB1954 reduction by NapA was very very low, the k_{cat}/K_m were also very low (figure 5.1: at 60 μM NADH= 0.0008 ± 0.0004 and at 200 μM NADH= 0.0005 ± 0.0002). The complete kinetic parameter table can be found in Appendix I section 3.

Nevertheless, the specificity constant for NapA with menadione was considerably higher than that with CB1954. In addition the Mann-Whitney U Rank Sum Test, which concluded that at 200 μM NADH there was a statistically significant difference observed concluding that the difference in median values observed for the rates of menadione and CB1954 by NapA is greater than that which would be expected by chance (P=0.032). However at 60 μM NADH there is no statistically significant difference between the rates of menadione and CB1954 by NapA (P= 0.843). Moving on, as the NapA was not pure and may have contained other proteins, the UV spectrum test should be conducted (and the steady state enzyme kinetics repeated. This would allow verification of the results and viability of the concluded theory that menadione is a better substrate for NapA.

Although the pro-drug is not a natural substrate for the enzyme, studies have shown that NapA has a higher specificity constant in comparison to the WT NfsB (Jackson *et al*, 2006; Grove *et al*, 2003). However in this project NapA has a lower specificity constant in comparison to the WT NfsB, which was due to the low expression of NapA in this study and the impurity within the sample.

Another explanation could be that there wasn't enough FMN bound to the enzyme and thus NapA could not reduce the substrate efficiently. To assess the level of bound FMN and NapA, a UV spectrum could be conducted at 280, 355 and 455 nm. The NapA and FMN, which can be bound or unbound, will give a peak at 280 nm, the FMN (unbound) will give a peak at 355 and finally the NapA (unbound) will give a peak at 455 nm. A normal and expected result would show a 4 x difference in the peaks observed at 280 and 355 nm. Finally by subtracting the values obtained for the unbound NapA (455nm) and unbound FMN (355 nm) from the peak which contains both bound/unbound FMN and NapA, the level of bound FMN can be determined (Hammill *et al*, 2007).

The SDS-PAGE illustrated that the WT NfsB, WT HT NfsB and WT CL NfsB were quite pure, however the main issue lies within whether the his-tag was successfully cleaved off the WT HT NfsB. The purified digested WT HT NfsB was assessed by SDS-PAGE and illustrated that only part of the protein had been cleaved. This could have been due to (i) that the protein was actually not digested enough; however (ii) it was more likely due to the column which did not remove the digested his-tag successfully (figure 3.2.4). This could be assessed by loading the digested sample on another NiNTA column and observing the fractions on a SDS-PAGE, in order to be certain of the results.

Moreover, the specificity constant of the three wild type proteins for the reduction of CB1954 were all quite low as the pro-drug is not a natural substrate for the NfsB (figures 5.1a/b).

The his-tag had a negative effect on the specificity constant, for example at 60 μM NADH, the k_{cat}/K_m value observed for the WT NfsB (0.0041) is double the k_{cat}/K_m value for WT HT NfsB (0.0022). Also once the his-tag is cleaved of the WT HT NfsB, the specificity constant increases, but doesn't fully regain the full efficiency of reducing the substrate (0.0026). A Similar pattern of results is also observed for 200 μM NADH (figures 5.1a/b).

The vector used for incorporating the histidine tag into the protein is pTrcHisA, which added a NH terminal his6-tag, in order to allow affinity purification. However the active site for the NfsB and sites which can interfere with the binding of the FMN cofactor and substrates is located near the N-terminal of the NfsB protein. Therefore the poly histidine tag could be interfering with the interaction between the substrate and the FMN cofactor. This would then result in a lower specificity constant observed for the WT HT NfsB in comparison to the WT NfsB (Rau and Stolz, 2003; Grove *et al*, 2003; Jackson *et al*, 2006). Furthermore, there is a slight increase in the specificity constant once the his-tag has been removed, however the value does not return to its original level. This is because the his-tag on the pTrcHisA vector is located between the bases 425-442, and the recombinant enterokinase cleaves the his-tag at the bases 491-505. Therefore there are several bases of the histidine tag left on the NfsB and some extra bases of the vector are cut. As the complete histidine tag is not removed, it is expected that the specificity constant will not be restored to the original level (Rau and Stolz, 2003).

To conclude whether there is an actual negative effect caused by the addition or the cleavage of the histidine tag, a Mann-Whitney U Rank A Sum Test was conducted, which concluded that in the case of NfsB reduction of CB1954 the histidine tag had no significant effect ($P > 0.05$). However in the case of menadione reduction, once cleaved there was a statistical significance observed when comparing to WT NfsB, and the difference in the

median values between the two groups is greater than that which would be expected by chance (P= <0.001 for 60 and 200 μM NADH).

Finally, although there is no statistical significance observed, in order to investigate why there is a higher specificity constant for the rate of menadione reduction with all the NfsB proteins a crystal structure of menadione with NfsB is essential. As this would determine how menadione interacts with the FMN cofactor, and the differences in this interaction which causes it to be a better substrate than CB1954.

The twinned crystal which was obtained from the WT CL NfsB could not be solved although it did diffract. This was due to several crystals sharing the same lattice points and thus causing an intergrowth of crystals. Generally in order to solve the diffraction pattern of a crystal, twinning can be a major problem as the different patterns of reflection from the crystal (as it is rotated and the diffraction pattern of each angle is collected) is from several crystals and thus nearly impossible to solve. The main system to solve a crystal as such is to obtain several crystals and therefore have multiple diffraction patterns which can then help solve the diffraction pattern and subsequently produce the crystal structure image (Nelson, 2011).

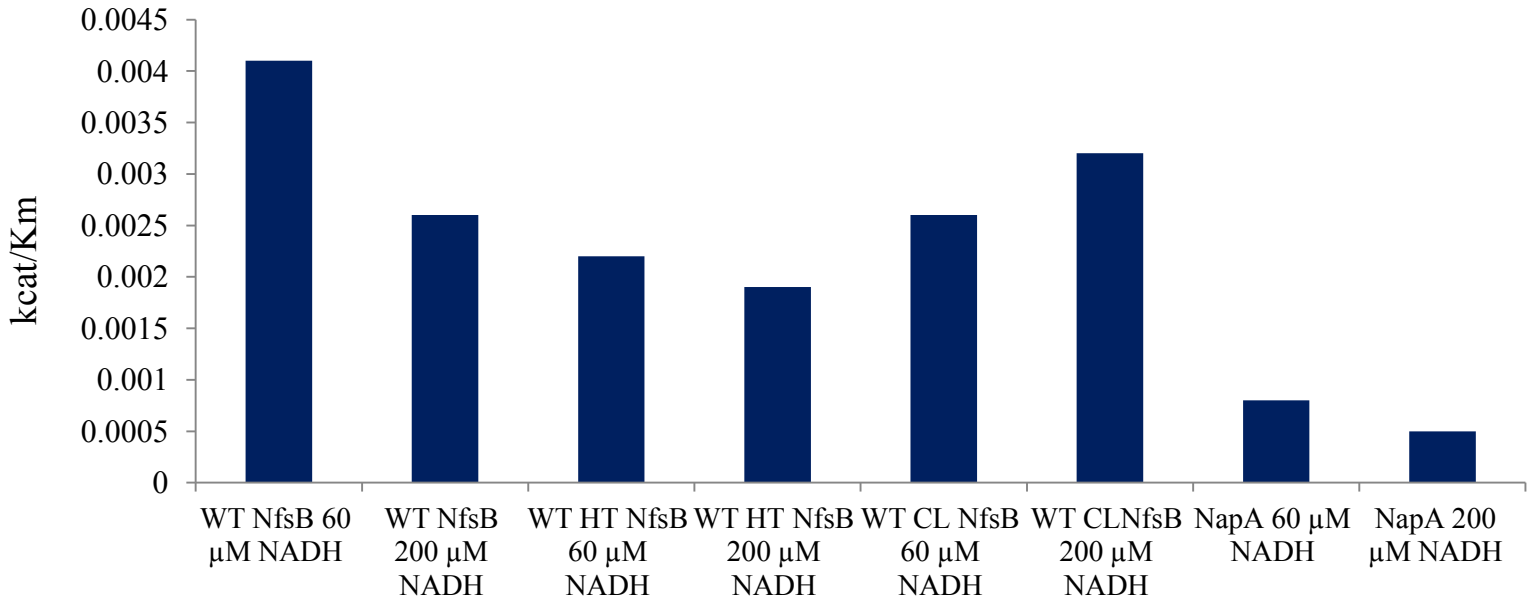

Figure 5.1a: The specificity constants for all NfsB proteins for the reduction of CB1954

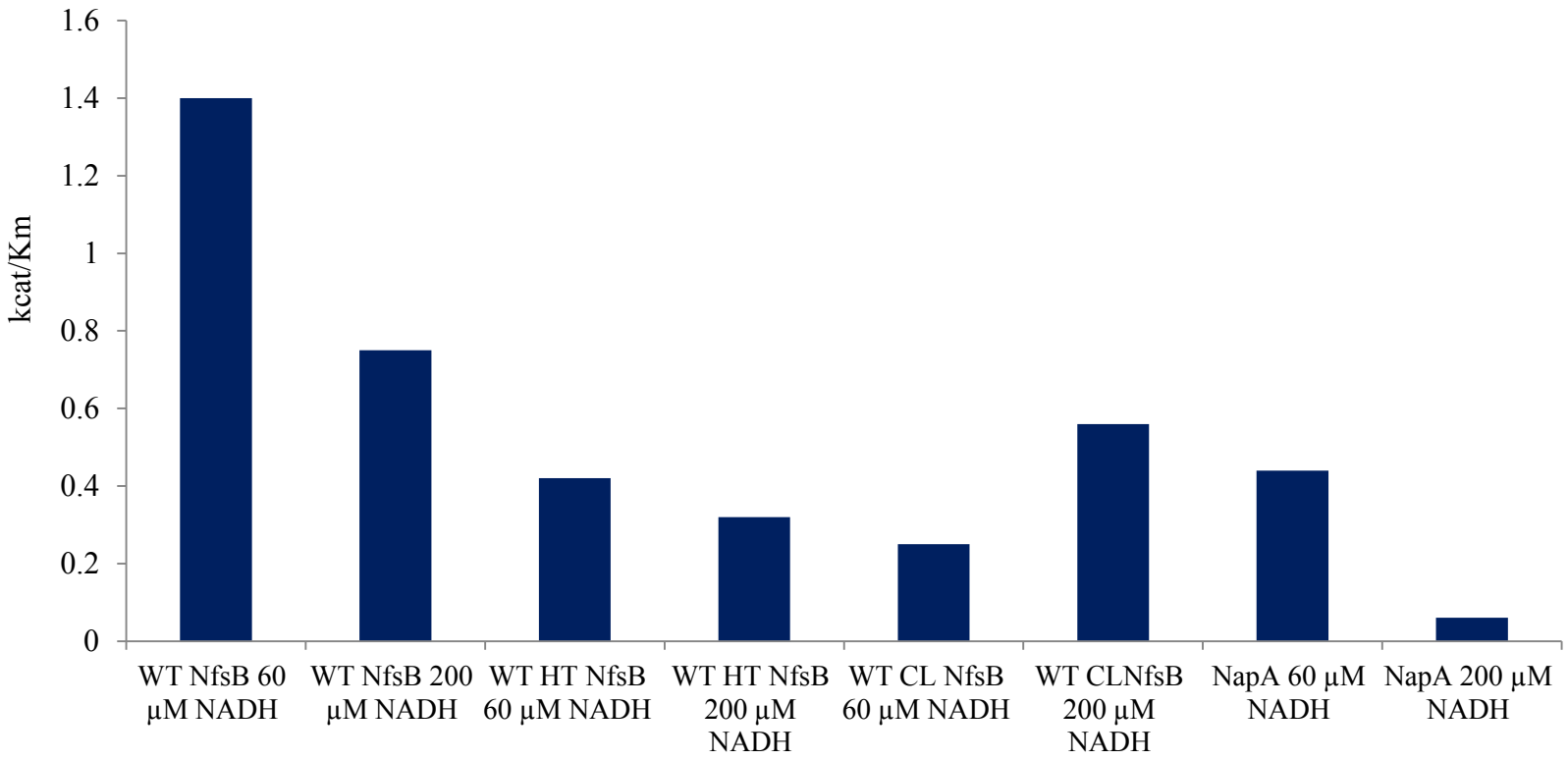

Figure 5.1b: The specificity constants for all NfsB proteins for the reduction of menadione

6. Conclusion and recommended further research

The conclusion of this project is that the histidine tag has an inhibitory effect on the specificity constant of the wild type NfsB for the substrates (CB1954 and menadione). However, statistically the histidine tag has only an inhibitory effect on the rate of menadione reduction. Furthermore menadione is a better substrate for NapA in comparison to CB1954, however to ensure this result is highly accurate; a repeat of NapA expression and purification is highly advisable in order to obtain viable results. Also the use of a cleavage enterokinase which cuts the entire histidine tag should be compared with the rEK used in this study, and whether the complete removal of the his-tag improves the specificity constant for the WT CL NfsB significantly. Finally, X-ray crystallography of menadione with NfsB would be extremely important in order to conclude why it is a better substrate for NfsB and subsequently, based on these results, improve NfsB activity with CB1954.

Appendix I

Section 1: The steady state kinetics of WT NfsB for the pro-drug CB1954 ; the effects of the 6 poly histidine tag on the rate of substrate reduction

[CB1954] µM	[NADH] µM	$k_{catapp}s^{-1}$	t	P	K_{mapp} µM	t	P	K_{cat}/K_m $\mu M^{-1}s^{-1}$	t	P
141-3525	60	5.8 ± 1.2	4.6	0.0004	1400 ± 700	1.9	0.067	0.0041 ± 0.0013	3.2	0.0058
141-3525	200	26 ± 3.5	7.4	<0.0001	9900 ±1700	5.8	<0.0001	0.0026 ± 0.000099	26	<0.0001

Table 1.1 The kinetic parameters of reduction of the pro-drug CB1954 by the WT NfsB.

[CB1954] µM	[NADH] µM	$k_{catapp}s^{-1}$	t	P	K_{mapp} µM	t	P	K_{cat}/K_m $\mu M^{-1}s^{-1}$	t	P
141-3525	60	10.7 ± 3.4	3.1	0.0064	4800 ± 2200	2.1	0.052	0.0022 ± 0.0004	6.0	<0.0001
141-3525	200	ND	-	-	ND	-	-	0.0019 ± 0.0002	8.4	<0.0001

Table 1.2 : The kinetic parameters of reduction of the pro-drug CB1954 by WT HT NfsB.

[CB1965] µM	[NADH] µM	$k_{catapp}s^{-1}$	t	P	K_{mapp} µM	t	P	K_{cat}/K_m $\mu M^{-1}s^{-1}$	t	P
141-3525	60	9.5 ± 2.3	4.2	0.0011	3700 ±1400	2.6	0.020	0.0026 ± 0.00040	6.8	<0.0001
141-3525	200	ND	-	-	ND	-	-	0.0032 ± 0.0004	8.5	<0.0001

Table 1.3: The kinetic parameters of reduction of the pro-drug CB1954 by the WT CL NfsB.

For all the kinetic parameters of wild type NfsB with CB1954, the pro-drug concentration was varied between 141 - 3525 µM with a fixed concentration of either 60 or 200 µM NADH. The kinetic parameters were estimated from the fit of each dataset to the Michaelis Menten equation (Figure 2.2.9 1).

Section 2: The steady state kinetics of WT NfsB for Menadione; the effects of the 6 poly histidine tag on the rate of substrate reduction

[Menadione] µM	[NADH] µM	$k_{catapp}s^{-1}$	t	P	K_{mapp} µM	t	P	K_{cat}/K_m $\mu M^{-1}s^{-1}$	t	P
0.5-300	60	5.8 ± 0. 44	13	<0.0001	4.2 ± 1.6	2.6	0.018	1.4 ± 0 .47	2.9	0.0079
0.5-300	200	13 ± 0.69	19	<0.0001	18 ± 3.3	5.4	<0.0001	0.75 ± 0.11	6.6	<0.0001

Table 2.1 : The kinetic parameters of reduction of the Menadione by the WT NfsB.

[Menadione] µM	[NADH] µM	$k_{catapp}s^{-1}$	t	P	K_{mapp} µM	t	P	K_{cat}/K_m $\mu M^{-1}s^{-1}$	t	P
0.5-300	60	6.2 ± 0.5	14	<0.0001	15 ± 4	3.7	0.0016	0.42 ± 0.095	4.5	0.0002
0.5-300	200	13 ± 0.6	22	<0.0001	41 ± 5.5	7.4	<0.0001	0.32 ± 0.032	9.8	<0.0001

Table 2.2: The kinetic parameters of reduction of the Menadione by the WT HT NfsB.

[Menadione] µM	[NADH] µM	$k_{catapp}s^{-1}$	t	P	K_{mapp} µM	t	P	K_{cat}/K_m $\mu M^{-1}s^{-1}$	t	P
0.5-200	60	2.6 ± 0.15	17	<0.0001	10 ± 2.2	4.6	0.0002	0.25 ± 0.043	5.7	<0.0001
0.5-200	200	9.3 ± 0.47	20	<0.0001	17 ± 3.1	5.4	<0.0001	0.56 ± 0.085	6.6	<0.0001

Table 2.3: The kinetic parameters of reduction of the Menadione by the WT CL NfsB.

The Menadione concentration is varied between 0.5 - 300 µM with a fixed concentration of either 60 or 200 µM NADH. The kinetic parameters were estimated from the fit of each dataset to the Michaelis Menten equation figure 2.2.9.1

Section 3: The steady state kinetics of NapA for the pro-drug CB1954

[CB1954] µM	[NADH] µM	$k_{catapp}s^{-1}$	t	P	K_{mapp} µM	t	P	K_{cat}/K_m $\mu M^{-1}s^{-1}$	t	P
141 -2820	60	0.53 ± 0.18	3.02	0.012	ND	-	-	0.0008 ± 0.0004	1.7	0.104
141 - 3525	200	1.2 ± 0.48	2.5	0.030	ND	-	-	0.0005 ±0.0002	2.8	0.015

Table 3.1: Displaying the kinetic parameters of reduction of the CB1954 by the NapA.

For the steady state kinetics of Napthylalanine NfsB with CB1954, the pro-drug concentration is varied between 141 - 3525 µM with a fixed concentration of either 60 or 200 µM NADH. The kinetic parameters were estimated from the fit of each dataset to the Michaelis Menten equation (figure 2.2.9.1).

Section 4: The steady state kinetics of NapA for Menadione

[Menadione] µM	[NADH] Mm	$k_{catapp}s^{-1}$	t	P	K_{mapp} µM	t	P	K_{cat}/K_m $\mu M^{-1}s^{-1}$	t	P
0.5 – 100	60	0.34 ± 0.012	28	<0.0001	0.77 ± 0.19	4.07	0.0009	0.44 ± 0.101	4.4	0.0004
0.5 – 100	200	1.5 ± 0.21	7.4	<0.0001	9900 ± 1700	3.01	0.0082	0.0606 ± 0.013	4.6	0.0003

Table 4.1: Displaying the kinetic parameters of reduction of Menadione by the NapA.

For the above table, the Menadione concentration is varied between 0.5-100 µM with a fixed concentration of either 60 or 200 µM NADH. The kinetic parameter were estimated from the fit of each dataset to the Michaelis Menten equation (figure 2.2.9.1).

References

Anlezark.G.M.(2002) Bacillus amyloliquefaciens orthologue of Bacillus subtilis ywrO encodes a nitroreductase enzyme which activates the prodrug CB 1954. **Journal of Microbiology.** 148:297–306

Balentine. J.R., Davis.C.P. (2012) **What is cancer** [online].New York City: MedicineNet. Available from http://www.medicinenet.com/script/main/art.asp?articlekey=12510[Accessed 5 December 2011

Both.G.W., (2009) Gene-directed Enzyme Prodrug Therapy for Cancer: A Glimpse into the Future. **Discovery Medicine**, 069.

Christoffersson.A.J. (2009) A Computational Investigation of the Mechanism of CB1954 Reduction by E.coli Nitroreductase.**University of Birmingham**

Cobb.L.M., *et al.*(1969)2, 4-Dinitro-5-ethyleneiminobenzamide (CB 1954): a potent and selective inhibitor of the growth of the Walker carcinoma 256. **Journal of Biochemical Pharmacology**, 18(6):1519–1527.

Davidoff.A.M., (2007) Gene therapy improved chemotherapy delivery**. Journal of Molecular Cancer Research.**

Friedlos.F.*et al.,* (1992) The properties of total adducts and interstrand crosslinks in the DNA of cells treated with CB 1954. Exceptional frequency and stability of the crosslink. **Journal of Biochemical Pharmacology**, 43(6):1249-54.

Genomics (2011) **Gene therapy.** [Online]. U.S. Department of Energy Genome Program's: HGP. Available from http://www.ornl.gov/sci/techresources/Human_Genome/medicine/genetherapy.shtml

[Accessed 5 January 2012]

Goldwein.J.W., Vachani.C. (2010) **Chemotherapy: the basics** [online].Pennsylvania: University of Pennsylvania. Available from http://www.oncolink.org/treatment/article.cfm?id=319&s=9&c=2 [Accessed 5 December 2011]

Green.N.K., *et al*. (2004) The Nitroreductase/CB1954 Enzyme-Prodrug System.. **Journal of Medicine**, 90, 459-477.

Grove.J.I. (2003) Generation of Escherichia coli nitroreductase mutants conferring improved cell sensitization to the prodrug CB1954. **Journal of Cancer Research**, 63:5532–5537.

Hammill.J.T. (2007) Preparation of site-specifically labeled fluorinated proteins for ^{19}F-NMR structural characterization. **Nature,** 2, 2601 – 2607.

Herod.M.R. (2010) Oncolytic Adenovirus Vectors for Nitroreductase Suicide Gene Therapy of Prostate Cancer. **University of Birmingham.**

Jackson.J.C. (2006).Improving Nature's Enzyme Active Site with Genetically Encoded Unnatural Amino Acids. **Journal of the American Chemical Society**, *128* (34), pp 11124–11127

Knox.R.J. (2001) Bioactivation of 5-(aziridin-1-yl)-2,4-dinitrobenzamide (CB 1954) by human NAD(P)H quinone oxidoreductase 2: a novel co-substrate-mediated antitumor prodrug therapy. **Journal of Cancer Research**,60;(15): 4179-86.

Koder.R.L. *et al* (2002) Flavin Thermodynamics Explain the Oxygen Insensitivity of Enteric Nitroreductases**. Journal of Biochemistry,** *41* (48), pp 14197–14205.

Kowalski.P. *et al (2002)* Modulation of the atypical multidrug-resistant phenotype by a hammerhead ribozyme directed against the ABC transporter BCRP/MXR/ABCG2**. The Journal of Cancer Gene and Cellular Therapies**, 9, 579–586

Krishna.R., Mayer.L.D. (1997) Liposomal Doxorubicin Circumvents PSC 833-Free Drug Interactions, Resulting in Effective Therapy of Multidrug-resistant Solid Tumors**. European Journal of Pharmaceutical Sciences**, 11: 265–283.

Lovering.A.L.(2001) The structure of *Escherichia coli* nitroreductase complexed with nicotinic acid: three crystal forms at 1.7Å, 1.8Å and 2.4Å resolution. **Journal of Molecular Biology,** 309:203–213.

Merkel.J.R., Steer.E. (1953) Relationship between ‘’Chloramphenicol Reductase Activity’’ and Chloramphenicol Resistance in Escherichia Coli.**Journal of Bateriology,** 66(4):389.

Mitchell.D.J., Minchin.R.F. (2008) E. coli nitroreductase/CB1954 gene-directed enzyme prodrug therapy: role of arylamine N-acetlytransferase 2Gene-directed enzyme prodrug therapy**. The Journal of Cancer Gene and Cellular Therapies,** 15, 758-764.

Nelson.S.A. (2011) **X-Ray Crystallography** [online]. New Orleans: Tulane University. Availble from http://www.tulane.edu/~sanelson/eens211/x-ray.htm [Accessed 29 February 2012]

Prosser.G.A. (2011) Discovery and Optimisation f Bacterial Nitroreductases for use in Anti-Cancer Gene Therapy. University of Wellington, research Archives.

Rau.J. ,Stolz.A. (2003) Oxygen-Insensitive Nitroreductases NfsA and NfsB of*Escherichia coli* Function under Anaerobic Conditions as Lawsone-Dependent Azo Reductases. **Journal of applied and environmental microbiology**, 69(6): 3448–3455

Ropert.C. (1999). Liposomes as a gene delivery system. Journal of Medical and Biological Research, 32: 163-16

Suzuki.R., *et al*. (2007) Effective gene delivery with novel liposomal bubbles and ultrasonic destruction technology. **International Journal of Pharmaceutics**, 10,034.

Thomas.H., Coley. H.M.(2003). Overcoming multidrug resistance in cancer: an update on the clinical strategy of inhibiting p-glycoprotein. **Journal of Cancer Research**, *57;* 5246

WCRFI. (2011) **General world cancer statistics** [online]. London; WCRFI. Available from http://www.wcrf.org/cancer_statistics/world_cancer_statistics.php [Accessed 5 December 2011]

World Health Organization (2008) **Cancer** [online].United Nations: WHO. Available from http://www.who.int/mediacentre/factsheets/fs297/en/ [Accessed 5 December 2011]

Wu.H.C.,Chand.D.K. (2010). Peptide-Mediated Liposomal Drug Delivery System Targeting Tumor Blood Vessels in Anticancer Therapy. **Journal of Oncology,** 10.1155/2010/723798

Xu.G., McLeod.H.L.(2001). Strategies for enzyme/pro-drug cancer therapy. **Clinical Cancer Research**, *7;* 3314

Second Thesis

Abstract

Platelet derived growth factors (PDGF) are one of the major abundant growth factors which control the proliferation, growth and division of many cells. The effects exerted by the PDGF isoforms are achieved by the binding to their structurally related tyrosine kinase receptors, PDGF receptor α and β, which become phosphorylated. The current hypothesis was that Protein Kinase C (PKC) is a point of signal integration for PDGF receptor recycling. In this study the G protein coupled cytokines fMLP and a LPA were investigated. fMLP was an un-investigated cytokine, where this study showed it to potentiate and stimulate PDGF β receptor phosphorylation as well as induce activation of PKC. Furthermore, the downstream effector molecule AKT was potentiated in response to PDGF β receptor phosphorylation. This is early data supporting the hypothesis that PKC is a point of signal integration for PDGF receptor recycling and that all signals which result in receptor recycling must activate PKC. Furthermore LPA has been previously shown to cause PDGF β receptor recycling and activation of PKC. This study re-confirmed these findings, however identified that downstream effector molecules AKT, ERK 1 and 2 are not potentiated in response, nonetheless this requires further investigation.

List of figures

Figure 3.8.5 Phosphorylation of ERK 2 in response to stimulation with LPA and PDGF-BB

Figure 3.8.6 Total ERK 2 protein available in response to stimulation with LPA and PDGF-BB

Abbreviations

PDGF	Platelet derived growth factor
GF	Growth factor
SDS-PAGE	Sodium dodecyl sulphate polyacrylamide gel electrophoresis
IP	Immunoprecipitation
WGA beads	Wheat germ agglutinin
SH domains	Src Homology Domains
SH2	Src Homology 2
SH3	Src Homolgy 3
PLCɣ	Phospholipase- C
[PI(4,5)P_2]	Phosphatidylinositol 4,5-bisphosphate
Ca^{2+}	Calcium

PI3 K	Phosphatidylinositol 3 Kinase
PKC	Protein Kinase C
[PI(3,4,5)P_3]	Phosphatidylinositol 3,4,5-trisphosphate
AKT	Protein kinase B
MAPK	Mitogen activated protein kinase
PTP	Protein Tyrosine Phosphatase
LPA)	Lysophosphatidic acid
fMLP	N-Formyl-Methionyl-Leucyl-Phenylalanine
FPR	N-formyl peptide receptors
MEF cells	Mouse embryonic fibroblast cells

1. Introduction

1.1Background

The research into growth factors (GFs) is of great importance as they play significant roles in the development of numerous cancers (Goustin *et al.*, 1986). GFs are generally classified as polypeptides which bind to a high affinity cell membrane receptor, resulting in the stimulation of cell proliferation and/or differentiation (Goustin *et al.*, 1986). Furthermore, GFs are exceptionally versatile; stimulating cell proliferation and/or differentiation in a vast number of diverse cell types, however some GFs are specific and thus stimulate only a particular cell type (King., 2012). The signalling pathways which under normal cellular conditions mediate the GFs are enhanced in cancer and the mitogenic signalling is affected by the oncogenes involved (Aaronson., 1991).

There is on average an estimated figure of 267 individuals per 100,000 diagnosed with cancer in the U.K alone, placing it in the 22nd position for the world's leading cancer rates (wcrfi., 2011). These figures have continued to increase significantly, with a reported death of 7.6 million individuals in 2008; stressing the need for a therapeutic intervention and highlighting the importance of research within this field (WHO., 2008).

1.2 Platelet derived growth factors and tyrosine kinase receptor

Platelet derived growth factor (PDGF) in particular are one of the major abundant GFs which control the proliferation, growth and division of many cells (Deuel & Huang., 1984). PDGF's were initially discovered during the investigation into lesions of atherosclerosis, which identified activated platelets releasing a growth promoting activity (Kohler & Lipton., 1974; Ross *et al*., 1974). PDGF's are major mitogens for connective tissue types such as smooth muscle cells and fibroblasts, as well as controlling significant embryonic developments (Shim *et al.*, 2010; Goustin *et al.*, 1986). The signalling network of the platelet derived growth

factor is similar in both mice and humans as it includes four ligands, which are A, B, C and D. PDGF is a dimeric glycoprotein, made up of polypeptide chains, and thus the ligands forms disulphide linked homo/hetrodimers; however among these, only the A and B ligands are capable of forming biologically active and functional dimers, with their related tyrosine kinase receptors (figure 1.2.1) (Shim *et al.*, 2010 ; Wu *et al.*, 2008; Heldin & Westermark., 1999; Karlsson., 2009). The PDGF isoforms, A and B polypeptide chains, are initially synthesized in a precursor form (immature), which will then be subjected to proteolytic processing (NH_2 terminal for A-polypeptide chains and COOH for the B-polypeptide chain) to produce the mature form of the PDGF isoform. These can be observed on simple *Sodium dodecyl sulfate* gels, which will illustrate the migration of the mature form of PDGF at 30 kDa in comparison to the immature reduced chains at 15 kDa (Heldin & Westermark., 1999). The mature A and B polypeptide chains are 100 amino acids in length and have 8 cysteine residues which are conserved, as two of the cysteine residues form key bonds in the dimer (2^{nd} and 4^{th}). However the remaining 6 residues are involved in intra-chain disulfide bonding (Heldin & Westermark., 1999). Furthermore, the A polypeptide chain is coded for by the gene on chromosome 7 and the B polypeptide chain gene is on chromosome 22, with both containing 7 exons. The exon function on both genes is highly similar as the first exon encodes the signal sequence, followed by the 2^{nd} and 3^{rd} exons, which are eventually removed as they both encode for the precursor sequence of the PDGF isoform. Subsequently exons 4 and 5 then contain the encoding for the mature PDGF protein, ending then with exon 7 which is non coding. Exon 6 differs in the two gene; in the B-polypeptide chain, this may be removed as proteolytic maturation occurs, whereas in the A polypeptide chain there are two splice forms, one which contain the exon 6 and the other where it has been spliced out (Heldin & Westermark., 1999).

The effects exerted by the PDGF isoforms are achieved by the binding to the structurally related tyrosine kinase receptors which are PDGF Receptor α and β (Hooshmand-Rad *et al.,* 1998). Binding to the PDGF α receptor (thus dimerizing + phosphorylating) controls the development of vital organs such as the skin, kidneys and lungs among others. In addition the activated PDGF β receptor is significantly involved in early heamopoiesis and angiogenesis (Shim *et al.*, 2010). The α receptor is able to form bonds with both the A and B polypeptide chains of the PDGF, however the β receptor bonds only to the B polypeptide chain (Andrae *et al.,* 2008 ; Hooshmand-Rad *et al.,* 1998) (Figure 1.2.1). Furthermore, both receptors are expressed on cell surfaces of glia cells fibroblasts, capillary endothelial cells, neuronal cells and other cells of mesenchymal origins (Hooshmand-Rad *et al.,* 1998). The molecular size of the PDGF α receptor is slightly lower (170 kDa) than the PDGF β receptor (180 kDa), as well as each receptor consisting of an intracellular, transmembrane and extracellular domains (Shim *et al.*, 2010; Heldin & Westermark, 1999). The extracellular division of both receptors consists of 5 domains which have a structure similar to immunoglobulins (D1-D5); this is linked to the intracellular part of the receptor through the transmembrane spanning region which leads to the split tyrosine kinase domain (Lokker *et al.*, 1997 ; Heldin & Westermark., 1999)

Due to the significant effects the activated tyrosine kinase receptors have, an over stimulation results in tumour growth via the malignant cells, as these are then stimulated through the autocrine pathway. In addition PDGF is one of the many endogenous stimulators of angiogenesis which activates the cascade resulting in the formation of new blood vessels; angiogensis within the tumour occurs in the case of over stimulated PDGF receptors (Shim *et al.*, 2010 ; Wu *et al.*, 2008). Furthermore, the increased activation of the tyrosine kinase receptors (PDGFRα or PDGFRβ) has also been observed in myeloid malignancies, lung cancers, gastrointestinal tumours, dermatofibrosarcoma protruberans to name a few, in

addition to many other tumours such as malignant gliomas (Shim *et al.*, 2010 ; Wu *et al.*, 2008). Therefore an abnormal increase in activated PDGF receptor stimulation results in an enhanced signalling cascade highlighting it to be a key characteristic in a vast number of diseases and consequently becoming a target to exploit for the use of novel anti cancer drug development and therapeutic treatment (Shim *et al.*, 2010 ; Wu *et al.*, 2008; Östman *et al* ., 2006)

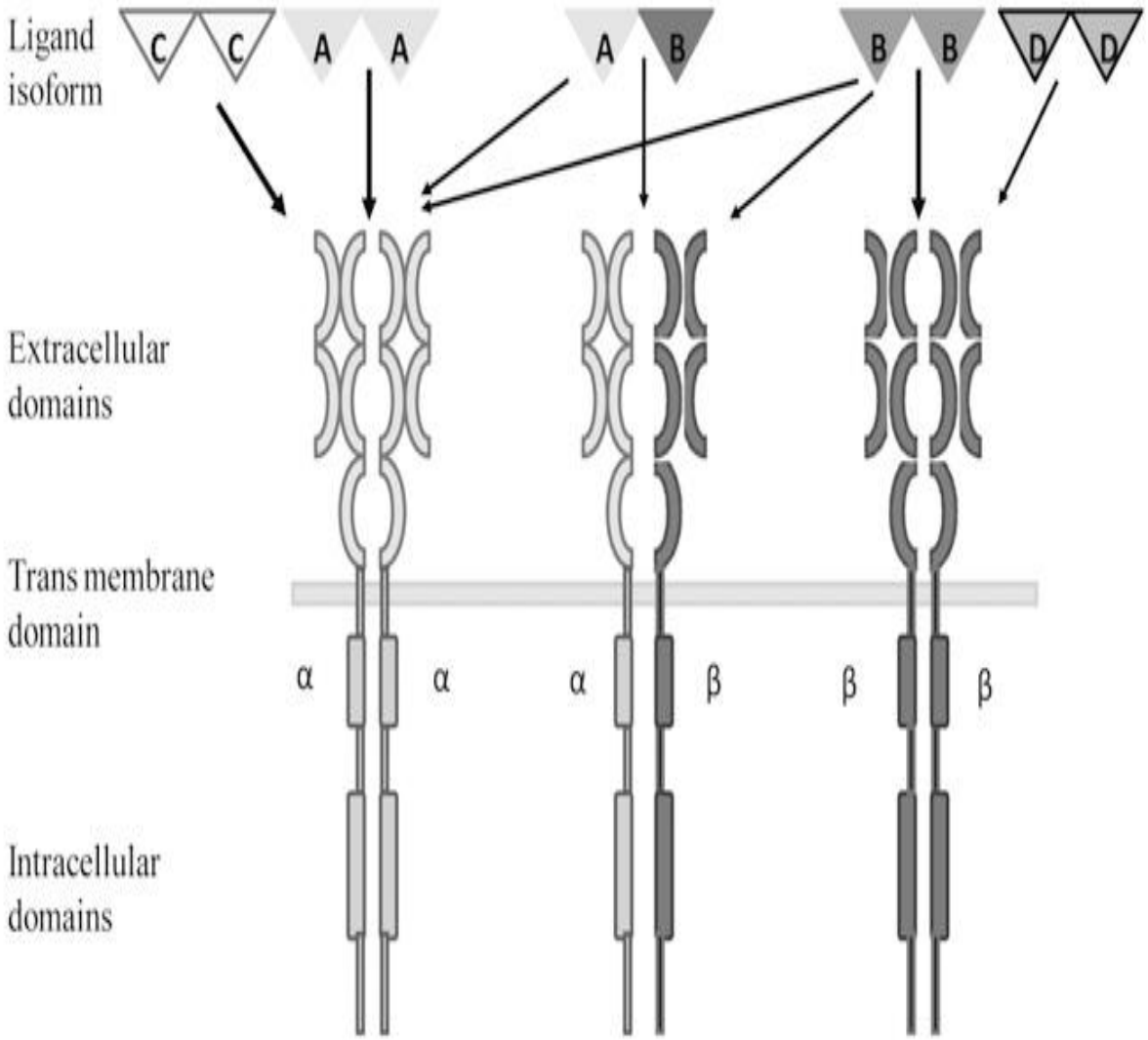

Figure 1.2.1: A schematic diagram of the PDGF isoforms and the binding to their corresponding tyrosine kinase receptors (PDGFRα or PDGFR β (Karlsson., 2009).

The PDGF isoforms bind the PDGFR with different affinities, forming the corresponding hetro/homdimers, complexed to their receptor. The PDGF homodimers (AA and CC) can only bind the PDGF α receptor. The PDGF hetrodimer (AB) can bind both the α and the β receptors. The PDGF homodimer (DD) can only bind the β receptor, finally the homodimer PDGF BB is the only isoform which can bind both receptors (Heldin & Westermark., 1999; Lokker *et al.*, 1997 ; Karlsson., 2009 ; Andrae *et al.,* 2008).

Generally once the PDGF ligand binds the PDGF β receptor it is internalized and endocytosis occurs as it is compartmentalized into clathrin coated vesicles. The vesicles then shed the clathrin coat resulting in the formation of early endosomes as the internalized vesicles fuse (van der sluis *et al.*, 2000). At this point the receptor is either degraded through lysosomal degradation via multivesicular bodies; a process which sorts the early endosomes into the late endosomal degradation pathway, or recycled back to the plasma membrane, for which Rab4a is a necessary protein (figure 1.2.2). The great family of monomeric GTPases, also known as Rab proteins, regulate important processes in the majority of vesicular sorting. In particular Rab4a is a central component of the recycling pathway, where it regulates the receptor recycling from early endosomes. Finally, the recycling of the PDGF β receptor back to the cell surface through Rab4a dependent recycling increases PDGF receptor activation (Hellberg *et al.,* 2009; Karlsson *et al.*, 2006).

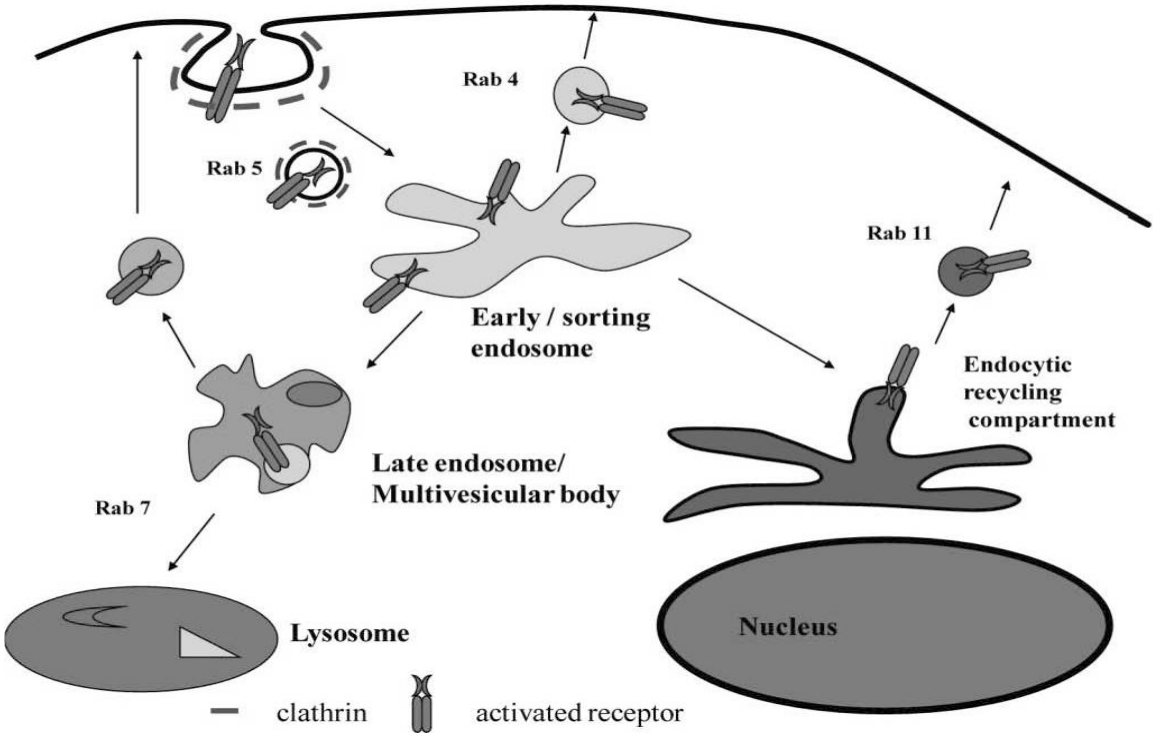

Figure1.2.2: The endocytic recycling and degradation processes of PDGF β receptor (Karlsson., 2009)

1.3 Intracellular signal transduction

The intracellular signalling cascade of the PDGF β receptor requires a vast and significant number of phosphorylation processes which are stabilised through protein kinases and phosphatases. However signal transduction occurs through signalling molecules which are employed to the receptor once it has been activated; through the use of the specific domains on the signalling molecules, interaction with the receptor is enabled (Heldin & Westermark., 1999). The binding of the PDGF ligand to its related tyrosine kinase receptor results in the dimerization and autophosphorylation of the PDGF receptor, which controls two significant functions depending on the tyrosine residues which are, phosphorylated (Heldin & Westermark, 1999). The phosphorylation of the conserved tyrosine kinase domains, tyrosine 849 PDGFRα and Tyrosine 857 PDGFRβ, results in an increased catalytic kinase, in comparison to the residues external of the conserved domains causing the transduction of molecules containing Src homology domains, via the formation of docking sites (Heldin & Westermark., 1999).

1.4 Src Homologies SH2 & SH3

The majority of signalling molecules use the specific domain SH2 to interact and bind to the phosphorylated PDGF receptor as it binds phosphotyrosines. The Src family consists of many tyrosine kinases which have a SH2 domains present in the catalytic segment as well as being activated via either binding to the autophosphorylated PDGF receptor or dephosphorylation of the receptor. In general it is an important domain which is involved in the mitogenic response of PDGF (Heldin & Westermark., 1999).

The SH3 domain is also present on the catalytic segment of many tyrosine kinases in the Src family and thus binds phosphorylated PDGFR, but it also distinguishes proline rich regions and the PDZ for the recognition of valine residues in the C terminal (Pawson & Scott., 1997)

Furthermore other transduction molecules which bind to the phosphorylated PDGFR include; PLCɣ, PI3 kinase, Src, SHP-2 and RasGAP (Heldin & Westermark, 1999; Karlsson, 2009). In addition there are the adaptor molecules including Grb2, Shc, Nck, Grb7 and Crk; finally there is the family of stat molecules (Heldin & Westermark, 1999).

1.5 Stimulation of cell growth, differentiation, migration and prevention of apoptosis

The activation of transduction molecules results in the stimulation of fundamental processes within the cells.

1.5.1 Phospholipase- C (PLCɣ)

PLCɣ cleaves phosphatidylinositol 4,5-bisphosphate [$PI(4,5)P_2$] into an inositol 1,4,5-trisphosphate and diacylglycerol, which causes an increased level of intracellular Ca^{2+} , which are mobilized. The change in intracellular Ca^{2+} levels causes the stimulation and activation of classic protein kinases ɣ, α, and β; these result in cell growth and migration (Heldin & Westermark., 1999). Furthermore, the PLCɣ is phosphorylated through binding to the PDGFR which causes increased catalytic activity of the transduction molecule as specific residues are phosphorylated (Heldin & Westermark., 1999). In addition, full activation of PLCɣ is dependent on PI3 Kinase (Heldin & Westermark., 1999).

1.5.2 Protein Kinase C (PKC)

PKC is a family of protein kinases, which are involved in the signal transduction cascade downstream of the PDGF β receptor. As mentioned before hand, activation of PKC occurs as the levels of diacylglycerol and intracellular Ca^{2+} increases. In particular the activation of PKC α is a critical step for the recycling of the PDGF β receptor as it promotes receptor recycling from early endosomes (Hellberg *et al.,* 2009; Karlsson *et al.*, 2006).

1.5.3 Phosphatidylinositol 3 Kinase (PI3 K)

The family of PI3 kinases consists of several members, however the ones that are activated by the PDGFR, or other tyrosine kinase receptors, contain a catalytic subunit (p110) and a regulatory subunit (p85). In comparison to the PLCɣ molecule, PI3 kinase phosphorylates the [$PI(4,5)P_2$] into phosphatidylinositol 3,4,5-trisphosphate [$PI(3,4,5)P_3$] (Heldin & Westermark., 1999). The PI3 K has a significant function as it generates the phospholipid PIP3 second messenger which binds AKT (protein kinase B) on the pleckstrin homology and activates AKT, a downstream effector molecule, through phosphorylation. This results in stimulation of cell growth and prevention of apoptosis. Other biological responses exerted by the activated PI3K include actin reorganization and chemotaxis (Heldin & Westermark., 1999).

1.5.4 Mitogen activated protein kinase (Ras-MAPK)

This pathway leads to the activation of important downstream effector molecules, activating the MAPK pathways, which stimulate cell growth, differentiation and migration (Heldin & Westermark., 1999; Andrae *et al.,* 2008). These processes occur as Grb2 (an adaptor molecule) binds Sos1, a guanine nucleotide exchange factor (GEF) site, through its SH3 domain resulting in the activation of Ras. This process occurs as the GEF allows the release of guanosine diphosphate from the Ras GDP and enables the binding of guanosine triphosphate forming the activated Ras GTP. Finally the activated Ras GTP activates RaF-1 initiating the Mitogen activated protein kinase cascade (MAPK) (Heldin & Westermark., 1999; Andrae *et al.,* 2008).

1.6 Receptor regulation

1.6.1 Protein Tyrosine Phosphatase (PTP)

Protein tyrosine phosphatases are a family of enzymes, which regulate important cellular processes such as cell growth, differentiation and oncogenic transformations via the removal of phosphate groups from phosphorylated proteins (figure 1.6.1a) (Fischer *et al.,* 1991). Recent research has shown that PTP's regulate receptor recycling of the PDGF β receptor via the dephosphorylation of this receptor; the loss of PTP resulted in the hyperphosphorylation of the receptor at position Y1021. In addition, recycling of PDGF β receptor to the cell surface was found to be reliant on Rab4a dependent recycling, as well as that PKC α being a critical signalling kinase regulating the Rab4a dependent recycling of the PDGF receptor (Hellberg *et al.,* 2009; Karlsson *et al.*, 2006).

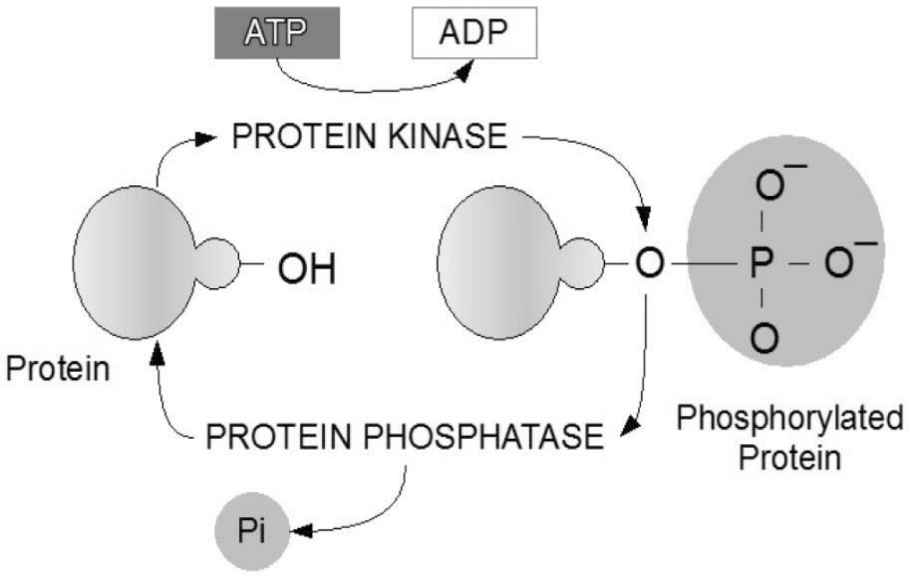

Figure 1.6.1a: The de/phosphorylation process of proteins regulated by PKC and PTP. (Karlsson *et al.,* 2009).

1.7 Cytokine-induced potentiation of PDGF receptor signalling

Previously established findings on Cytokine induced potentiation of PDGF β receptor signalling:

The use of the G protein coupled cytokine lysophosphatidic acid (LPA) , has proved to increase PDGF β receptor phosphorylation as it activates PKC which in turn activates PDGF β receptor recycling (Hellberg *et al.,* 2009; Karlsson *et al.*, 2006). Furthermore, it has been hypothesised that PKC is a point of signal integration for PDGF β receptor.

1.7.1 Lysophosphatidic acid (LPA)

The phospholipd LPA is a cytokine which acts as a signalling molecule and binds to its lysophospholipid receptor, a G protein coupled receptors. Once bound to its receptor and activated, depending on the cell type, a variety of effects are exerted within the cell. LPA activates PKC and therefore results in an increase of receptor recycling leading to an increase in activated PDGF β receptor; calcium levels are mobilized as it is released from the endoplasmic recticulum, via phospholipase-mediated inositol 1,4,5-trisphosphate and diacylglycerol (Yuan *et al.*, 2002). In addition downstream receptor activation by LPA activates Ras and Rho. Rho is a downstream signalling GTPase molecule of PI3 K and thus leads to similar effects as the AKT/PKB; Ras activates the MAPK/ERK pathway (Yuan *et al.*, 2002).

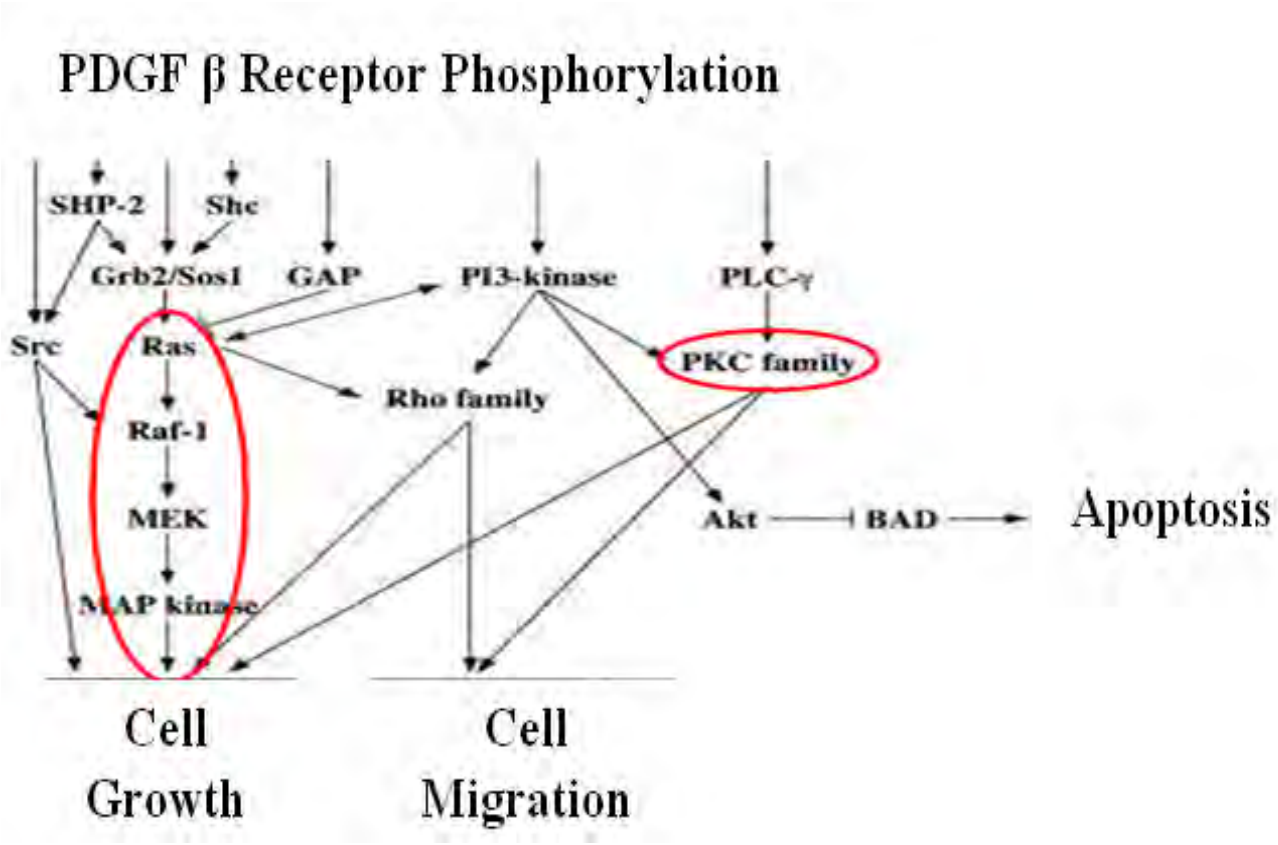

Figure 1.7.1: Activated downstream effector molecules by LPA (Heldin *et al.,* 1998)

1.7.2 N-Formylmethionyl-leucyl-phenylalanine (fMLP)

N-Formylmethionyl-leucyl-phenylalanine (fMLP) is a strong chemo-attractant, more specifically for polymorphonuclear neutrophils, by binding to their specific N-formyl peptide receptors (FPR) which are seven rhodopsin like helical transmembrane G protein coupled receptors of the cells (Murphy, 1994). In neutrophils, early work has proved that this cytokine induces activation of phospholipase C β , which in turn results in the generation of inositol 1,4,5-trisphosphate and diacylglycerol; PKC activation (Ding and Badweyt, 1993). Furthermore, many researchers have proved that fMLP stimulates tyrosine phosphorylation in the MAPK family and extracellular signal regulated kinases (ERK) in neutrophils (Kusunoki *et al*., 1992; Torres *et al* .,1993; Grinstein & Furuya, 1992; Rollet *et al* .,1994). However

fMLP induced phosphorylation of the PDGF β receptor is still unknown. Although the neutrophil cells used in previous studies employed transfection of cells with the FPR receptor, similar results may be expected for the PDGF β receptor (Kusunoki *et al*., 1992; Torres *et al* .,1993; Grinstein & Furuya, 1992; Rollet *et al* .,1994).

1.8 Benefits of project

The investigation of the projects allows more knowledge to be gained on downstream effector molecules of PDGF β receptor and a greater understanding of intercellular signalling mediated by the receptor phosphorylation. Also investigating the effects of the cytokines on PDGF receptor phosphorylation allows a greater understanding of how cytokines potentiate the signal and whether it is through the established receptor recycling pathway or perhaps other unexplored possibilities. Finally the findings will provide valuable findings on the early hypothesis that PKC is a point of signal integration for PDGF receptor recycling.

1.9 Summary of project aims and objectives

The research project was separated into two sections:

1. The first part of the project investigated whether fMLP potentiates the ability of the PDGF-BB ligand to phosphorylate the PDGF β receptor and whether all downstream signalling effector molecules were affected.

2. The second part of the project expanded on the findings of LPA, therefore whether the phosphorylation of all downstream signalling effector molecules of PDGF β receptor are potentiated.

2. Materials and Method

2.1 Reagents

Lysophosphatidic acid (LPA) and fMLP (N-formyl-methionine-leucine-phenylalanine) were purchased from Sigma-Aldrich. The primary antibodies MARCKS, P-TYR, PERK and the PDGF-BB ligand were all purchased from Santa Cruz Biotechnology. The primary antibodies CTB, PMARCKS, AKT, PAKT and ERK were all purchased from Cell signalling technologies. The HRP Goat-anti-mouse and anti-rabbit IgG were both purchased from Invitrogen. Dulbecco's Modified Eagle's Medium purchased from Lonza Bio-Whittaker and Fetal bovine serum from BioSera. Lysis buffer make, 2 x loading sample buffer, Tween 20, NaOH, Wheat Germ Agglutinin beads, Penicillin and Streptomycine were purchased from Sigma Aldrich. Finally Coomassie plus protein assay reagent was fromThermo Scientific.

2.2 PDGF β receptor phosphorylation and Downstream signalling molecules

The project employed the use of PDGF-BB as a ligand to simulate the receptors as this is the only isoform which can bind both receptors (Heldin & Westermark., 1999; Lokker *et al*., 1997). In addition wild type mouse embryonic fibroblast (MEF) cells were used from littermate wild type mice according to the protocol described previously in the paper *You-Ten et al 1997.*

There are several downstream signalling molecules of PDGF β receptor phosphorylation which were investigated in order to determine whether the effect of the cytokines subsequently affected the phosphorylation of the downstream effector molecules.

The monoclonal mouse antibodies to phosphotyrosine P-Tyr (py99) was employed to detect total tyrosine phosphorylation of the PDGF receptor as this antibody binds phosphotyrosine

residues located within the receptor cytoplasmic domains. Furthermore, C terminal β antibody was used as to specifically bind the PDGF β receptor and measures the phosphorylation of this receptor.

The phosphorylation of downstream effector molecules which were investigated are MARCKS, AKT, ERK 1 and ERK 2.

2.3 Cell Culturing

Wild type mouse embryonic fibroblast (MEF) cells were derived from littermate wild type mice described previously in the paper You-Ten et al 1997 and were a gift from Canada Institute of Health and Research. The cells were grown in Dulbecco's Modified Eagle's Medium (Lonza Bio-Whittaker) containing 10% Fetal bovine serum (BioSera) and 1% Penicillin and Streptomycine (Sigma Aldrich).

2.4 MEF cell stimulation and lysis

The cells were split into thirteen T 25^3 cell culture flask (Cell Star Greiner Bio-One) and starved overnight in Dulbecco's Modified Eagle's Medium only (Lonza Bio-Whittaker). One flask was unstimulated; four flasks were stimulated with 5 ng/ml PDGF-BB ligand, the following four with 10 μM LPA or 100 nM fMLP and the final four with both 5 ng/ml PDGF-BB and 10 μM LPA or100 nM fMLP. Each batch of cells was stimulated for 10, 20, 40 and 60 minutes in 37^0C incubators. The stimulation was stopped by placing the T 25^3 flasks on ice and finally rinsing twice with ice cold Phosphate buffered saline (PBS). Subsequently the cells were lysed in150 μl of lysis buffer for 15 minutes, which consisted of; 0.5% Trition X-100, 0.5% deoxycholic acid, 150 mM NaCl, 20 mM Tris (pH 7.5), 10 mM EDTA, 0.5 mM Na_3VO_4 and 1 mg/ml aprotinin (Sigma Aldrich). The lysates were cleared via centrifugation (Biofuge Heraeus Sepatech) for 15 minute at 13,000 rpm in 4^0C. For the total cell lysate samples, 40 μl was removed and added to the same volume of 2 x loading

sample buffer (4% SDS, 20% Glycerol, 0.12M Tris pH 6.8, and 10% BME, all from Sigma Aldrich), which was heated for 5 minutes at 95^0C.

2.5 Immunoprecipitation (IP)

The immunoprecipitation of the PDGF receptors was conducted by mixing equal amounts of the proteins with lysis buffer, making it up to a 1 ml volume. This was determined via a protein assay which measured (Softmax Molecular Devices-Precision Microplate reader) the optical density of 5 µl of the total cell lysate sample mixed with 200 µl Coomassie plus protein assay reagent (Thermo Scientific).

Approximately 5 µg/ml of CTβ antibody was added to the mixture and incubated end over end overnight at 4^0C. Then 30 µl of protein A beads was added and incubated end over end for 1 hour at 4^0C. Subsequently the beads were washed 3 x by adding 1 ml of lysis buffer, re-suspending the beads and then using a magnetic strip to separate the beads from the lysis buffer. On the last wash the lysis buffer is removed, leaving the beads, and 30 µl of the 2 x sample loading buffer was added. The samples were heated for 5 minutes at 95^0C.

2.6 WGA bound PDGF receptor

A volume of 40 µl of WGA (wheat germ agglutinin from Sigma Aldrich) beads was added to the mixture and was incubated end over end for 1 hour at 4^0C . The beads were washed 3 x by adding 1 ml of lysis buffer, re-suspending the beads, and centrifuging for 3 minutes at 13,000 rpm (Biofuge Heraeus Sepatech). On the last wash the lysis buffer is removed, leaving the beads, and 40 µl of the 2 x sample loading buffer was added. The samples were heated for 5 minutes at 95^0C.

2.7 SDS-PAGE, Western Blot and membrane development

The samples were separated using SDS-PAGE (Sodium dodecyl sulfate polyacrylamide gel electrophoresis) according to the Laemmli Protocol 1970 (Bio Rad multicasting Kit). The gels were either 7%, for PDGF receptor, MARCKS and AKT detection and 10% for ERK detection. Finally they were transferred onto a nitrocellulose membrane (Transblot Turbo Transfer Pack BioRad).

The membrane was blocked using PBS containing 5 % Fetal bovine serum (BioSera) for 1 hour and incubated overnight with the primary antibody made up according to manufacturers protocol. Following the membrane was washed 6 x for 5 min each, using PBS containing 0.01% Tween 20 (Sigma Aldrich) and incubated for 1 hour with the secondary antibody followed by the same procedure of membrane washing. Finally, the bound antibodies were visualized and quantified via enhanced chemiluminescence using ECL reagents 1 and 2 (Gene Flow LTD) the softwares GeneSnap and GeneTools on the UV Transilluminator Syngene from Gene Flow.

2.8 Membrane stripping and re-blotting

Once the membrane had been developed it was incubated with 0.4 M NaOH (Sigma Aldrich) for 10 minutes and subsequently washed for 5 minutes (6 x) with PBS containing 0.01% Tween 20. It was then re-blocked using PBS containing 5 % Fetal bovine serum (BioSera) and the following primary antibody is re-probed.

2.9 Blotting of primary and secondary antibodies

Depending on which receptor signal being investigated, different antibodies were used and made up according to the manufacturer's protocol:

▪ P-Tyr (mouse source - Santa Cruz Biotechnology) primary antibody for detecting tyrosine phosphorylation of proteins containing tyrosine. Secondary antibody is HRP Goat-anti-mouse IgG H + L (Invitrogen).

▪ C Terminal antibody (rabbit source- home made) primary antibody specific for PDGF β receptor phosphorylation. Secondary antibody is HRP Goat-anti-rabbit IgG OS GRD (Invitrogen).

▪ MARCKS (mouse source -Santa Cruz Biotechnology) primary antibody for MARCKS protein. Secondary antibody is HRP Goat-anti-mouse IgG H + L (Invitrogen).

▪ PMARCKS (rabbit source- Cell signalling technology) primary antibody for detecting phosphorylated MARCKS protein. Secondary antibody is HRP Goat-anti-rabbit IgG OS GRD (Invitrogen).

▪ ERK (rabbit source- Cell signalling technology) primary antibody for ERK protein. . Secondary antibody is HRP Goat-anti-rabbit IgG OS GRD (Invitrogen).

▪ PERK (rabbit source- Santa Cruz Biotechnology) primary antibody for detecting phosphorylated ERK protein. Secondary antibody is HRP Goat-anti-rabbit IgG OS GRD (Invitrogen).

▪ AKT (rabbit source -Cell signalling technology) primary antibody for AKT protein. Secondary antibody is HRP Goat-anti-rabbit IgG OS GRD (Invitrogen).

▪ PAKT (rabbit source- Cell signalling technology) primary antibody for the detection of phosphorylated AKT protein. Secondary antibody is HRP Goat-anti-rabbit IgG OS GRD (Invitrogen).

3. Results

3.1 fMLP stimulation of PDGF receptor phosphorylation

The effects of the cytokine fMLP on the PDGF β receptor was determined by stimulating the mouse embryonic fibroblast cells in 13 T 25^3 cell culture flask; four flasks with 5 ng/ml PDGF-BB, the following four with 100 nM fMLP and the final four with the two combined; the last remaining flask was unstimulated. For each batch of the cells, a stimulation period of 10, 20, 40 and 60 minutes was conducted. The total cell lysates (TCL) were boiled in 2 x sample loading buffer and separated on SDS-PAGE gels; subsequently followed by a Western blot. The membranes were immunoblotted with P-Tyr to detect total tyrosine phosphorylation and then stripped and re-probed with PDGF β receptor antibody (CTB).

3.1.1 Total cell lysate samples stimulated with fMLP

The fMLP stimulated as well as potentiated tyrosine phosphorylation of the PDGF β receptor. There was a pattern on the western blot results which illustrated that the combination of fMLP with the PDGF-BB ligand increased the ligands ability to phosphorylate the PDGF receptor (figure 3.1.1a). However in order to analyse the data accurately the bands observed on the Western blot were quantified using the software GeneTools (figures 3.1.1b/c).

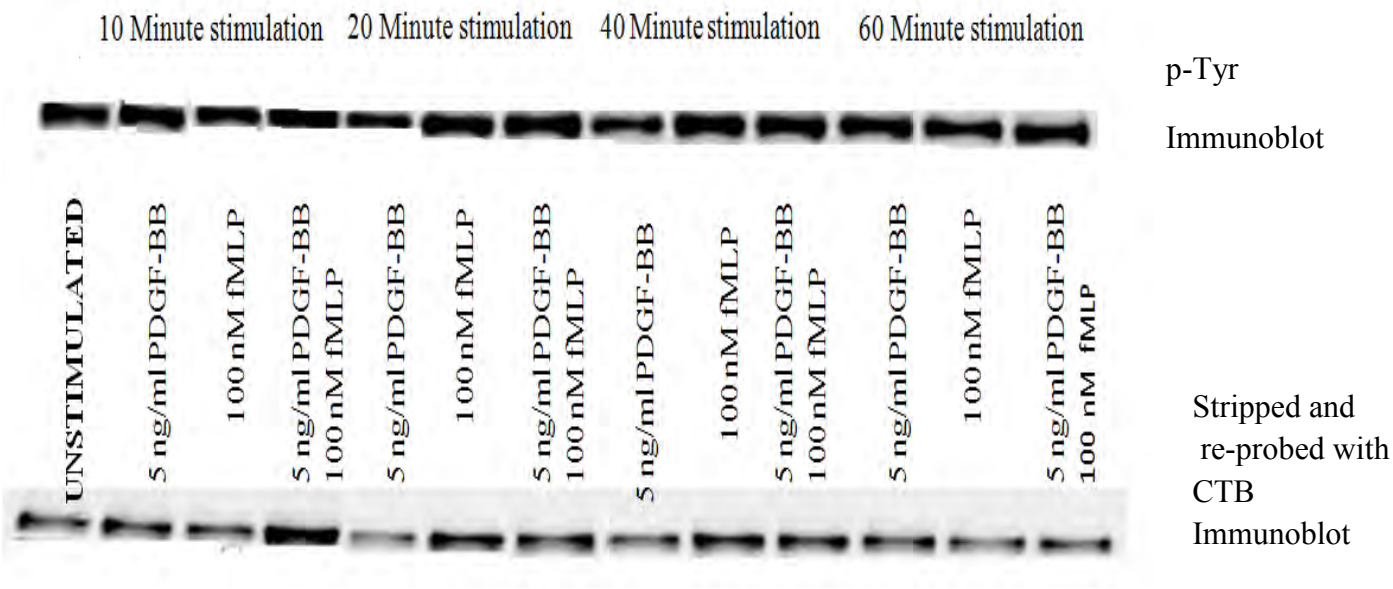

Figure 3.1.1a: Western Blot of PDGF receptor phosphorylation at 190 kDa stimulated with fMLP and PDGF-BB

Quantified p-Tyr Blot for total tyrosine phosphorylation of the PDGF receptor in the total cell lysate

There was a clear high level of background banding in the unstimulated sample. Throughout the stimulation time points, the samples containing both the fMLP and PDGF-BB illustrated increased levels of phosphorylation in comparison to PDGF-BB and fMLP stimulations alone. In comparison at 10 minutes, there was a high level of phosphorylation for stimulation with PDGF-BB, which decreased as the stimulation time increased. There is a strange pattern in the PDGF-BB stimulations as the phosphorylation increased again after 20 minutes stimulation. However at 10 minutes stimulation with fMLP there were low levels of phosphorylation, but these significantly increased as the stimulation time prolonged and remained fairly constant at 60 minutes stimulation.

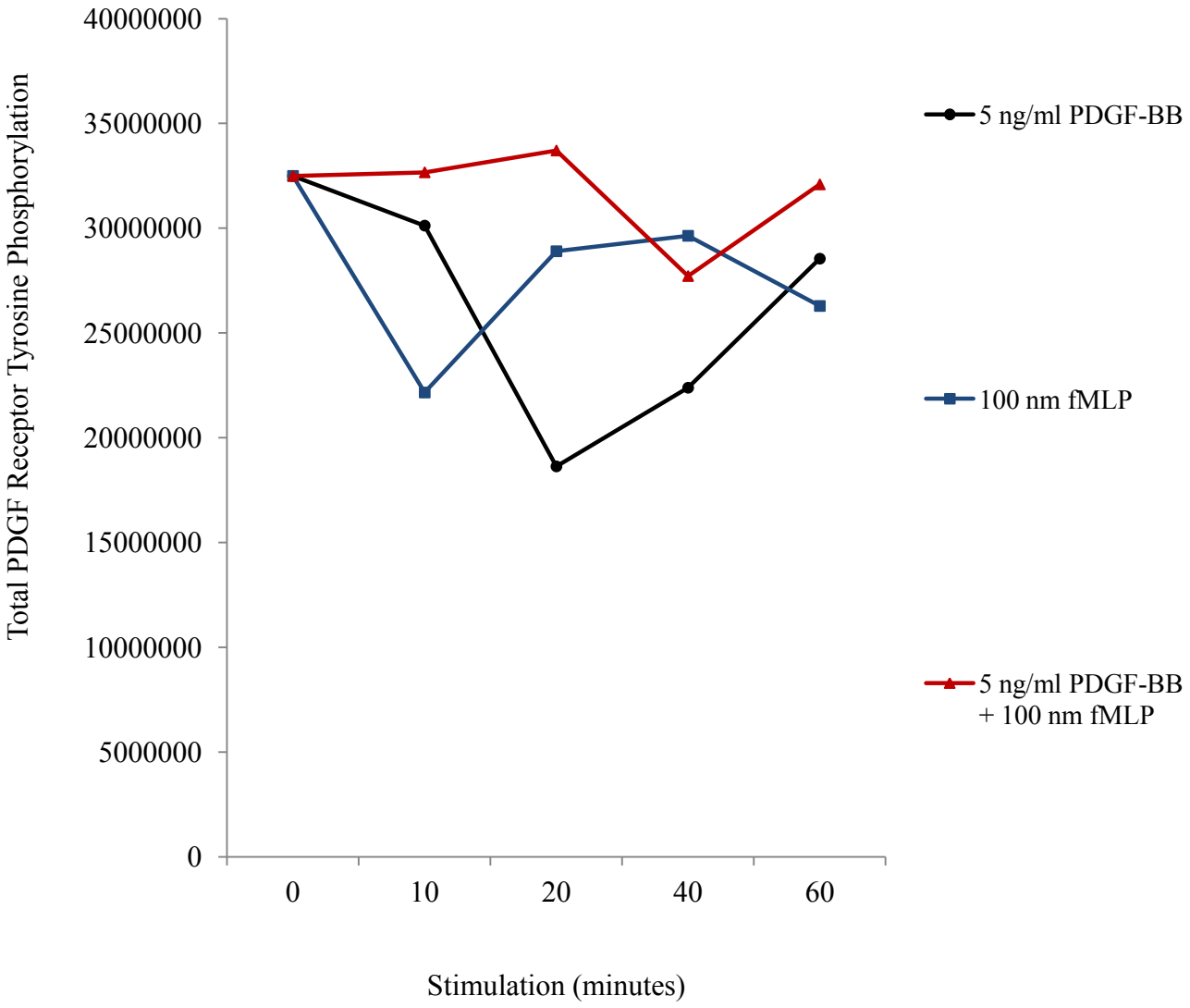

Figure 3.1.1b: PDGF receptor tyrosine phosphorylation in response to stimulation with fMLP and PDGF-BB

Quantified CTB Blot for phosphorylation of the PDGF β receptor in the total cell lysate

The membrane was stripped and re-probed with PDGF β Receptor antibody

Again there was a clear high level of background banding in the unstimulated sample. The fMLP and PDGF-BB combined stimulation was increased significantly at 10 minute stimulation, however as the time prolonged, the phosphorylation decreased after 20 minutes. PDGF-BB stimulation alone increases the phosphorylation at 20-40 minutes and then decreases after 40 minutes. The same pattern was observed for fMLP stimulation.

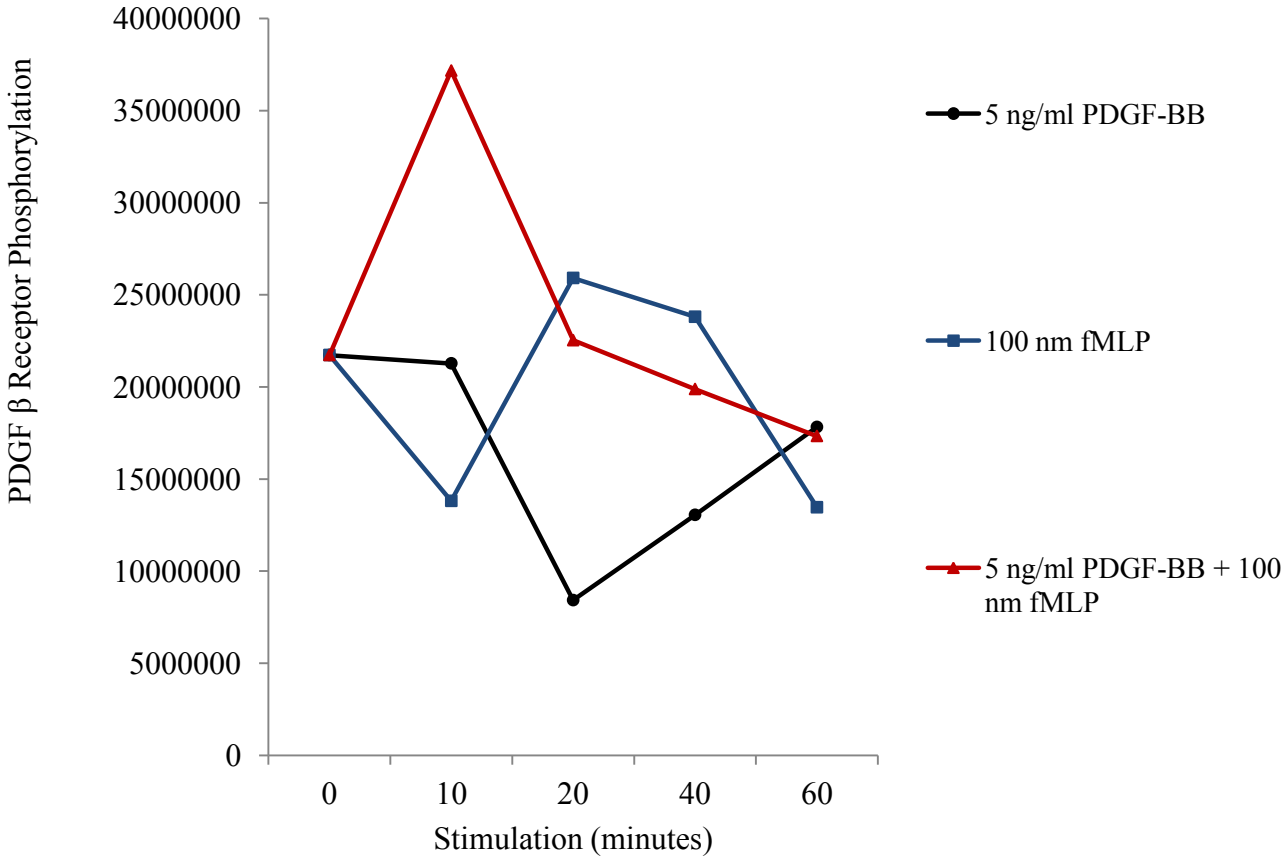

Figure 3.1.1c: Phosphorylation of PDGF β receptor in response to stimulation with fMLP and PDGF-BB

3.2 WGA bound PDGF receptor phosphorylation

Due to the high levels of background banding, other proteins that are phosphorylated are also detected on the membrane as the total cell lysate samples were used, therefore the results for this would be inaccurate. In order to solve this problem an Immunoprecipitation was conducted to precipitate out the PDGF receptor. This employed 5 µg/ml of CTB antibody to bind the PDGF receptor in the total cell lysate and protein A beads to bind the complex. However this method failed as the PDGF receptor could not be precipitated out and detected at 190 kDa on the western blot (figure 3.2.1).

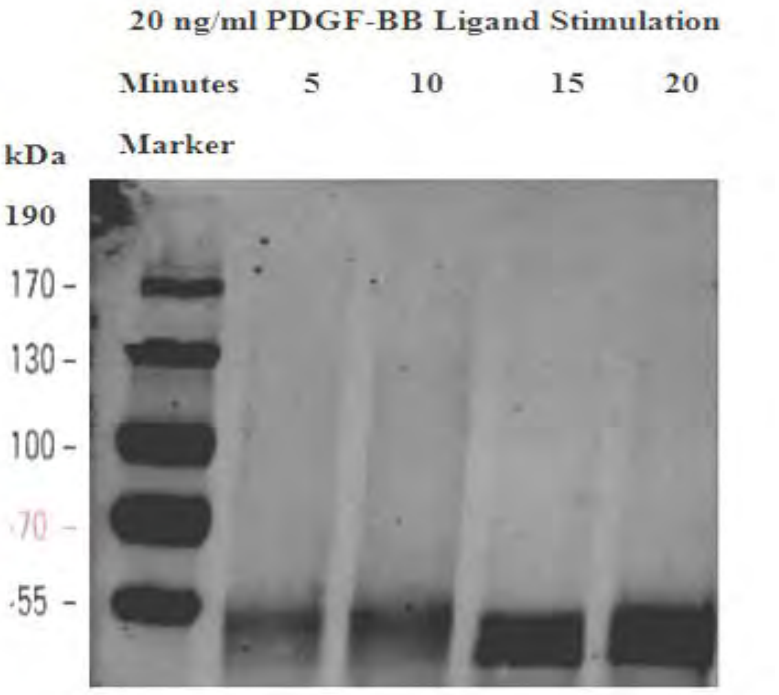

Figure 3.2.1: No signal detection for PDGF receptor immunoprecipitation.

The membrane was blotted with PDGF β Receptor antibody; however there is no signal detected at 190 kDa. There are clear antibody bands (IgG) at 55 kDa

Following the failure of the immunoprecipitation method, WGA beads were employed to precipitate the PDGF receptor out of the total cell lysate samples. The WGA beads were added and bound all glycosylated proteins, namely the PDGF receptor. This method was successful and the background banding was reduced significantly (figure 3.2.2). Furthermore, the bands observed on the membrane for the samples with WGA beads were not as clear and clean as those on the TCL. This method still requires further optimization in order to obtain clearer and cleaner membranes, nonetheless the results presented that fMLP does indeed potentiate PDGF-BB ligands ability to phosphorylate the PDGF receptor.

Furthermore, the results observed for the WGA bound PDGF receptor on the p-Tyr and CTB blots both illustrate the increase in PDGF receptor phosphorylation as fMLP and PDGF-BB ligand are combined (figures 3.2.2). However to obtain accurate results, the bands observed on the western blots were quantified using the software GeneTools (3.2.3/4).

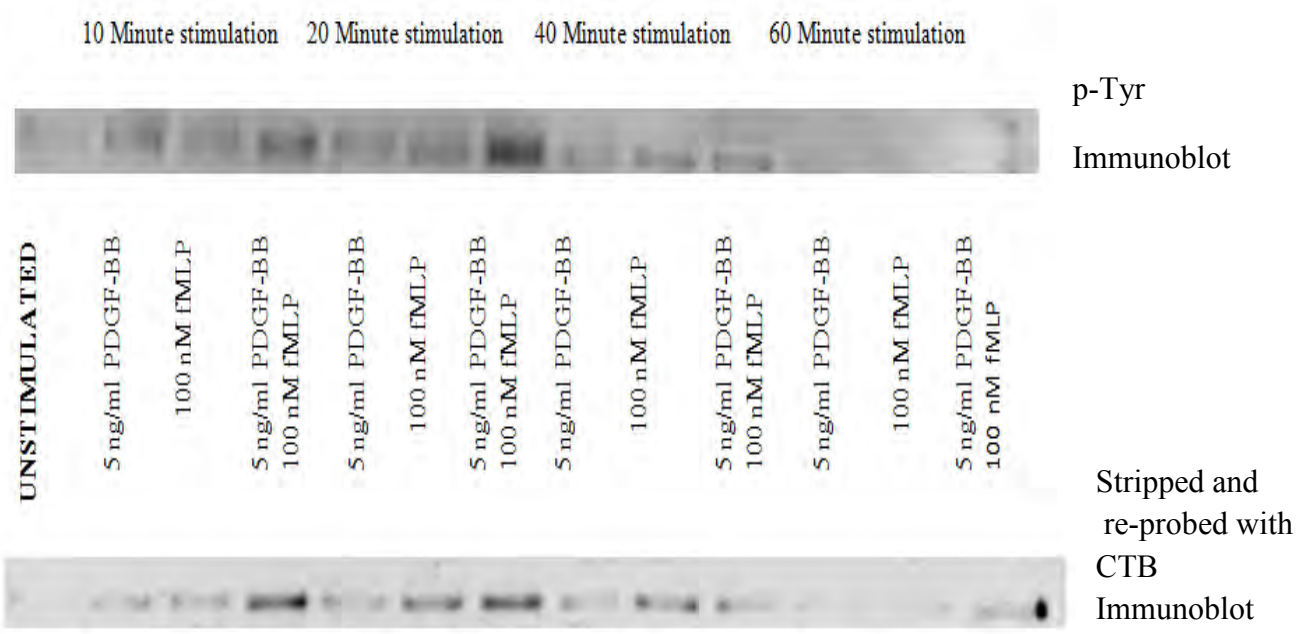

Figure 3.2.2: Western Blot of WGA bound PDGF receptor phosphorylation at 190 kDa stimulated with fMLP and PDGF-BB

Quantified p-Tyr Blot for total tyrosine phosphorylation of the WGA bound PDGF receptor

The background banding in the unstimulated sample was reduced significantly. The stimulation with PDGF-BB and fMLP combined resulted in the highest level of phosphorylation. This was followed by the samples stimulated with fMLP alone and finally those stimulated with PDGF-BB. All samples showed a period of phosphorylation followed by dephosphorylation. Samples which were stimulated with fMLP maintained a longer period of phosphorylation.

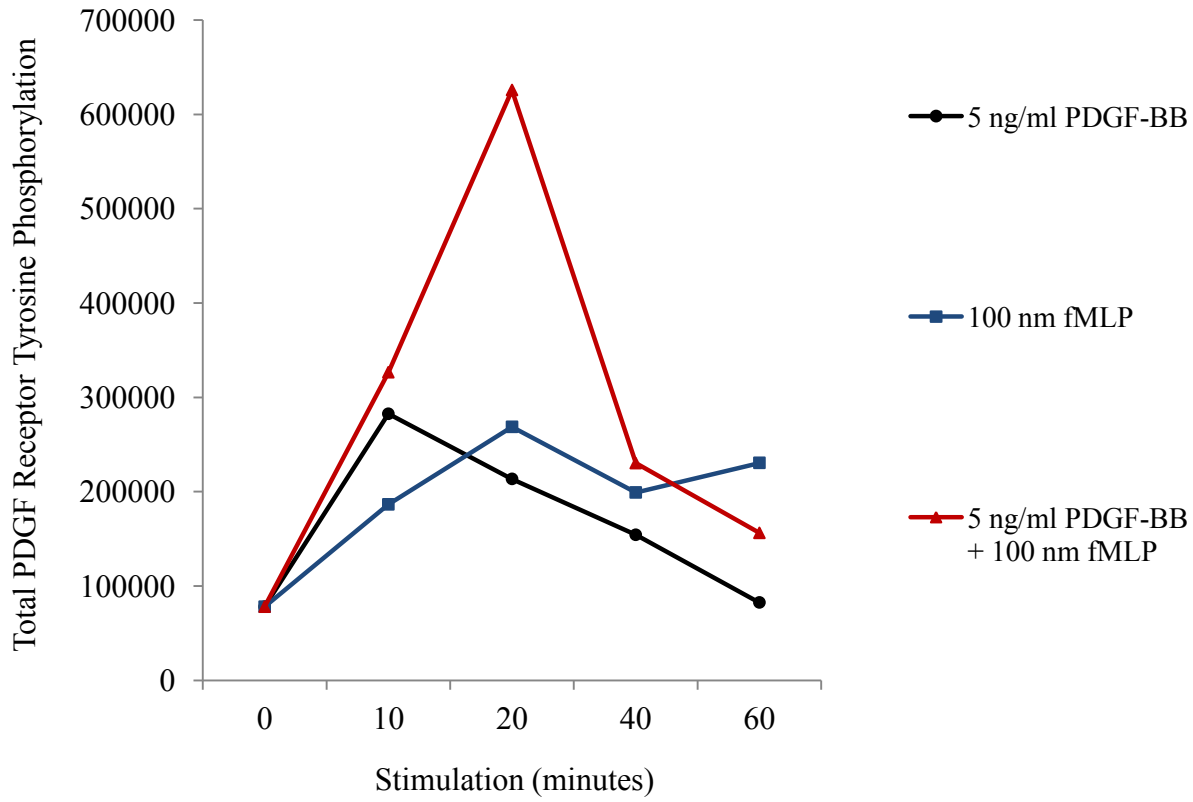

Figure 3.2.3: Phosphorylation of WGA bound PDGF receptor in response to stimulation with fMLP and PDGF-BB

Quantified CTB Blot for phosphorylation of the WGA bound PDGF β receptor

The membrane was stripped and re-probed with PDGF β Receptor antibody

Again the background banding was reduced significantly. The result is very clear as the PDGF β receptor is phosphorylated the most once fMLP and PDGF-BB are combined. This is followed by fMLP stimulation alone and finally the PDGF-BB ligand. A period of de-phosphorylation follows for all stimulations after 20 minutes. These results indicate that not only does fMLP increase PDGF receptor phosphorylation; it can still do so in the absence of the PDGF-BB ligand, hence fMLP stimulation results in higher phosphorylation than PDGF-BB ligand alone.

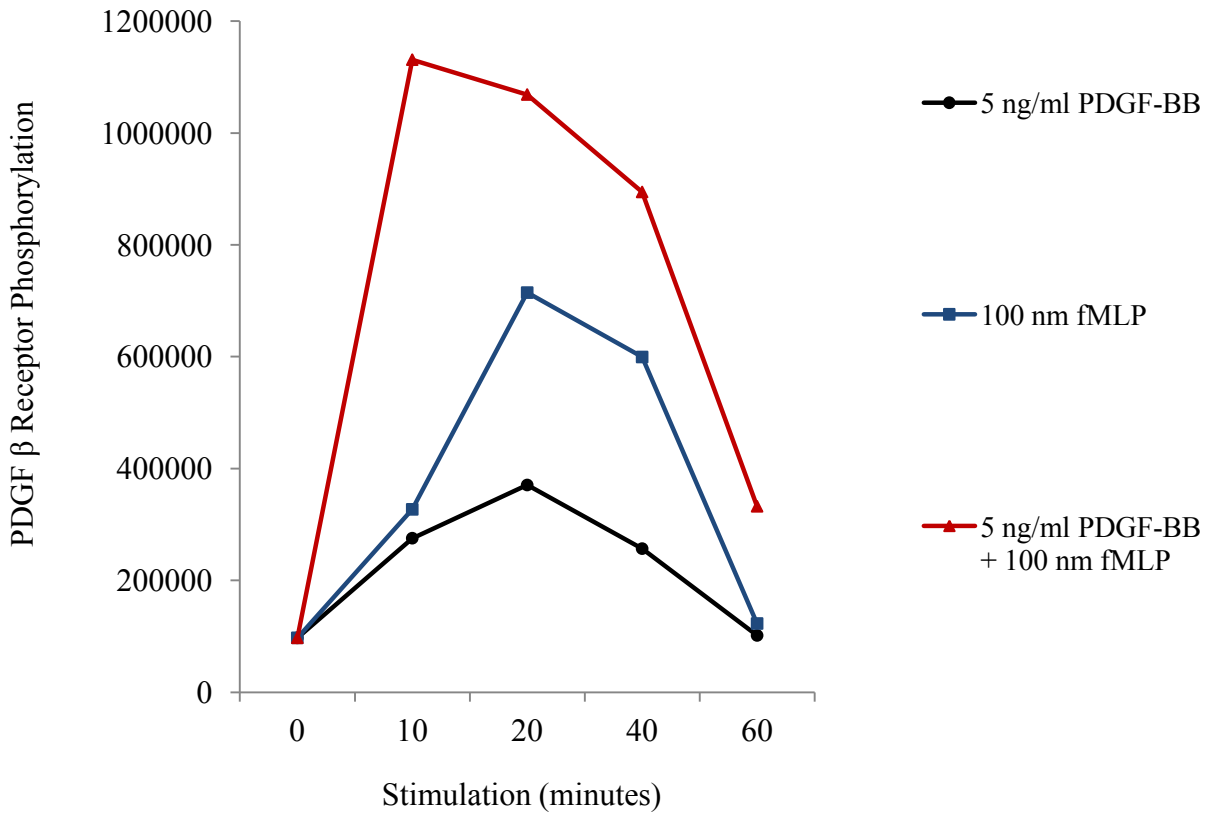

Figure 3.2.4: Phosphorylation of WGA bound PDGF β receptor in response to stimulation with fMLP and PDGF-BB

3.3 Downstream signalling effector molecules phosphorylation by fMLP

The signalling molecules downstream of the PDGF β receptor, which were investigated, were MARCKS and AKT (Protein kinase B). The phosphorylation was determined by separating the Total cell lysate samples by SDS-PAGE followed by western blot to transfer the samples onto a nitrocellulose membrane. This was immunoblotted with the phosphorylated protein antibody, and then the membrane was stripped and re-probed with the protein antibody.

3.3.1 The effect of fMLP on MARCKS phosphorylation

The phosphorylation of MARCKS (Myristoylated alanine-rich C-kinase substrate), a major substrate for protein kinase C, was investigated in order to assess if protein kinase c was activated in response to PDGF β receptor stimulation. Once the TCL samples were separated out and transferred onto the nitrocellulose membrane, it was immunoblotted with PMARCKS (phosphorylated MARCKS antibody) followed by stripping and re-probing with MARCKS protein antibody. Furthermore, the results observed for the PMARCKS blot illustrated the increase in phosphorylation as fMLP and PDGF-BB ligand are combined (figures 3.3.1a). However to obtain accurate results, the bands observed on the western blots were quantified using the software GeneTools (3.3.1b/c).

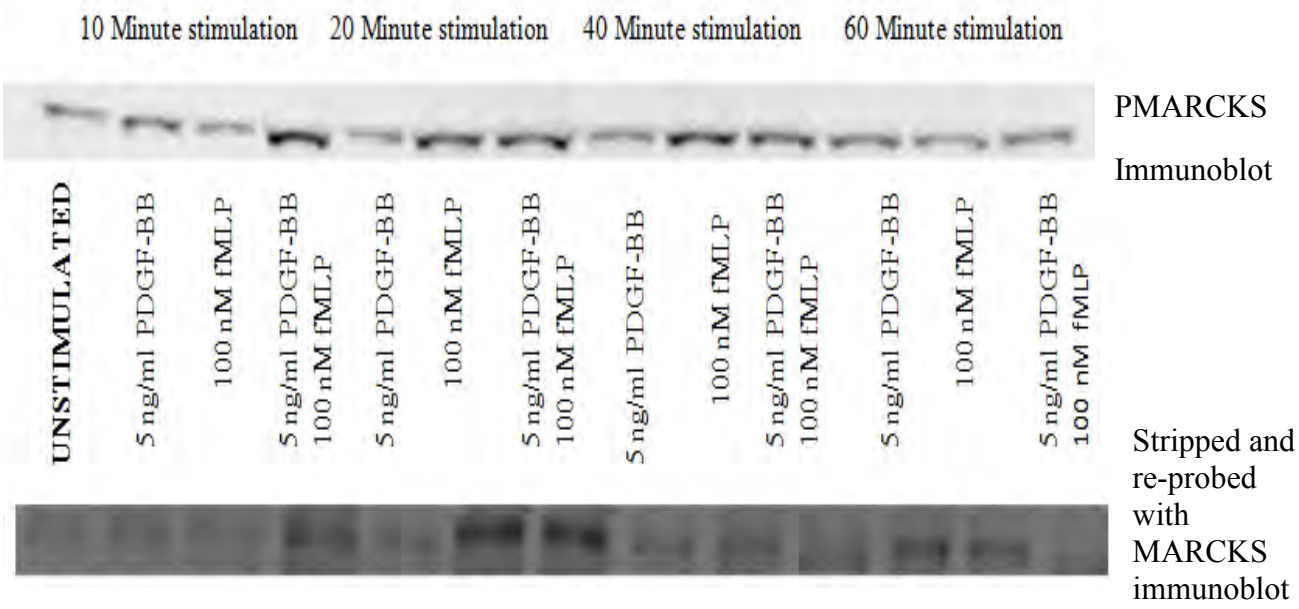

Figure 3.3.1a: Western Blot of MARCKS phosphorylation at 75 kDa stimulated with fMLP and PDGF-BB

MARCKS phosphorylation and total MARCKS protein available

In both figures, the combination of fMLP with the PDGF-BB ligand resulted in the highest level of MARCKS phosphorylation as well as in the amount of MARCKS protein available (3.3.1b/c).

There was a clear difference observed once the stimulation had begun in comparison to the unstimulated samples, therefore validating the results. Furthermore the lowest levels of protein available as well as phosphorylated protein were in the samples which were stimulated with PDGF-BB ligand alone. At 20 minutes, stimulation with fMLP alone and that combined with the PDGF-BB ligand were very similar, however the combined stimulation de-phosphorylates slightly faster. Finally for the PDGF-BB ligand stimulation, there is a slight (yet insignificant in comparison to the other two) increase at 40-60 minutes.

Therefore fMLP stimulation alone already increases levels of MARCKS phosphorylation (and thus PKC activity) as well as in addition to PDGF-BB ligand.

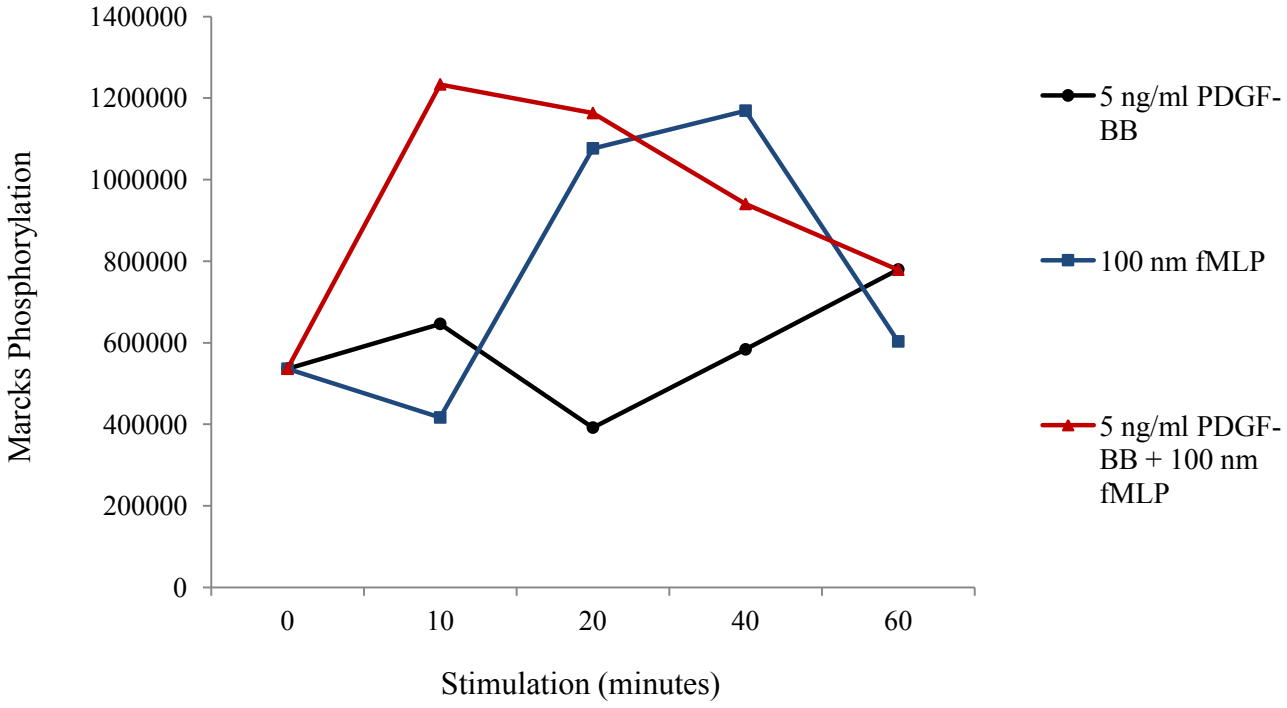

Figure 3.3.1b: Phosphorylation of MARCKS in response to stimulations with PDGF-BB and fMLP

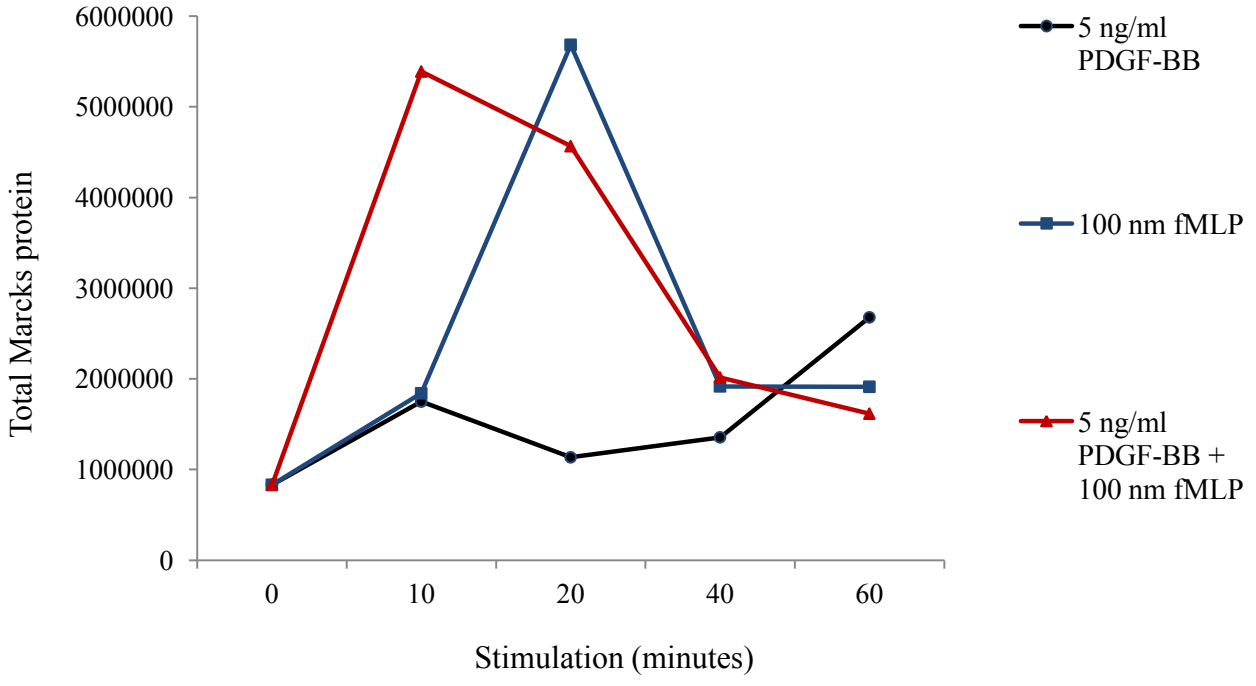

Figure 3.3.1c: Total MARCKS protein available in response to stimulations with PDGF-BB and fMLP

3.3.2 The effect of fMLP on AKT (protein kinase B) phosphorylation

The TCL samples were separated out and transferred onto the nitrocellulose membrane, which was then immunoblotted with PAKT (phosphorylated AKT antibody) followed by stripping and re-probing with AKT protein antibody. Furthermore, the results observed for the AKT blot illustrated the increase in phosphorylation as fMLP and PDGF-BB ligand are combined, however stimulation with PDGF-BB ligand alone also results in a high level of AKT phosphorylation (figures 3.3.2a). Furthermore in order to obtain accurate results, the bands observed on the western blots were quantified using the software GeneTools (3.3.2b/c).

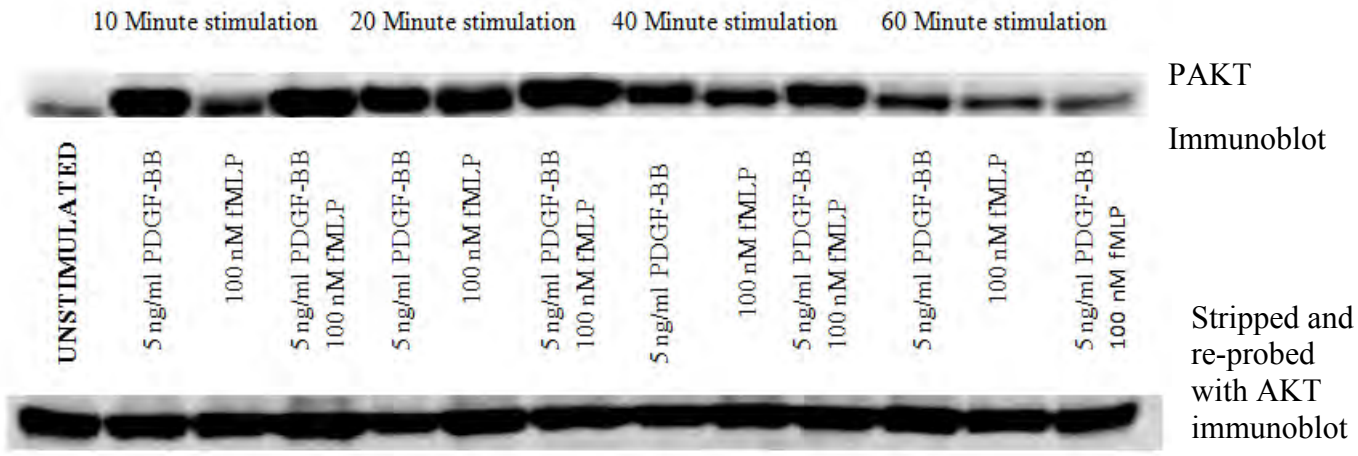

Figure 3.3.2a: Western Blot of AKT phosphorylation at 60 kDa stimulated with fMLP and PDGF-BB

AKT phosphorylation and total AKT protein available

The level of phosphorylation in the unstimulated sample is very low in all 3 stimulations (figure 3.3.2b), although there is a high level of protein available (figure 3.3.2c). At 10 minutes, the stimulation with combined fMLP and PDGF-BB has the highest phosphorylation, followed by PDGF-BB alone and finally fMLP. Comparing this to figure 3.3.6, the protein levels in the combination sample remain high, however those of PDGF-BB and fMLP alone decreases significantly, and continues to do so until 20 minutes.

After 20 minutes, the period of phosphorylation ends for PDGF-BB and fMLP combined where it has reached a peak, and begins to undergo dephosphorylation and thus decrease. Nonetheless the protein levels still remain high but dip slightly at 40-60 minutes.

After 10 minutes, the period of phosphorylation ends for PDGF-BB and fMLP stimulations alone, reaching a slight peak. However although it decreases, there are high protein levels available which continue to increase. This doesn't seem to affect the phosphorylation as dephosphorylation has already begun.

Therefore as fMLP is combined with the PDGF-BB ligand, higher levels of AKT phosphorylation are observed.

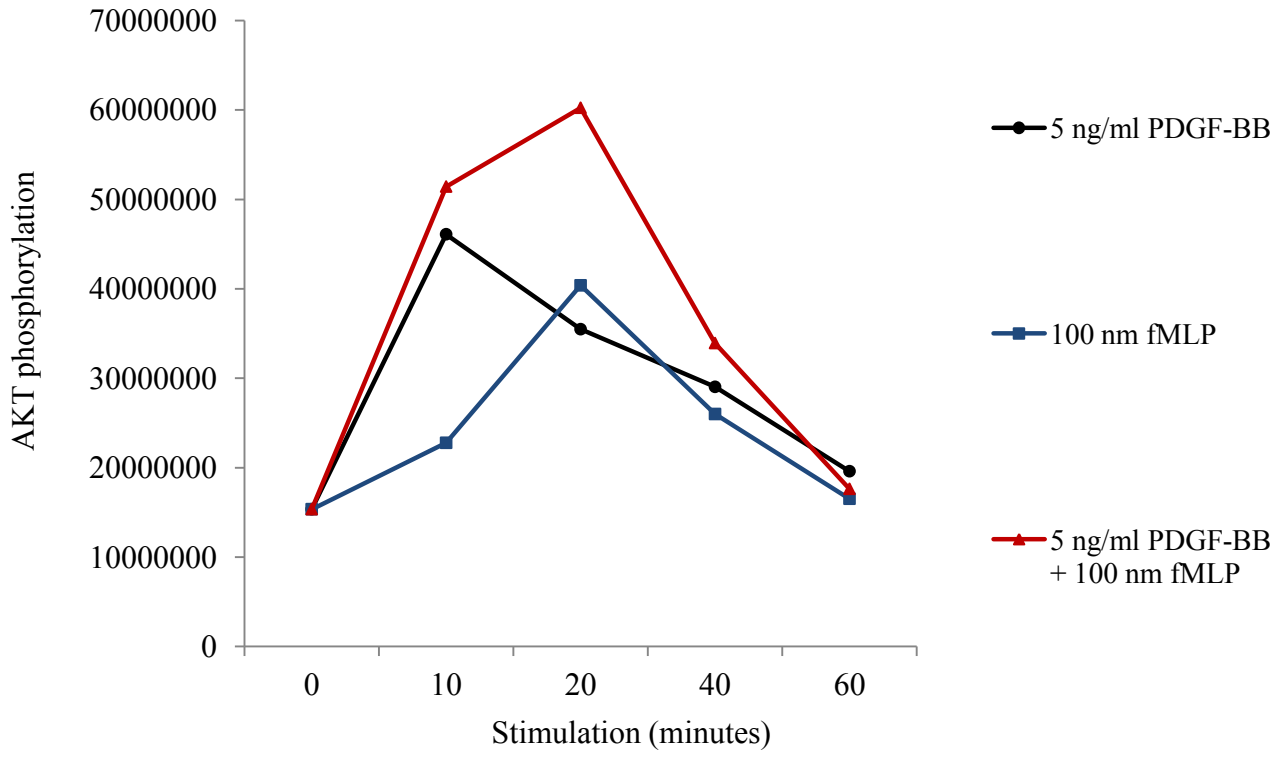

Figure 3.3.2b: Phosphorylation of AKT in response to stimulation with fMLP and PDGF-BB

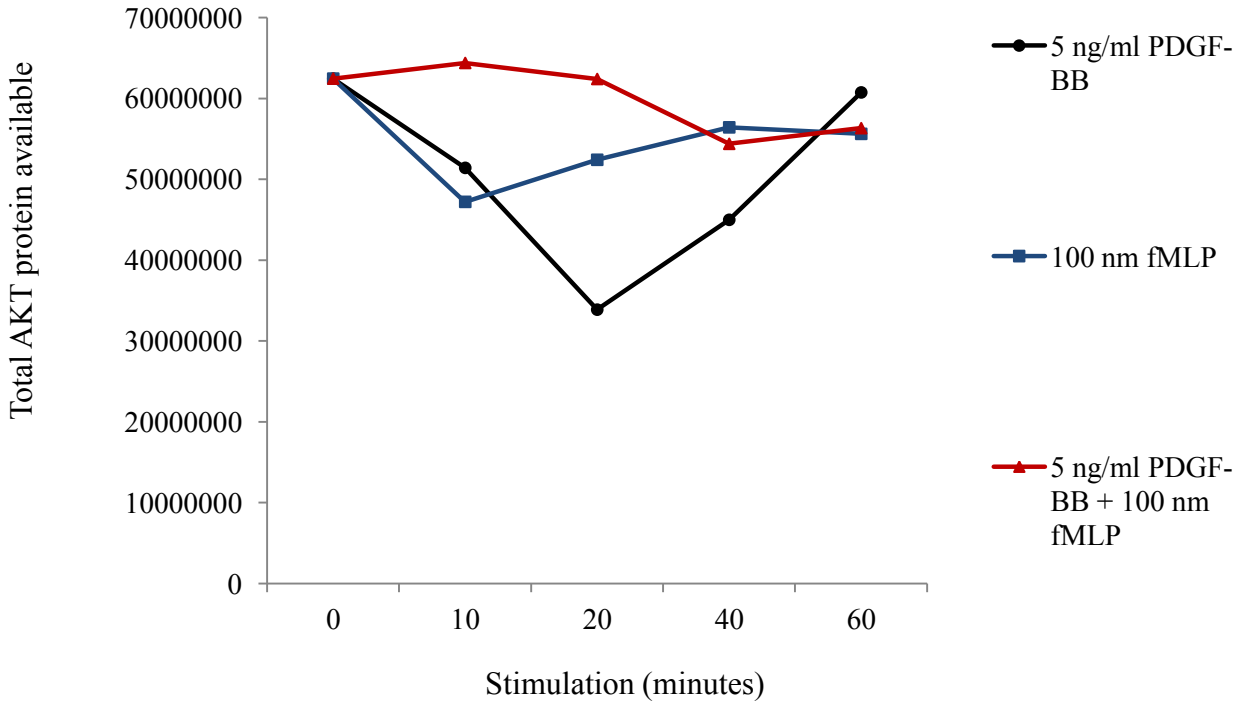

Figure 3.3.2c: Total AKT protein available in response to stimulation with fMLP and PDGF-BB

3.4 Expanding on previous findings of Lysophosphatidic acid (LPA)

In order to expand on the previous established findings that LPA potentiates the ability of PDGF-BB to phosphorylate the PDGF receptors, a control experiment was conducted to assess this. Four T 25^3 cell culture flasks were stimulated with and without LPA in the following stimulation orders; all stimulations were for 5 minutes.

1 ng/ml PDGF-BB

1 ng/ml PDGF-BB + 10 μm LPA

5 ng/ml PDGF-BB

5 ng/ml PDGF-BB + 10 μm LPA

20 ng/ml PDGF-BB

The total cell lysate was separated out via SDS-PAGE and the samples transferred onto a nitrocellulose membrane for western blotting. Once visualized via enhanced chemiluminescence the results confirmed previously established findings (figure 3.4.1).

Furthermore, to visualize this data clearly, the bands were quantified using the software GeneTools (figure 3.4.2)

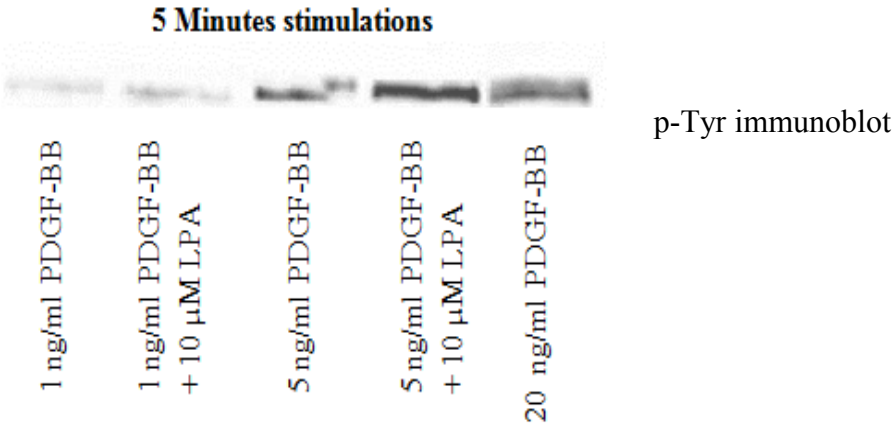

Figure 3.4.1: Western blot of PDGF receptor phosphorylation at 190 kDa stimulated by PDGF-BB ligand and LPA

PDGF receptor tyrosine phosphorylation

The ability of the PDGF-BB ligand to phosphorylate the phosphorylation of the PDGF receptor is clearly potentiated. The combination of LPA induces a two fold increase in phosphorylation. Furthermore the addition of LPA produces phosphorylation results slightly higher than stimulation with even 20 ng/ml PDGF-BB ligand. Therefore previously established findings are re-confirmed.

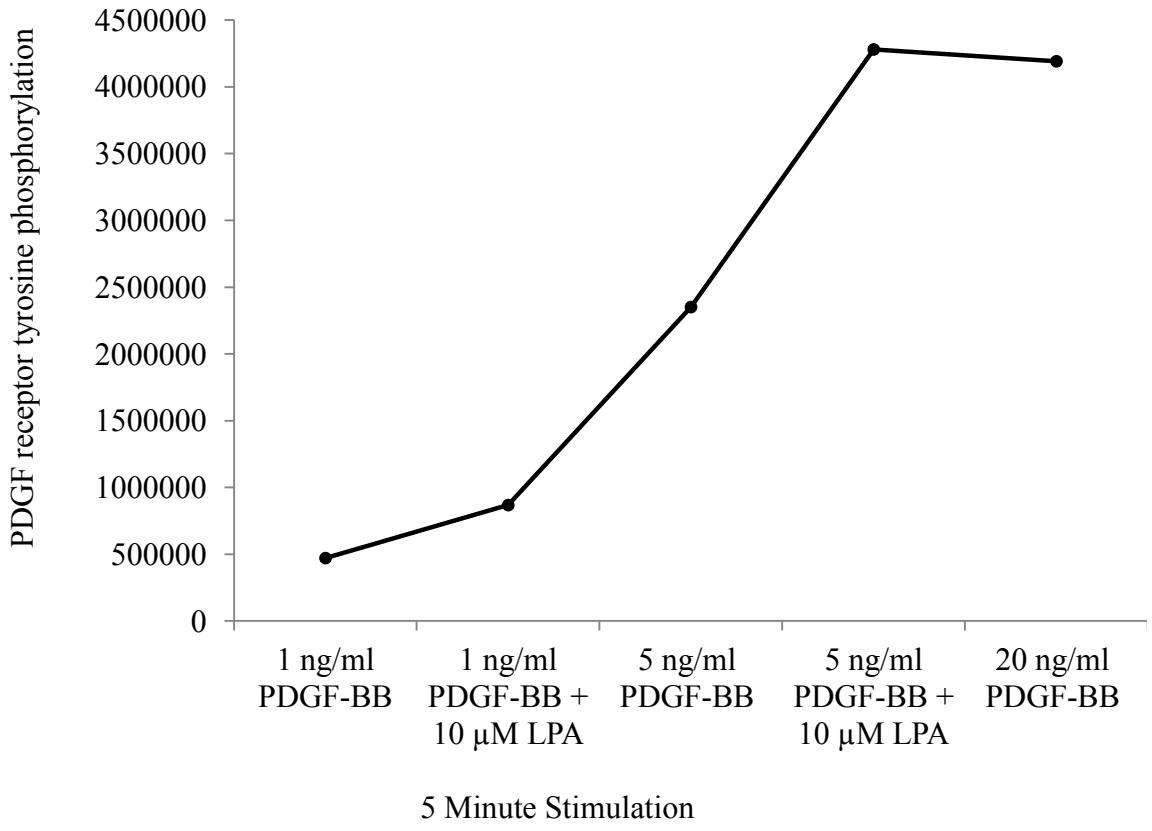

Figure 3.4.2: Phosphorylation of the PDGF receptor in response to stimulation with PDGF-BB and LPA

3.5 Total PDGF receptor tyrosine phosphorylation & PDGF β receptor by stimulation with LPA

Furthermore to further assess the effects of LPA on the PDGF receptors, stimulations over a period of an hour were assessed. The TCL were separated via SDS-PAGE and transferred onto a nitrocellulose membrane using western blotting. Once visualized via enhanced chemiluminescence (figure 3.5.1) the results were also quantified to assess the data more accurately (3.5.2/3).

There is a high level of background banding in the unstimulated samples, as the total cell lysate were used. However the main pattern which can be detected from the western blot is that as time prolongs, the PDGF receptor phosphorylation decreases; finally in the samples which contain the combination of LPA and PDGF-BB this only seems to be increasing. Unfortunately the IP with CTB antibody for this did not work, neither did the WGA beads.

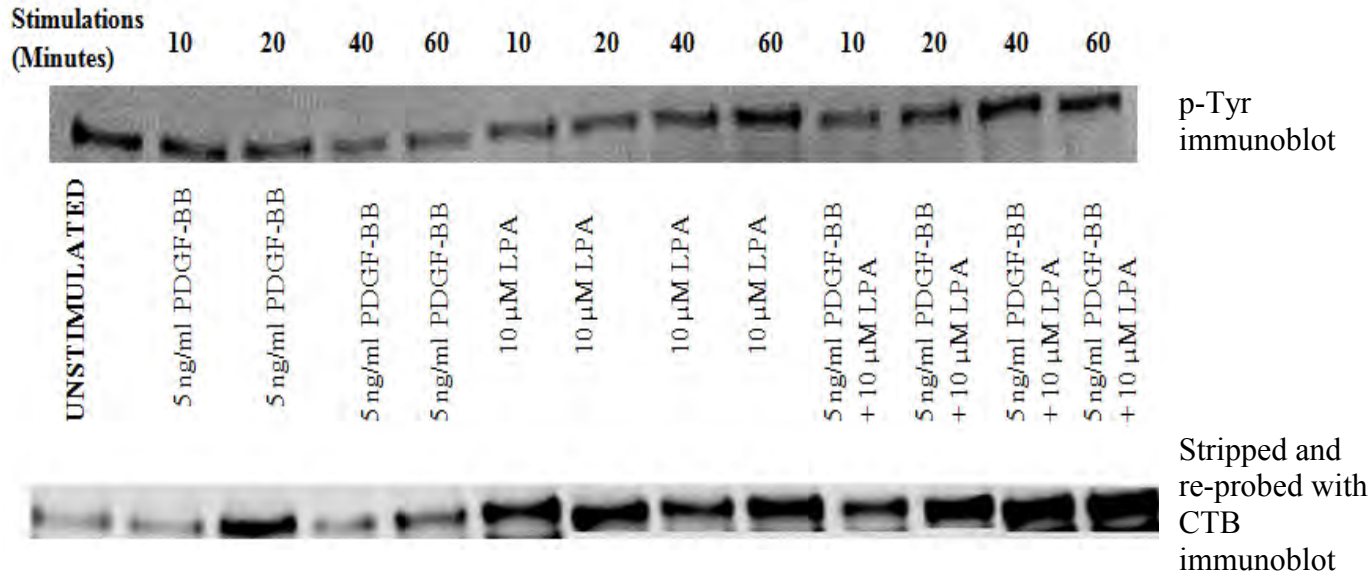

Figure 3.5.1: Western blot of PDGF receptor phosphorylation at 190 kDa stimulated by PDGF-BB ligand and LPA

Quantification of p-Tyr and CTB immunoblots stimulated with PDGF-BB and LPA

On figure 3.5.2 the clear background banding can be observed as a peak.

p-Tyr immunoblot:

If the unstimulated sample point were to be dis-regarded, the data shows positive results that LPA does induce and potentiate PDGF receptor phosphorylation. At ten minutes the highest phosphorylation is recorded for the sample containing the PDGF-BB alone, however this decreases almost immediately and dephosphorylation occurs.

For the samples containing LPA alone and also the combination both illustrate low levels of phosphorylation initially at 10 minutes, but these increase immediately and continue to do so even at 60 minutes.

CTB immunoblots:

When observing the phosphorylation of the PDGF β receptor, lower levels of background banding is present in the unstimulated sample. At 10 minutes stimulation the phosphorylation of the sample containing both the LPA and PDGF-BB is fairly low but continues to increase, surpassing the other two stimulations and continues to have high levels of phosphorylation even at 60 minutes. LPA alone results in higher phosphorylation levels than PDGF-BB, however both increase then reach a peak at 20 minutes, after which they undergo de-phosphorylation until 40 minutes, before slightly increasing again.

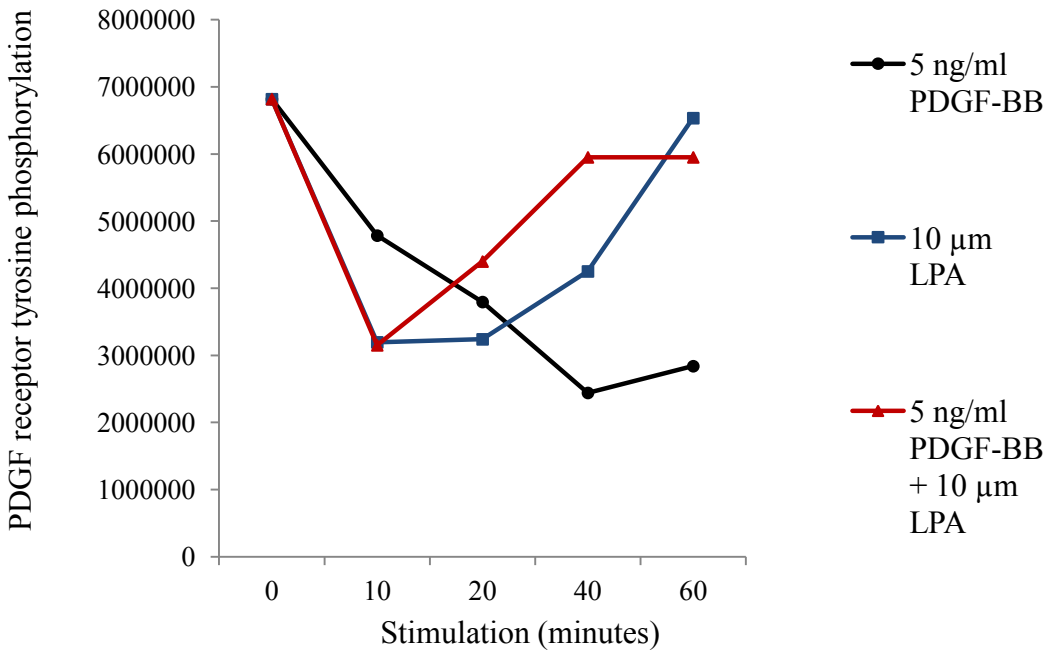

Figure 3.5.2: Phosphorylation of PDGF tyrosine receptor in response to stimulation by LPA and PDGF-BB

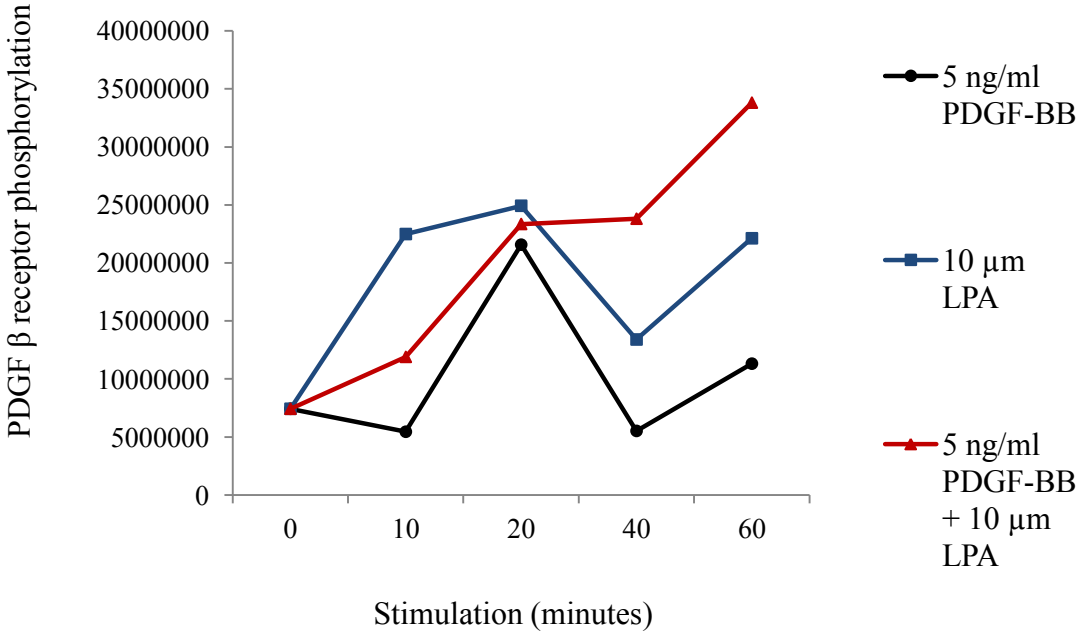

Figure 3.5.3: Phosphorylation of PDGF β receptor in response to stimulation with LPA and PDGF-BB

3.6 The effect of LPA on MARCKS phosphorylation

The phosphorylation of MARCKS, a major substrate for protein kinase C, was investigated in order to assess if protein kinase c was activated in response to PDGF β receptor stimulation with LPA. Once the TCL samples were separated out and transferred onto the nitrocellulose membrane, it was immunoblotted with PMARCKS (phosphorylated MARCKS antibody) followed by stripping and re-probing with MARCKS protein antibody. Furthermore, there was a minor error made when stimulating the samples, resulting in the use of Dulbecco's Modified Eagle's Medium containing 10% Fetal bovine serum and 1% Penicillin and Streptomycine for the stimulations. Therefore the stimulation medium contained growth factors which can increase and affect the levels of phosphorylation observed.

The results observed for the P/MARCKS blot (figure 3.6.1) were difficult to interpret on the western blot and thus were quantified using the software GeneTools (figures 3.6.2/3).

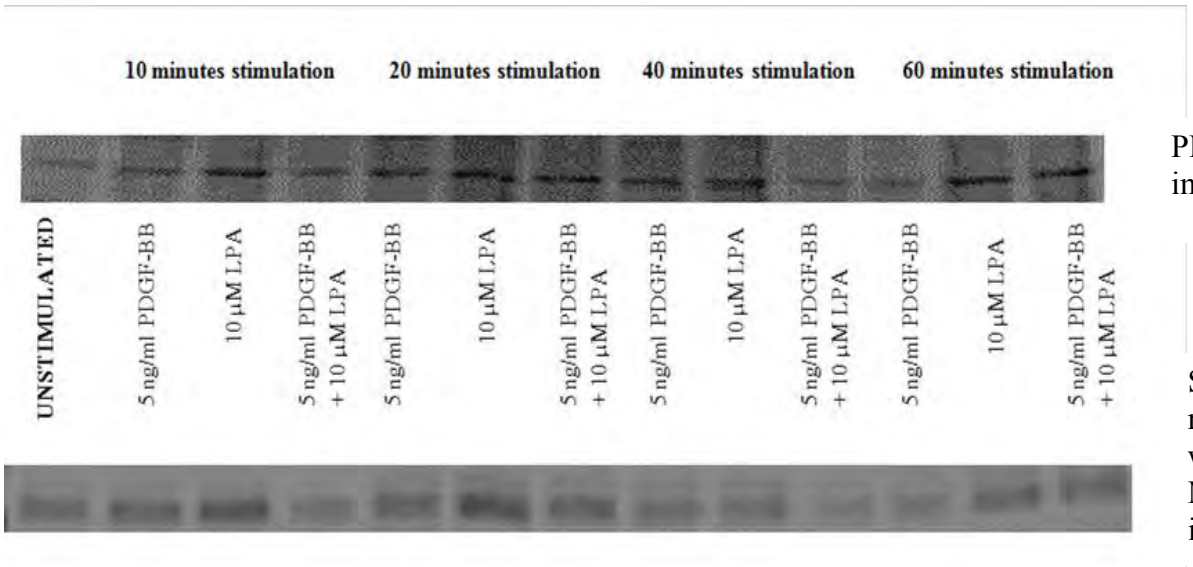

Figure 3.6.1: Western blot of MARCKS phosphorylation at 75 kDa stimulated by PDGF-BB ligand and LPA

MARCKS phosphorylation and total MARCKS protein available

During the first 10-20 minutes stimulations the combination of LPA with the PDGF-BB ligand has low levels of MARCKS phosphorylation. There are higher levels of MARCKS phosphorylation with fMLP and PDGF-BB lone stimulations (figure 3.6.2). This is translated in the level of MARCKS protein available as the sample with the combination has the lowest protein level.

However after 20 minutes, there is a sudden increase in both the level of MARCKS protein available as well as the phosphorylation of it. This exceeds both the level of MARCKS phosphorylation observed for the samples with the lone stimulations. Therefore the increase noted in MARCKS phosphorylation after combining LPA with PDGF-BB ligand requires a period of time, but it does activate MARCKS.

Furthermore as noted beforehand, the addition of medium which contained growth factors could have had a significant effect on the results observed. Therefore a repeat is crucial.

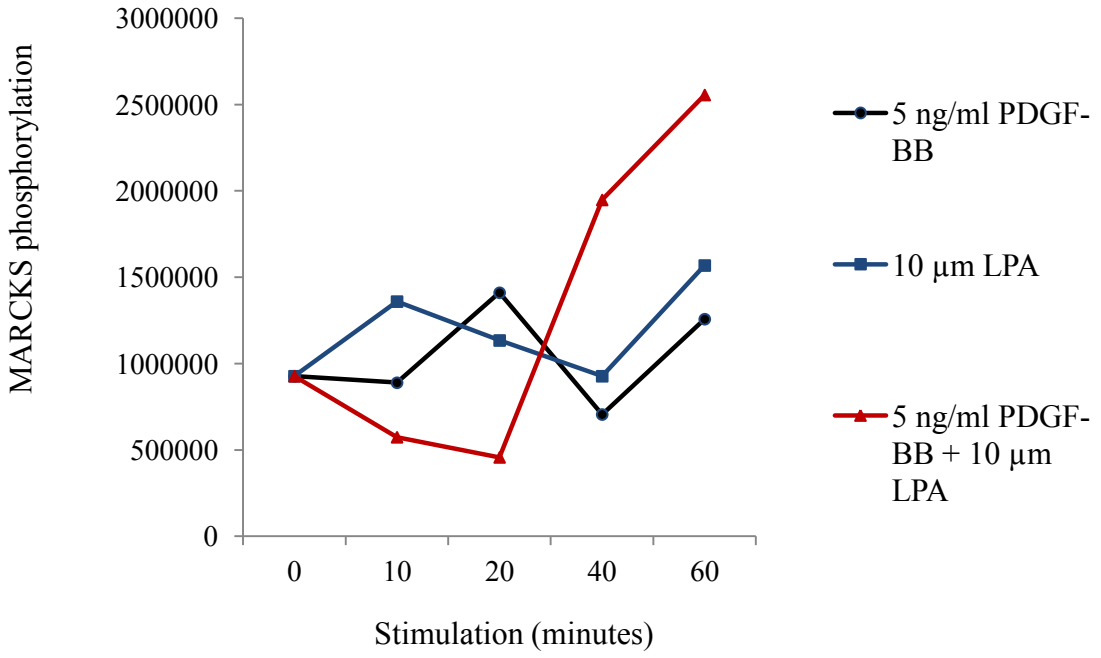

Figure 3.6.2: Phosphorylation of MARCKS in response to stimulations with PDGF-BB and LPA

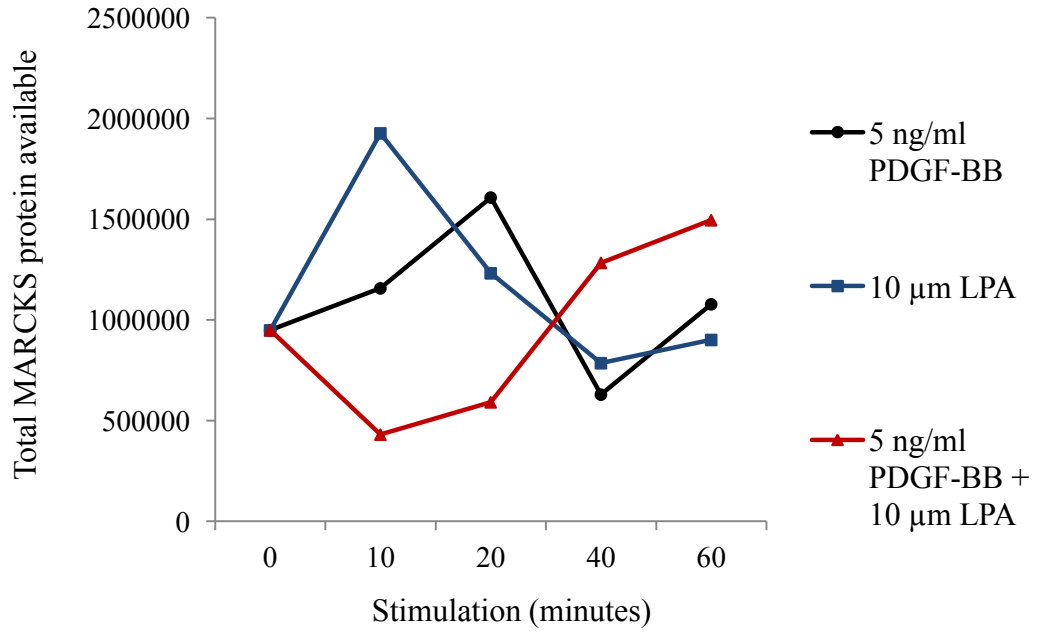

Figure 3.6.3: Total MARCKS protein available in response to stimulations with PDGF-BB and LPA

3.7 The effect of LPA on AKT (protein kinase B) phosphorylation

The TCL samples were separated out and transferred onto the nitrocellulose membrane, which was then immunoblotted with PAKT (phosphorylated AKT antibody) followed by stripping and re-probing with AKT protein antibody. Furthermore, there was a minor error made when stimulating the samples, resulting in the use of Dulbecco's Modified Eagle's Medium containing 10% Fetal bovine serum and 1% Penicillin and Streptomycine for the stimulations. Therefore the stimulation medium contained growth factors which can increase and affect the levels of phosphorylation observed. It was difficult to analyse the western blot from the bands alone (figure 3.7.1) thus they were quantified using the software GeneTools (figure 3.7.2/3).

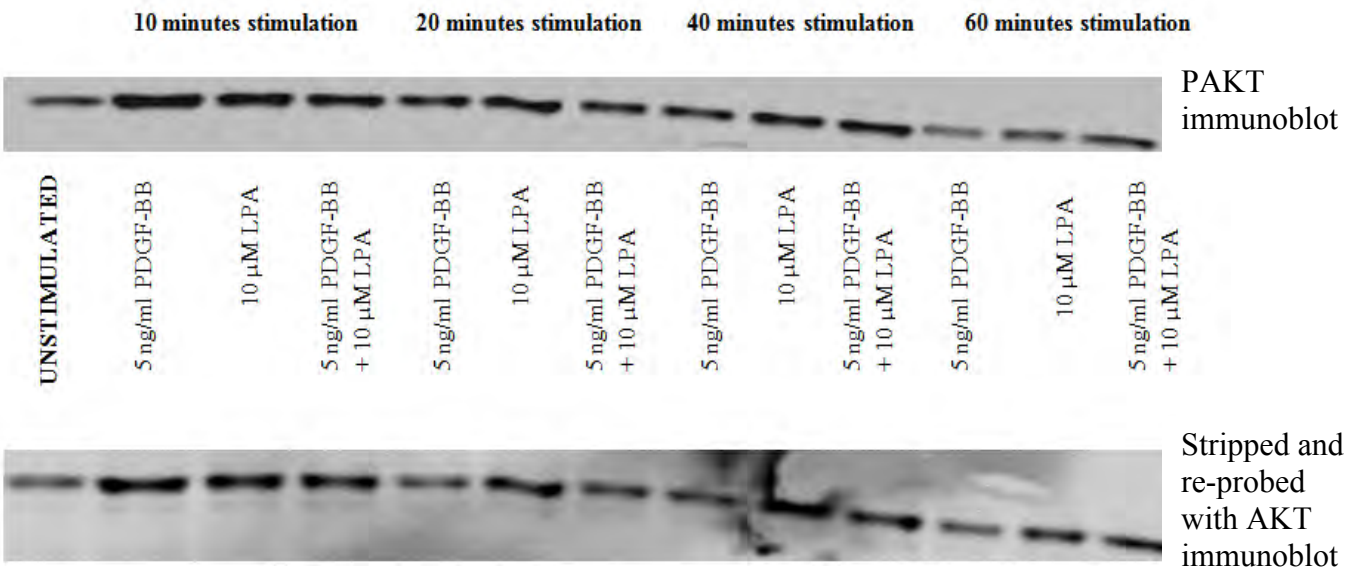

Figure 3.7.1: Western Blot of AKT phosphorylation at 60 kDa stimulated with LPA and PDGF-BB

AKT phosphorylation and total AKT protein available

The sample containing both LPA and PDGF-BB has the lowest level of phosphorylation. Initially at 10 minutes, the highest level of AKT phosphorylation is observed for the sample stimulated with PDGF-BB ligand alone. This then decreases almost immediately undergoing de-phosphorylation. However with the LPA lone stimulation the phosphorylation is slightly lower than PDGF-BB alone, also peaking at 10 minutes and then gradually decreasing.

The levels of protein correspond to the level of phosphorylation. Although due to the error of using medium which contained growth factors, the phosphorylation may be exaggerated, particularly within the sample stimulated with PDGF-BB ligand alone and thus preventing any noticeable change in phosphorylation.

A repeat is crucial.

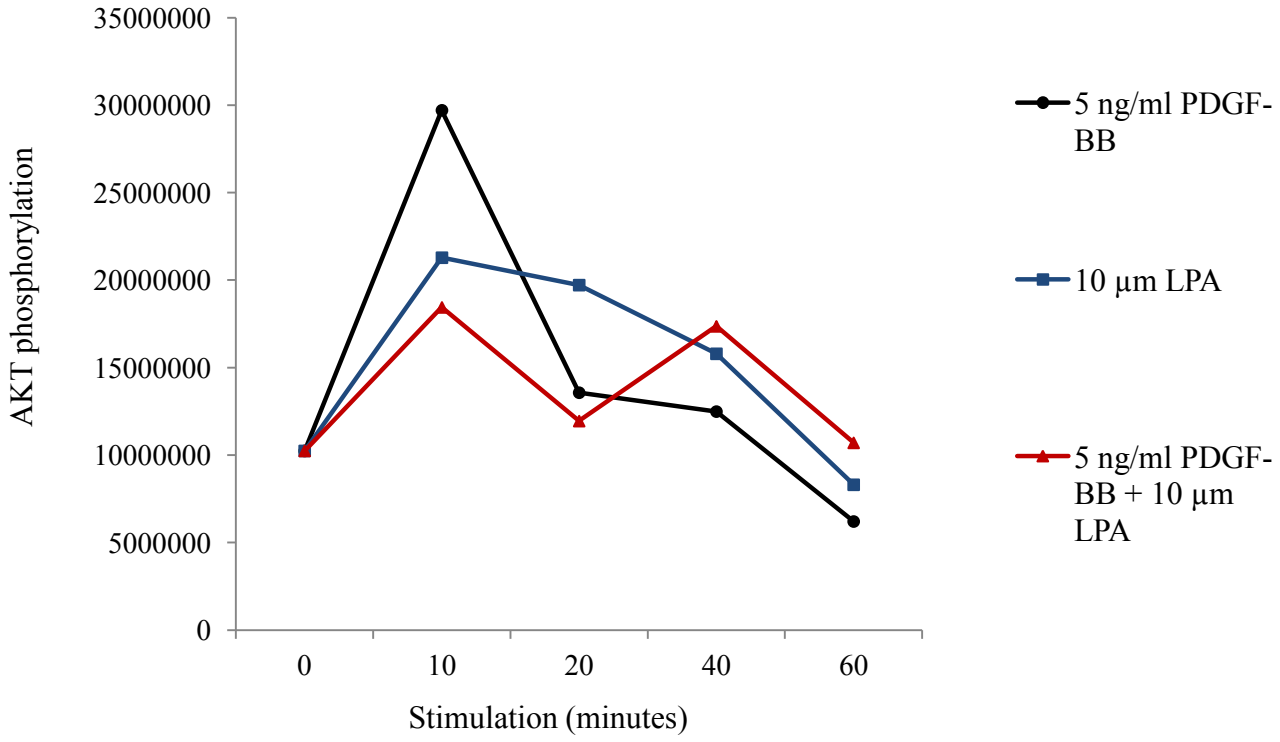

Figure 3.7.2: Phosphorylation of AKT in response to stimulation with LPA and PDGF-BB

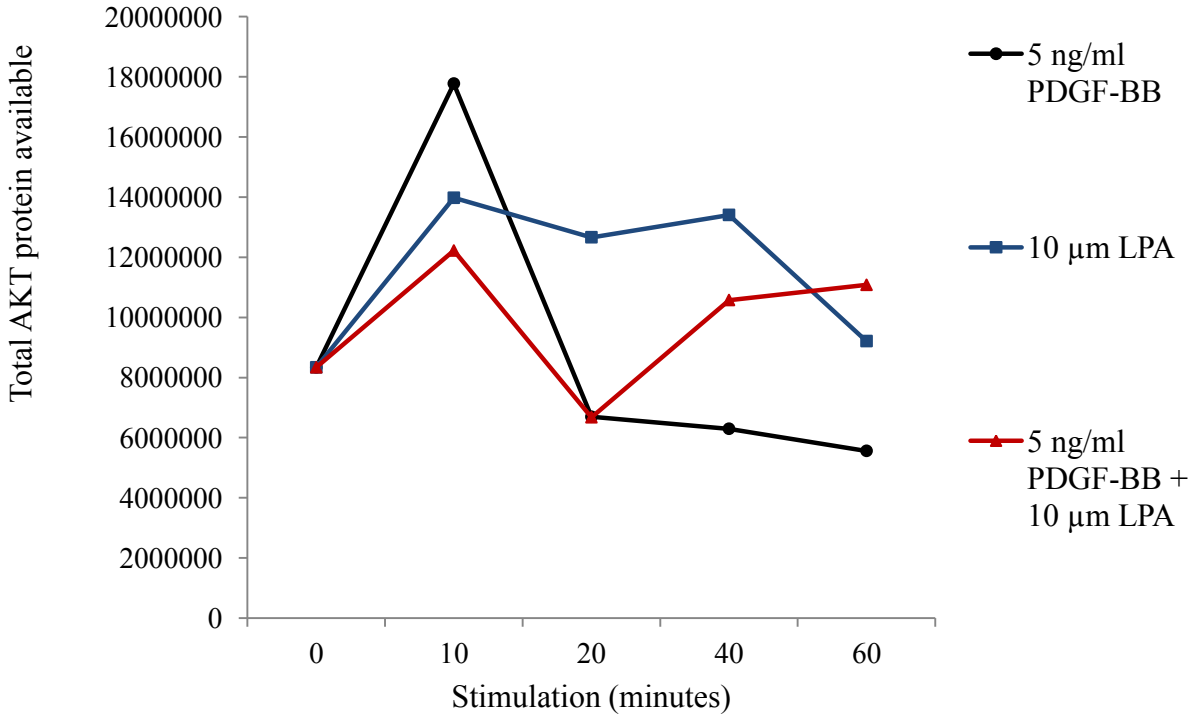

Figure 3.7.3: Total AKT protein available in response to stimulation with LPA and PDGF-BB

3.8 The effect of LPA on ERK protein phosphorylation

The last downstream effector molecule which was investigated for stimulations with LPA was the phosphorylation of ERK 1 at 44 kDa and ERK 2 at 42 kDa. This stimulation also employed the error which used medium that contained growth factors for stimulation. The TCL samples were separated out and transferred onto the nitrocellulose membrane, which was then immunoblotted with PERK (phosphorylated ERK antibody) followed by stripping and re-probing with ERK protein antibody, which will both bind the two different proteins (figure 3.8.1). Again the bands were quantified as it was too difficult to assess the results otherwise (figures 3.8.2/3).

ERK 1 Phosphorylation:

Figure 3.8.1: Western Blot of ERK 1 phosphorylation at 44 kDa stimulated with LPA and PDGF-BB

ERK 1 Phosphorylation

ERK 1 phosphorylation is not increased by the combination of LPA with PDGF-BB.

The highest level of phosphorylation is observed for the sample which was stimulated with the PDGF-BB ligand alone. This is followed by the sample stimulated with LPA alone and finally that which was stimulated with the combination.

However when observing the levels of ERK 1 protein available, the highest levels are observed for samples which had been stimulated with LPA. In comparison the lowest levels of ERK 1 protein is observed in the sample where only PDGF-BB has been used to stimulated.

These results could indicate that all of the protein (or most of it) was phosphorylated with the stimulation of PDGF-BB, however this could be a major error due to the medium used.

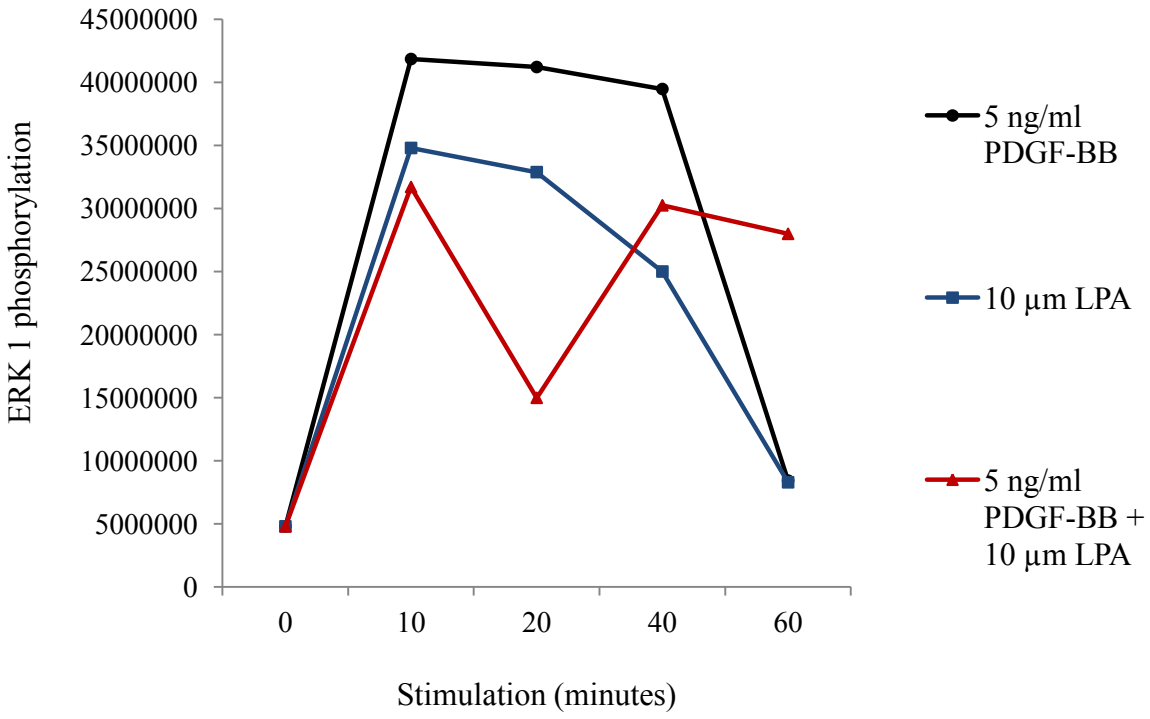

Figure 3.8.2: Phosphorylation of ERK 1 in response to stimulation with LPA and PDGF-BB

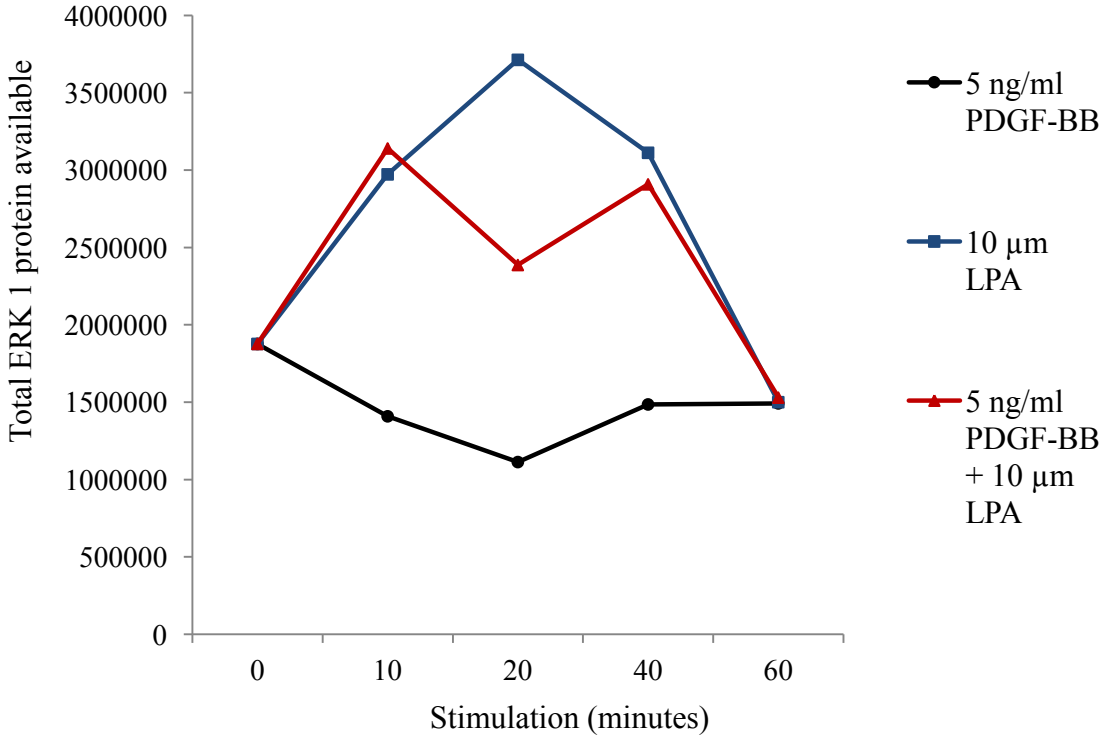

Figure 3.8.3: Total ERK 1 protein available in response to stimulation with LPA and PDGF-BB

ERK 2 Phosphorylation:

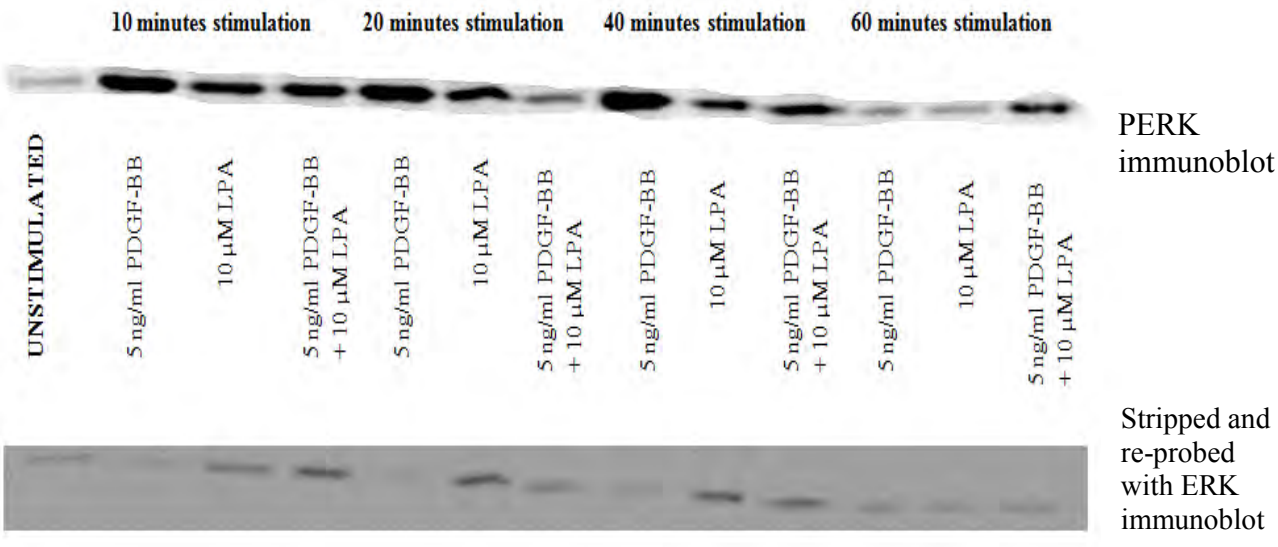

Figure 3.8.4: Western Blot of ERK 2 phosphorylation at 42 kDa stimulated with LPA and PDGF-BB

The bands were quantified using the software Genetools (figures 3.8.5/6).

ERK 2 phosphorylation is not increased by the combination of LPA with PDGF-BB. The same pattern is observed as for ERK 1.

There are high levels of protein available for samples stimulated with LPA; however these illustrate very low levels of phosphorylation. In comparison there are very low levels of protein available for the sample stimulated with PDGF-BB ligand alone, and yet it has the highest level of phosphorylation.

This could conclude that PDGF receptor phosphorylation doesn't activate ERK 2; however this could also be a major error due to the medium used. Therefore a repeat is crucial

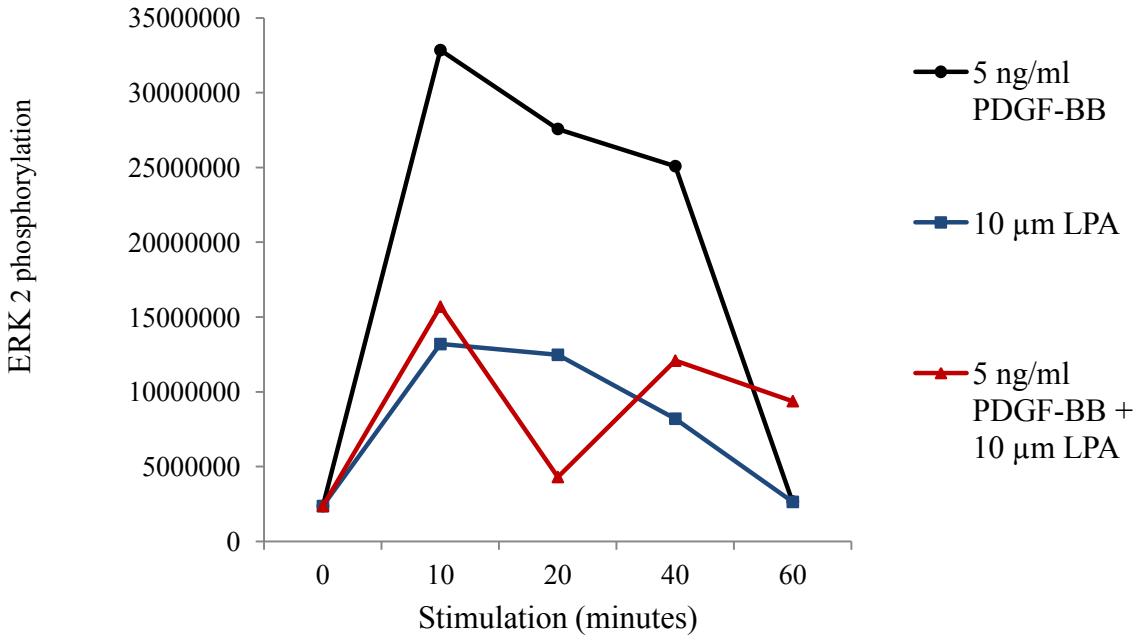

Figure 3.8.5: Phosphorylation of ERK 2 in response to stimulation with LPA and PDGF-BB

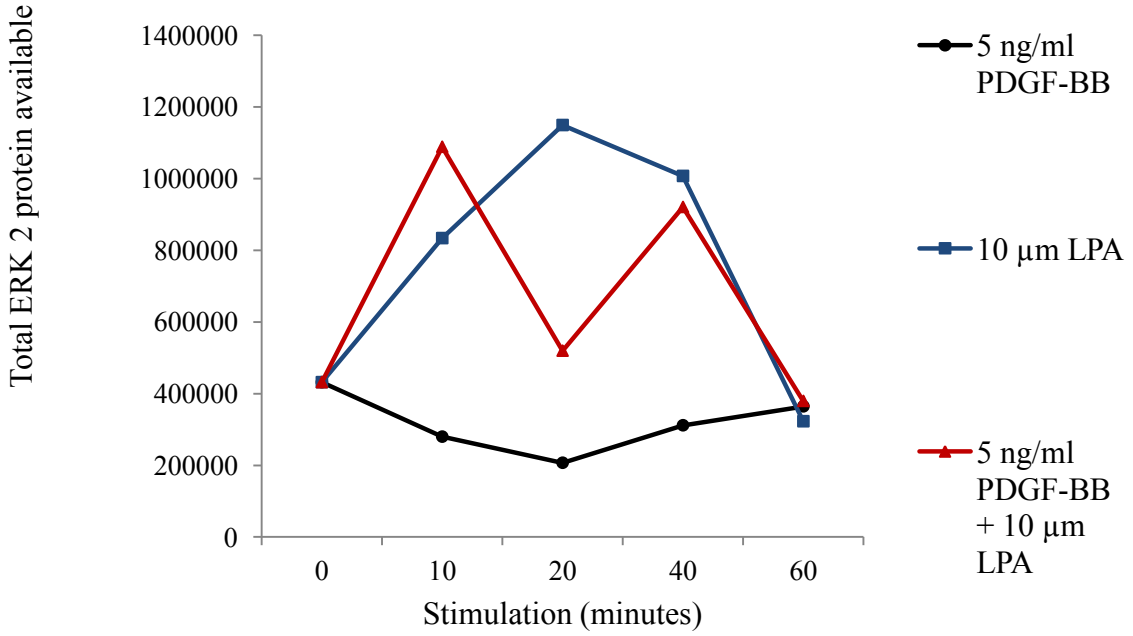

Figure 3.8.6: Total ERK 2 protein available in response to stimulation with LPA and PDGF-BB

4. Discussion

4.1 fMLP potentiates PDGF-BB ligand ability to phosphorylate the PDGF receptors

The bands observed on figure 3.1.1a, which were the total cell lysate samples stimulated with fMLP and PDGF-BB, clearly illustrated that there was a high level of background banding on both the p-Tyr and CTB immunoblots. In order to assess the extent of background banding, the bands were quantified using the software GeneTools, and a significant level was observed. This was a problem as there could not be a real change in phosphorylation observed due to the peak in the unstimulated sample. This was due to the fact that the total cell lysate contains many other proteins as this has not been specifically purified for the PDGF receptor. Therefore it is expected that there will be many other proteins present in the sample, and thus results in a high background banding. It is very important to eliminate the background banding, as this gives an inaccurate result and the phosphorylation cannot be observed correctly.

Unfortunately the IP method with CTB antibody did not work (figure 3.2.1) as there was a problem with the protein A beads and the antibody itself. An extensive period was spent attempting to precipitate the PDGF receptor out, however these were all futile and had no success. Therefore WGA beads were used, which contains lectin, this binds all glycosylated proteins within the sample e.g. PDGF receptor (Piercenet., 2012). However the problem with this method was that it still required an extensive amount of optimization as the bands observed on figure 3.2.2 are not clean and clear in comparison to those observed on the total cell lysate immunoblots. Again with the use of WGA beads, glycosylated proteins are bound; this could bind other proteins and therefore result in slightly higher levels of phosphorylation

observed. It would have been more appropriate to have used the IP method which employed the C terminal antibody which would have directly bound to the PDGF β receptor.

Although the method employing the WGA beads still required some optimization, the results observed on the western blot figure 3.2.2 were quantified using the software GeneTools, and the data obtained was very good. The background banding in the unstimulated sample had been reduced significantly on both the immunoblots (figures 3.2.3/4). When analysing the data from the p-Tyr blot, it was very clear that PDGF tyrosine phosphorylation was enhanced significantly in the samples stimulated with the combination of 5 ng/ml PDGF-BB ligand and 100 nM fMLP. The second highest phosphorylation observed was in the samples stimulated with fMLP alone and then finally PDGF-BB stimulation alone. The same results were observed on the CTB immunoblots. This data suggests that even in the absence of PDGF-BB ligand stimulation, fMLP is still capable of activating and phosphorylating the PDGF receptors. Therefore this would implicate that fMLP is directly activating PKC since recent studies have shown it to be a crucial point of activation as it promotes receptor recycling from early endosomes (Hellberg *et al.,* 2009; Karlsson *et al.*, 2006).

In order to further investigate this new finding, the phosphorylation of MARCKS was monitored in response to stimulation with fMLP and PDGF-BB ligand. Myristoylated alanine-rich C-kinase substrate also known as MARCKS, is encoded for by the MARCKS gene and is regulated by PKC. Therefore the higher levels of activated PKC, the higher levels of phosphorylated MARCKS.

The western blot on figure 3.3.1a clearly illustrated the increase in MARCKS phosphorylation in the samples which were stimulated with fMLP, in comparison to stimulation with PDGF-BB ligand alone. Once this was quantified the data was much more easily to analyse and the highest peaks of phosphorylation are observed for the samples

stimulated with the combination and with fMLP alone. The phosphorylation reaches a peak at 20-40 minutes where it then gradually begins to decrease. The levels of MARCKS phosphorylation observed for the samples stimulated with PDGF-BB ligand alone have very low levels. The MARCKS protein available corresponds with the phosphorylation observed (low levels of protein in sample stimulated with PDGF-BB alone etc). Furthermore, after a peak is reached in all the three different stimulations, the level of phosphorylation decreases. This is due to Protein tyrosine phosphatases as recent research has identified that this family of enzymes regulate dephosphorylation via the removal of phosphate groups from the phosphorylated proteins (figure 1.6.1a). The loss of this enzyme results in the hyperphosphorylation of the PDGF receptor which leads to the formation of tumours as cell growth and differentiation is uncontrolled (Hellberg *et al.,* 2009; Karlsson *et al.*, 2006; Fischer *et al.,* 1991). Therefore since the cells used were wild type, a period of phosphorylation followed by dephosphorylation was expected. Finally, MARCKS phosphorylation is significantly increased with the combination of fMLP with PDGF-BB and thus confirms the activation of PKC.

An important aspect to consider is that scientifically it is required to clearly show that the phosphorylation observed really is what it is perceived to be and that receptor recycling is occuring. Therefore to complete this data set initially PDGF receptor recycling and phosphorylation must be confirmed by using confocal analysis to analyse the PDGF β receptor sub-cellular localization. In addition to confirm that the receptor recycling is Rab4a dependant, by transfecting the cells with Rab4 dominant which inhibits Rab4a. An inhibitory effect of receptor phosphorylation would confirm that recycling is due to Rab4a.

Finally there are no error bars displayed on the figures, as more time was required to repeat each experiment in addition to obtaining good results (due to optimization and duration of

experiments). Therefore these experiments should be repeated in order to show that the results are reproducible.

4.2 fMLP potentiates downstream effector molecule AKT phosphorylation

The phosphorylation of the downstream effector molecule AKT was investigated. Protein kinase B also known as AKT is a protein kinase which can be either serine or threonine specific. In this project a serine 473 specific AKT was employed. The AKT protein is activated and thus phosphorylated by PIP3 second messenger. The PI3 K generates phospholipids PIP3 second messenger which binds AKT and phosphorylates it. AKT plays key roles within the cell as it stimulates cell growth and prevents apoptosis resulting in cell survival. This has been implicated in many cancers (Majewski *et al.,* 2004).

From the western blot figure 3.3.2a, the results are quite difficult to determine, with a slight indication that the combination stimulation results in the highest level of AKT phosphorylation. Therefore the bands observed were quantified using GeneTools and the graphs analysed. From figure 3.3.2b (AKT phosphorylation), the samples stimulated with PDGF-BB alone and those with the combination have a peak at 10 minutes. Subsequently, the phosphorylation of samples stimulated with PDGF-BB alone decreases almost immediately at 10 minutes and continuous to do so. However up until 20 minutes, samples stimulated with fMLP continue to rise in phosphorylation and then gradually dephosphorylate.

This was then compared to the total levels of AKT protein available, which corresponded with the results. There were higher levels of protein available for fMLP stimulation in comparison to PDGF-BB alone.

Therefore it can be assume that AKT phosphorylation is potentiated when fMLP is combined with PDGF-BB as fMLP activates PKC. A possible mechanism is that once PKC is activated the PDGF receptor is recycled which results in PDGF receptor phosphorylation. In addition this will then activate and phosphorylate PI3 K which leads to the phosphorylation and activation of AKT via PIP3 second messenger and thus AKT phosphorylation (Hellberg *et al.,* 2009; Karlsson *et al.*, 2006; Fischer *et al.,* 1991).

As mentioned beforehand there are no error bars displayed on the figures, as more time was required. Therefore these experiments should be repeated in order to show that the results are reproducible

4.3 LPA stimulated PDGF receptor phosphorylation

Previous studies have already established that LPA potentiates the ability of PDGF-BB ligand to phosphorylate the PDGF receptor and that this is due to receptor recycling as well as the activation of PKC. However before the findings on LPA were expanded, these experiments were repeated in order to obtain the same preliminary data and then continue on to investigate other downstream effector molecules as a control.

The control experiment illustrated on the western blot on figure 3.4.1 was quantified and the graph (figure 3.4.2) illustrated that LPA does potentiate PDGF receptor phosphorylation. However this experiment was only stimulated for a period of 5 minutes and thus the kinetics for LPA with PDGF-BB was not established yet. Unfortunately from this point onwards, the medium used for stimulation contained 5 % fetal bovine serum. This means the stimulation medium contained growth factors and thus could affect the results by means of increasing the levels of phosphorylation recorded, or causes inaccurate fluctuations in the phosphorylation curve. Nonetheless the results were analysed, as it was already expected for LPA to potentiate

PDGF receptor and MARCKS phosphorylation. Therefore if this is the same then it can be assumed that the use of the wrong medium did not have such devastating effects on the results. However this data should be repeated using the correct medium.

The kinetics for LPA combined with PDGF-BB ligand stimulations were conducted for its affect on PDGF receptor phosphorylation. The data is illustrated on the western blot figure 3.5.1, which was the total cell lysate sample immunoblotted with CTB and p-Tyr antibodies, showed that there was a significant level of background banding in the unstimulated samples. Unfortunately the WGA beads did not work for this stimulation as this method still requires extensive optimization, and as previously mentioned the IP method was not functioning. Therefore, the peaks for the unstimulated samples were disregarded and the other time points were assessed. On the p-Tyr immunoblots (figure 3.5.2) illustrating the total tyrosine phosphorylation of the PDGF receptor, the data was positive that the combination of LPA with PDGF-BB ligand increases phosphorylation. This is followed by LPA stimulation alone and finally the lowest phosphorylation was observed for stimulation with PDGF-BB alone. The same result was observed on the CTB immunoblots (figure 3.5.3).

Since the data obtained is what has been previously established and also expected for this experiment, it is assumed that the medium did not have a significant effect. Therefore the next step was to confirm that MARCKS phosphorylation is proportionately.

The western blot on figure 3.4.6 and the quantification on figures 3.4.7/8, for the phosphorylation of MARCKS and the total MARCKS protein available confirmed previous findings that it is activated in response to combination of LPA with PDGF-BB. The increase in phosphorylation occurs after 20 minutes, where it continues to increase and remain high even after 60 minutes. Therefore the increase noted in MARCKS phosphorylation after combining LPA with PDGF-BB ligand requires a period of time, but it does activate

MARCKS. At this point the downstream effector molecules AKT and ERK1/2 phosphorylation was investigated.

It was observed on the western blot figures and quantifications for AKT that there was no increase in phosphorylation. In fact very high phosphorylation levels were observed for the sample stimulated with PDGF-BB ligand alone. This raises suspicion that perhaps due to the growth factors in the stimulation medium, very high levels were observed. In addition the phosphorylation levels observed for LPA were not low either; therefore this is most likely the cause for the results observed.

Finally ERK 1 and ERK 2 are a chain of proteins activating the MAP kinase pathway within the cell and eventually resulting in the activation of transcription. As with AKT the same results were observed, where there is an abnormal high level of phosphorylation in the sample stimulated with PDGF-BB ligand alone leading to the conclusion that although the wrong medium did not affect the PDGF receptor and MARCKS phosphorylation; it did affect the downstream signalling molecules and their response to the stimulations.

4.4 Conclusion & future research

The first conclusions which can be derived from this project is that the previously un-investigates cytokine fMLP has been shown to significantly potentiate the ability of PDGF-BB ligand to phosphorylate the PDGF receptor. In addition this increase in phosphorylation also occurs in the absence of PDGF-BB, strongly suggesting that PKC is directly activated. Finally all downstream effector molecules of the PDGF receptor including MARCKS and AKT both have enhanced levels of phosphorylations when stimulated with fMLP. However this must be repeated several times to ensure the results are reproducible and that a confocal analysis of PDGF receptor localization is conducted to confirm receptor recycling. Finally the

cells should be transfected with Rab4 dominant which will inhibit the important Rab4a, and therefore assess whether the receptor recycling is dependent on this factor.

The second conclusion is that the previous findings on LPA's ability to increase PDGF receptor phosphorylation and activate protein kinase have been re-confirmed. However the downstream effector molecules were affected by the wrong medium which was used and thus this does require repetition to expand on the findings of LPA.

Moving on, due to the important findings on fMLP, the hypothesis that PKC is a point of signal integration for PDGF receptor recycling is supported and is now a crucial point which must be investigated. This should be done by repeating the experiments on fMLP and also employing other G protein coupled cytokines, assessing whether these also result in PDGF receptor recycling. It is though that this will be found and that MARCKS will also be activated. Therefore if all cytokines result in the recycling of PDGF receptor, then they all must activate PKC and this then must be a point of signal integration for receptor recycling.

If it found that PKC is indeed a point of signal integration it will be a major breakthrough as PKC is also a major and crucial point of activation for receptor recycling (Hellberg *et al*, 2009). Therefore this can then be targeted for novel anti cancer treatment and therapies.

5. References

1. Aaronson,S.A. (1991) Growth factors and cancer. **PubMed,** 254(5035):1146-53.

2. Andrae,J. *et al*. (2008) Role of platelet-derived growth factors in physiology and medicine. **Genes and Development**, 22:1276-1312

3. Deuel,T.F. and Huang,J.S. (1984) Platelet-derived growth factor. Structure, function, and roles in normal and transformed cells. **The Journal of Clinical Investigation**, 74(3): 669–676.

4. Ding,J. and Badweyt,J.A. (1993) Stimulation of Neutrophils with a Chemoattractant Activates Several Novel Protein Kinases That Can Catalyze the Phosphorylation of Peptides Derived from the 47-kDa Protein Component of the Phagocyte Oxidase and Myristoylated Alanine-rich C Kinase Substrate. **Journal of Biological Chemistry**, 268, 17326-17333.

5. Fischer,E,H. et al. (1991) Protein tyrosine phosphatases: a diverse family of intracellular and transmembrane enzymes. **Science**, 253;5018. 401-406.

6. Grinstein,S. and Furuya,W. (1992) Chemoattractant-induced tyrosine phosphorylation and activation of microtubule-associated protein kinase in human neutrophils. **Journal of Biological Chemistry**, 267; 25. 18122-18125

7. Goustin,A.S. *et al* (1986) Growth factors and cancer. **Cancer Research**, 46; 1015

8. Heldin, C.H. and Westermark,B. (1999) Mechanism of Action and In Vivo Role of Platelet-Derived Growth Factor. **American Physiological Society,** 79; 4. 1283-1316

9. Hellberg,C. *et al.* (2009) Activation of Protein Kinase C α Is Necessary for Sorting the PDGF β-Receptor to Rab4a-dependent Recycling. **Molecular Biology Of The Cell**, 20**;** 12**.** 2856-2863
10. Hooshmand-Rad,R. *et al*. (1998) PDGF α-receptor mediated cellular responses are not dependent on Src family kinases in endothelial cells. **Journal of Cell Science**, 111, 607-614.
11. Karlsson,S. *et al.* (2006) Loss of T-Cell Protein Tyrosine Phosphatase Induces Recycling of the Platelet-derived Growth Factor (PDGF β Receptor but Not the PDGF **α** Receptor). **Molecular Biology Of The Cell**, 17; 4846–4855.
12. King,M.W. (2012) **Growth factors** [online] US: Indiana State University. Available from http://themedicalbiochemistrypage.org/growth-factors.php#intro [Accessed 2nd May 2012]
13. Kohler,M. and Lipton,A. (1974) Platelets as a source of fibroblast growth-promoting activity. **Experimental Cell Research**, 87, Issue 2, 297–301
14. Kusunoki,T. *et al.* (1992) Tyrosine phosphorylation and its possible role in superoxide production by human neutrophils stimulated with FMLP and IgG. Elsevier,183; 2.789–796
15. Lokker, N.A. *et al*. (1997) Functional importance of platelet-derived growth factor (PDGF) receptor extracellular immunoglobulin-like domains. Identification of PDGF binding site and neutralizing monoclonal antibodies. **PubMed,** 272(52):33037-44.
16. Majewski,N. *et al.* (2004) Akt Inhibits Apoptosis Downstream of BID Cleavage via a Glucose-Dependent Mechanism Involving Mitochondrial Hexokinases. **Molecular and Cellular Biology**, 24; 2. 730-740.

17. Murphy,P.M. (1994) The molecular biology of leukocyte chemoattractant receptors. **PubMed**, 12:593-633

18. Östman,A. *et al* .(2006) Protein-tyrosine phosphatases and cancer. **Nature**, 6, 307-320

19. Pawson,T. and Scott,J.D. (1997) Signaling through scaffold, anchoring, and adaptor proteins.**PubMed**, 278(5346):2075-80.

20. PierceNet (2012) **Pierce Glycoprotein Isolation Kits** [Online] USA: Thermo Fisher Scientific. Available from http://www.piercenet.com/browse.cfm?fldID=BE7B5F09-27C9-4257-8C74-28A3E709B8B7 [Accessed 3rd May 2012]

21. Rollet,E. *et al* .(1994) Tyrosine phosphorylation in activated human neutrophils. Comparison of the effects of different classes of agonists and identification of the signalling pathways involved. **Journal of Immunology**,153; 1. 353-363

22. Ross,R. (1974) A Platelet-Dependent, Serum Factor That Stimulates the Proliferation of Arterial Smooth Muscle Cells In Vitro**. Proceedings of the National Academy of Sciences**. 71;4,1207-1210

23. Shim,A.H. *et al.* (2010) Structures of a platelet-derived growth factor/propeptide complex and a platelet-derived growth factor/receptor complex. **Proceedings of the National Academy of Sciences**. 107; 25. 11307–11312

24. Torres,M. *et al* (1993) Stimulation of human neutrophils with formyl-methionyl-leucyl-phenylalanine induces tyrosine phosphorylation and activation of two distinct mitogen-activated protein-kinases. **Journal of Immunology**, 150:1563-77

25. Van Der Sluijs,P. *et al*. (2000) Rabaptin4, a novel effector of the small GTPase rab4a. **Biochemistry Journal**, 346, 593-601.

26. WCRFI. (2011) **General world cancer statistics** [online]. London; WCRFI. Available from http://www.wcrf.org/cancer_statistics/world_cancer_statistics.php [Accessed 3rd May 2012]

27. World Health Organization (2008) **Cancer** [online].United Nations: WHO. Available from http://www.who.int/mediacentre/factsheets/fs297/en/ [Accessed 3rd May 2012]

28. Wu,E. et al. (2008) Comprehensive Dissection of PDGF-PDGFR Signaling Pathways in PDGFR Genetically Defined Cells.**PLOS.**

29. Yuan,J. et al. (2002) Cooperation of G_q, G_i, and $G_{12/13}$ in Protein Kinase D Activation and Phosphorylation Induced by Lysophosphatidic Acid. **The Journal of Biological Chemistry**, 278, 4882-4891.